Particle size, morphology, phase transition and energy efficient applications of hydrothermally produced VO_2(D)

Diana C. Teixeira G.

A dissertation submitted in partial fulfillment
of the requirements for the degree of
Doctor of Philosophy
of
University College London.

Department of Chemistry
University College London

August 26, 2018

I, Diana C. Teixeira G., confirm that the work presented in this thesis is my own. Where information has been derived from other sources, I confirm that this has been indicated in the work.

Abstract

Thin films of thermochromic vanadium(IV) oxide, VO_2(M), were synthesized using sol-gel/spin coating techniques and aerosol assisted chemical vapour deposition (AACVD). The effect of precursor solution aging, thickness and annealing temperature was studied.

A recently reported vanadium dioxide phase, VO_2(D), was studied in this work. Its structure (reported in the literature) is discussed and another possible structure is presented and analyzed in this work.

VO_2(D) nanoparticles of 20-30 nm were synthesized for the first time using vanadium pentoxide as a precursor *via* hydrothermal synthesis. The phase transition from VO_2(D) to thermochromic VO_2(M) was studied and reported to be the lowest phase transition temperature (165 °C) in order to obtain thermochromic VO_2. The pH conditions of the starting solution were studied and reported to be a critical and important feature in the reaction.

Different morphologies of VO_2(D) microparticles were prepared using ammonium metavanadate as a precursor by hydrothermal synthesis. VO_2(D) microparticles from 1 to 5 micron in size were reported with star shape, round-ball, elongated particles shape among others at different pH. The effect of the starting pH solution in the final product was studied. Thermochromic VO_2(M) microparticles were obtained after mild calcination.

Finally, thermochromic polymeric films were prepared using VO_2(M) nanoparticles obtained after low temperature calcination of VO_2(D) nanoparticles. The nanoparticles were encapsulated into a

polyvinylpyrrolidone matrix and deposited *via* spin coating onto a glass substrate.

Acknowledgements

I would like to thank my supervisors, Dr. Robert Palgrave and Professor Ivan Parkin for guidance, advice, encouragement and mentoring through my PhD. You both were the best professors. Thanks for your patience, time and thank you for your trust in me. I would also like to thank Professor Sankar and my supervisor in Singapore Dr. Gregory Goh, for all their help, teaching and guidance during the past years, their contribution has been invaluable.

I would also like to thank to Dr. Zhimei Du, for all the help and advice through all the exchange process. Thanks also to Mrs. Teo Yi Wen who managed all my attachments in Singapore, thanks to her, the process was easier and smoother.

I also wish to thank all my friends and colleagues that make my life amazing and happy during my years in London, to Dr. Raul Quesada for helping me at anytime, for his advice and unconditional friendship. To Dr. Carlos Sotelo for being my friend and supporting me during the whole process. You both were a key part of my adaptation to the non Spanish speaking environment. To Dr. Michael Powell for all his invaluable help and knowledge. Thanks for the time and dedication you put to teach me everything about vanadium. To Dr. Ian Godfrey for all his time, dedication and knowledge. To Dr. Steve Firth for his help, good talks and knowledge imparted to me. To Sayd to welcome me every day with a big smile, that make my days better. A big thanks for my office friends, Yaomin, Min, Roberta, Emily, Clara, Miguel and Matthew. Special thanks to my friends (that feels like family), Hafi and

Francesco, you two were an important part of this process, you make my life easier and amazing, thanks for the talks, the coffees and all the lovely experiences together.

I have to thank to my colleagues in Singapore, they make my time there even more fantastic. Special thanks to Ola for her guidance and time to show me everything around Singapore.

To my college friends who where always there for me, Jessica, Gaby, Aura, Laura and Ligia, thanks for supporting me every day.

To my new family, Cote, Michael, Marisol and Miguel thanks for always supporting me and cheering me up.

Special thanks to my family, parents and grandmother for being my pillar, supporting me everyday, encouraging me and make me what I am today. You are the best family I could have and this achievement is dedicated to you.

And last but not least, to my lovely husband, the most important person in this puzzle, who was there everyday and every night to cheer me up and walking by my side. This is for you, without your company I could not have done it. I love you.

Contents

List of Figures

List of Tables

Chapter 1

Introduction

1.1 General introduction and aims

This thesis presents the preparation and analysis of nanoparticles, microparticles, thin films and polymeric films of different phases of vanadium dioxide (VO_2) synthesized *via* hydrothermal synthesis [2] [3] [4] and sol-gel methods. Vanadium dioxide presents thermochromic behavior in its monoclinic form (VO_2(M)), and demonstrates a reversible metal to insulator transition at 68 °C. Due to its thermochromic properties, vanadium dioxide is a very interesting material to be used for architectural purposes such as smart coatings.

Considering the difficulty of producing nanoparticles of VO_2(M) in one step, a new easy and reproducible way to do so is presented in this work. Moreover, a newly reported phase of vanadium dioxide is studied and characterized.

In this chapter, a detailed description of vanadium dioxide thermochromic properties, structure and phases is presented, as well as a description of solar control coatings. This will be followed by a description of the techniques used in this work to synthesize particles and films of vanadium dioxide.

1.2 Novelty of work

Vanadium dioxide has several applications including architectural glazing, Li-ion batteries [5] [6], super capacitors [7] [8] [9], switching de-

vices [10] [11], among others. For each application, the morphology, particle size and crystallographic phase of vanadium dioxide used is very important. In this work a newly reported phase of vanadium dioxide is synthesized with different morphologies and sizes that can be used for different applications. Moreover, nanoparticles of the new phase are prepared and used to obtain thermochromic VO_2 *via* low temperature calcination. Polymeric films with thermochromic properties were prepared using VO_2(D) calcined nanoparticles.

In order to understand the vanadium synthesis process, thin films are prepared *via* sol-gel/spin-coating and aerosol-assisted chemical vapour deposition.

1.3 VO_2 for solar control coatings

Vanadium(IV) oxide has been largely studied due to its thermochromic properties that can be used for dynamic solar control coatings, for example, in windows of buildings with the aim of maintaining a comfortable temperature inside the installations without the excessive use of a cooling or heating system, that additionally contribute to energy demand.

According to the European Commission, 40% of the energy consumption and 36% of the CO_2 emissions in the European Union comes from buildings. Moreover the use of heating and cooling systems in buildings are estimated to account for around 60% of global energy consumption in buildings and the world sales of air conditioning systems in 2012 increased 13% compared to 2011 [12].

The international Energy Agency declare that if no actions are taken to improve energy efficiency in buildings, the energy demand is expected to rise by 50% in 2050 [12]. There is a real concern about these numbers and the need to lower them. In order to do so, the European Commission proposed in November 2016 to revise the the Energy Performance of Buildings Directive in order to encourage the use of smart technology in buildings [13]. Vanadium(IV) oxide can be used as part of the smart technologies for buildings.

Nowadays, static solar control coating technologies are being used in countries where constant hot/sunny weather or cold weather during the whole year are the rule. For example, reflective coatings or films are used in hot weather to repel the solar heat, thus to keep the inside of the building at a convenient temperature reducing in this way the excessive cost of cooling systems. On the other hand, in cold weather the aim is to retain the heat inside the building, this can be done using an indium doped tin dioxide (ITO) coating. This coating allows the sunlight to enter the building creating blackbody radiation. Due to the material properties, the blackbody radiation and the heat generated by people inside, the warmth will not be able to easily escape the building through the windows thus reducing the use of heating systems [14].

However, the commercial uses of the coatings does not include places with dramatically changing temperature throughout the year, for example central and northern Europe as well as north east USA where very cold winters and very hot summers occur.

The dynamic thermochromic properties of the vanadium (IV) oxide will allow the use of these coatings in places with variable temperatures during the year, as the material can behave as a reflective coating to reflect the sun heat or as a transparent one to allow the near infra-red radiation to enter the building. The main problem of using the vanadium(IV) dioxide commercially is the low luminous transmittance (T_{lum}) of the VO_2 while trying to have high solar modulation (T_{sol}) [15]. The ideal thermochromic films of VO_2 should have a transition temperature close to ambient temperature $\approx$ 25 °C, an integrated luminous transmittance (T_{lum}) $\geq$ 40% and a solar modulation ability $\geq$ 10% [16].

Luminous transmittance is defined as the ratio of the luminous flux transmitted by a body to the flux incident upon it, equation 1.1. Where $\bar{y}$ is the standard photopic luminous efficiency of the human eye by the Commission Internationale de l'Eclairage's (CIE) and $T(\lambda)$ is the transmission of the VO_2 film at different temperatures [17].

$$T_{lum} = \frac{TransmittedLight}{IncidentLight} = \frac{\int_{\lambda=380nm}^{780nm} \bar{y}(\lambda)T(\lambda)d\lambda}{\int_{\lambda=380nm}^{780nm} \bar{y}(\lambda)d\lambda} \tag{1.1}$$

$$T_{sol} = \frac{\int_{\lambda=300nm}^{2500nm} AM_{1.5}(\lambda)T(\lambda)d\lambda}{\int_{\lambda=300nm}^{2500nm} AM_{1.5}(\lambda)d\lambda} \tag{1.2}$$

The solar modulation is defined in equation 1.2 as the weighted solar irradiance spectrum, at a tilt angle of light on a south facing surface at 37°from horizontal solar irradiance spectrum ($AM_{1.5}$) times the transmission of the VO_2 film by $AM_{1.5}$. The $AM_{1.5}$ weighting spectrum is taken from the solar averaged transmittance calculated by Taylor *et al.* [17] representing the yearly average for mid-latitudes. The spectrum is shown in Figure 1.1

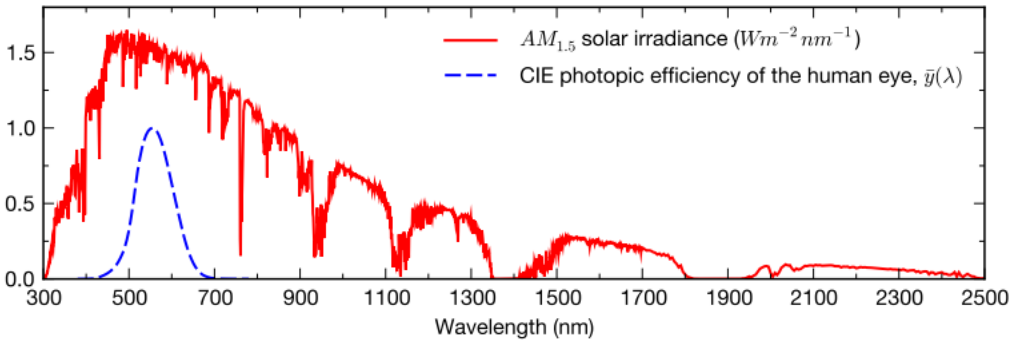

Figure 1.1: Spectra used to weight the transmittance functions in equations 1.1 and 1.2. The photopic luminous efficiency of the human eye, y(λ), and the AM1.5 solar irradiance spectrum. Used with permission of the authors [17].

Figure 1.2 shows a sketch of how a thermochromic film of vanadium(IV) oxide will work when used as a windows coating. The material has a critical temperature where it switches from transparent to reflective.

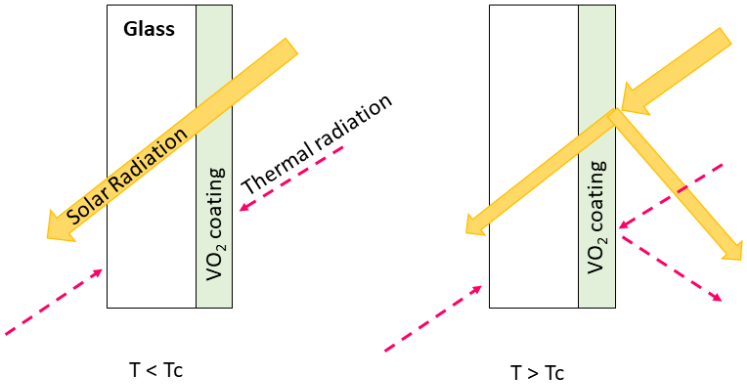

Figure 1.2: Schematic demonstration of the performance of thermochromic films in windows

Below the critical temperature (68 °C for bulk VO_2) the material is transparent and allows solar radiation to pass through the glass thus heating the interior of the building. On the other hand, when the temperature is above the switching temperature, the material is infrared reflective avoiding most of the thermal radiation coming from the sunlight that passes through the glass. The coating at this temperature is still visually transparent.

The transition temperature for the bulk vanadium(IV) oxide is too high to be used for solar control coatings in buildings, however, this temperature can be tuned by adding impurities to the compound like molybdenum [18], magnesium [19], fluorine [20], tungsten [21] and niobium [22] to mention the most common ones.

1.4 Vanadium overview and phases

Vanadium is a transition metal discovered by mineralogist Andres Manuel del Rio in 1801 [23]. It naturally occurs in about 65 different minerals, including vanadate, the ore of lead and vanadium.

In the late 1950s the thermo-conductive properties of several transition metal oxides were studied by Morin [14], and the most promising material investigated in terms of technological applications was vanadium(IV) oxide, as this material in its monoclinic phase present a re-

versible phase transition from monoclinic to tetragonal structure at 68 °C [24] [25] [26]. This phase change and the changes in the material properties were first studied by Goodenough [27].

The material is used for optical and electrical switching devices [10], multifunctional spintronics [28], and many military applications from IR sensors [29] [30], night vision equipment (as coatings) in order to prevent detection by reducing IR transmittance of blackbody emitters [31], to missile seeking sensors, and various other applications [32].

VO_2 has many other interesting and important applications in green construction or sustainable building [33] due to its thermochromic properties. Vanadium dioxide exhibits a reversible phase transition from a low temperature, monoclinic phase with insulating properties (VO_2(M)) to a high temperature, the so called rutile phase (VO_2(R)) has a tetragonal crystal form, with metallic properties (above 68 °C) [34]. This metal to semiconductor phase transition (MST) is related to an increase in the reflectivity in the near infrared spectrum which in turn modifies the near IR optical properties of the VO_2 with temperature.

The transition temperature of the material (68 °C) can be tuned down close to room temperature, to make it suitable for architectural purposes by doping the material using tungsten [35]. Vanadium dioxide is a candidate to be used as a coating in windows of building in order to regulate/maintain a pleasant temperature inside them without the need of the excessive use of heating or cooling systems due to its metal to insulator switching properties. Moreover, due to the growth of world population and the increase of the energy demand in buildings (industrial and residential), that nowadays reach up to 60 % of the energy consumption [36] [12], VO_2 coatings are good candidates to be used in order to diminish the energy usage in buildings and reduce the CO_2 emission (that only in US reach 43 % of carbon dioxide emissions) coming from them [37].

Vanadium's ground state electron configuration is [Ar]$3d^3 4s^2$ [38].

Vanadium thus has 5 valence electrons that can participate in the formation of chemical bonds. One common characteristic of transition metals is their ability to adopt multiple oxidation states. Vanadium has four commonly observed oxidation states: 5+, 4+, 3+ and 2+ and each one of them can be easily distinguished by their colour, as we can see from Figure 1.3 [39]. This is characteristic of the transition metal ions where the change of colours can be potentially used to predict the course of a redox reaction.

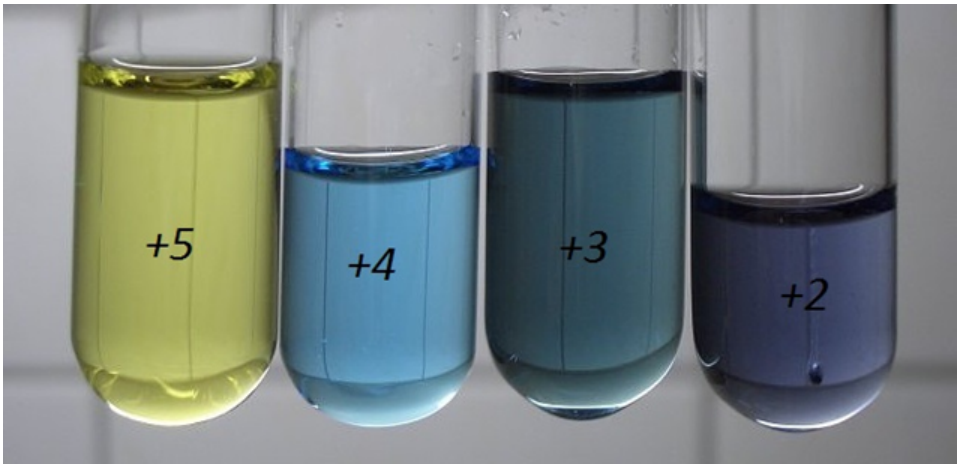

Figure 1.3: Different colours adopted by vanadium ions depending on their oxidation state

Each oxidation state is associated to a vanadium oxide phase, for example VO is associated to V^{2+} and V_2O_5 is associated with V^{5+}, etc., however, phases in between can be found as well, these phases are called Magneli phases [40] and have a general formula to represent them, V_nO_{2n-1}, with $3 \geq n \geq 9$. All the Magneli phases present a metal to insulator transition at different temperatures, except for V_7O_{13} which is metallic at all temperatures [41]. The metal to insulator transition temperatures for each Magneli phases are shown in Table 1.1.

Despite the fact that some Magneli phases present a MST temperature they are not being used for architectural purposes as the transition temperatures are too low or too high to work. For example, as well as vanadium(IV) oxide, vanadium(V) oxide (V_2O_5) also shows ther-

mochromic transitions at 257 °C, and it is usually used as a catalyst in industrial processes [42], in the manufacture of solid-state lithium ion batteries, and in gas-sensing applications [43], but not in architectural applications.

Table 1.1: Transition temperatures of the vanadium Magneli phases in the series V_nO_{2n-1} [41].

Compound (V_nO_{2n-1})	*Metal to Insulator transition temperature (K)*
V_2O_3	168
V_3O_5	430
V_4O_7	250
V_5O_9	135
V_6O_{11}	170
V_7O_{13}	metallic
V_8O_{15}	70
V_9O_{17}	-
VO_2	340

The Magneli phases are easier to obtain as the reaction times and conditions are less restrictive than those for pure phases, moreover, obtaining a pure phase V_xO_y is challenging as vanadium is stable over a wider range of oxidation states. For industrial purposes this is an advantage, moreover, Magneli phases are easier to dope because the dopant fills the vacancies in the structure and results in the change of the transition temperature as well as improvement in the transmission properties [41].

VO_2(D) is a relatively newly reported meta-stable phase [44] that is being investigated widely in the VO_2 field as a direct transition to VO_2(M) is allowed at relatively low temperatures (250 - 400 °C) [45] [46] under a controlled environment. Furthermore, once the transformation from VO_2(D) to VO_2(M) is achieved, the typical metal to semiconductor transition temperature of the thermochromic VO_2(M) is lower (61 °C) than the one reported in the literature for bulk VO_2(M) which is 68 °C [45].

This recently discovered vanadium dioxide phase VO_2(D) acts as a semi-conductor material with a band gap of 0.33 eV [44]. Its electronic

structure is still subjected of discussion as the few works that reported this new phase is similar in structure to the monoclinic nickel tungstate ($NiWO_4$) because the VO_2(D) X-Ray diffraction pattern is structurally similar. However, this assignment will be critically assessed in this thesis.

The research of this new phase is still ongoing, however, in this work two different syntheses are shown in oder to obtain VO_2(D) micro and nanoparticles. Different morphologies and sizes of this VO_2(D) phase are obtained and characterized in this work. This will be discussed in chapter 5.

1.5 Properties and structure of vanadium(IV) oxide

Vanadium dioxide (VO_2) has six known crystal structures. VO_2(A) [47] [48], VO_2(B) [49], VO_2(C) [45] [50], VO_2(D) [44] which will be widely discussed in this work, VO_2(M) and VO_2(R), with only VO_2(M) to VO_2(R) phases displaying a reversible switch induced by a temperature change close to room temperature.

Monoclinic VO_2 acts as a semi-conductor with a band gap of 0.7 eV [51] while for tetragonal VO_2 the gap becomes zero showing a metallic behavior [52]. Tetragonal VO_2, also known as VO_2(R), due to its structural resemblance to rutile TiO_2 phase, has semi-metallic properties, is a good electrical conductor and is highly reflective at near IR wavelengths.

These phases consist of coordinated V^{4+} ions with linkages of octahedra producing different crystal structures [53]. VO_2(A) has a reversible metal to insulator transition (MIT) temperature at 162 °C and is used as a cathode for lithium ion batteries [47] [54]. The solid material is thermally stable and resistant to oxidation in the presence of air below 400 °C [55].

VO_2(B) has been widely used as a convenient precursor to obtain

the VO_2(M) phase by calcination of the sample at temperatures above 500 °C under controlled atmosphere [44]. However in the past years VO_2(B) has been more studied in order to improve its electrochemical performance and also as a promising material to be used as a cathode in the Li-ion batteries [56].

Figure 1.4 shows the structures of V_2O_3, V_2O_5 and the stable phases of VO_2(B) and VO_2(A) for comparison.

The metal to semiconductor transition reflects a structural phase transformation from monoclinic (for temperatures below 68 °C) to tetragonal (for temperatures above 68 °C).

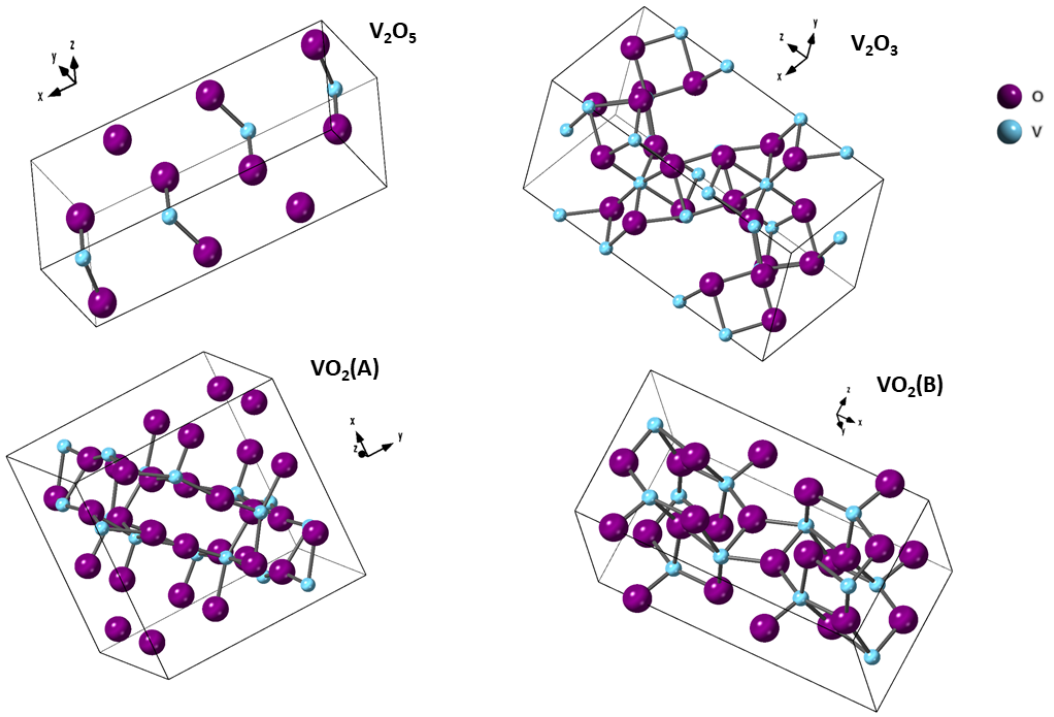

Figure 1.4: Representation of the V_2O_5, V_2O_3, VO_2(B) and VO_2(A) crystal structures

This metal to semiconductor transformation has been widely studied and diverse theories have been suggested in the literature to explain this process, however reasons for this are still being debated. The most accepted theory to explain the transition is the one from Goodenough [27]. Figure 1.5 shows the schematic band structure based on his work. When the material is at $T \geq T_c$, the crystal structure is tetragonal with

space group p$4_2/mnm$. Due to change of the temperature, the V 3d t_{2g} band separates into two sub-bands, $d_{||}$ and Π^*. The fusion of the V π^* band and the O 2pπ band provokes the π^* band to be moved upwards, while the weak hybridization (fusion) between $d_{||}$ and O 2p band leaves the $d_{||}$ band in the lowest state of all V 3d bands. The metallic behavior of the tetragonal phase is due to the partially filled $d_{||}$ and π^* band. The band gap, corresponding to an optical change is denoted as E_g and is the distance between the Fermi level and the O 2p band [57].

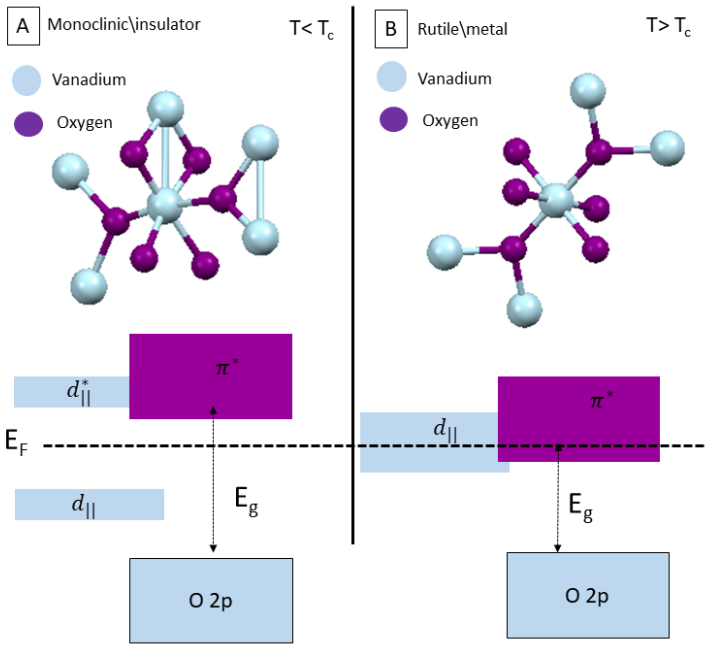

Figure 1.5: (A) VO_2(M) crystal and band structure (B) VO_2(R) crystal and band structure

On the other hand, when the material is at T $< T_c <$ 68 °C, the vanadium atoms combine and form a zig-zag along the c-axis, causing the distortion into a monoclinic structure with space group p21/c. The $d_{||}$ band splits into two bands: $d_{||}$ and $d^*_{||}$. The $d_{||}$ band is completely filled leaving thus the π^* band empty [57].

In other words, when the MST occurs the planes in the monoclinic vanadium atom shift. This shift is enough to break the V^{4+}-V^{4+} pair forming a tetragonal phase with metallic conductive properties [14].

1.6 Doping of VO_2 to decrease metal-to-semiconductor transition

Different materials have been used as VO_2 dopant in order to reduce (or increase) the critical transition temperature to make the material suitable for architectural purposes, to enhance the luminosity and transparency of the material and to improve the colour of the material, that otherwise is not really attractive.

The ionic radius of octahedral v^{4+} is 0.58 $\AA$ and studies reveal that ions with greater ionic radius, can be used as dopant to decrease the transition temperature, while ions with ionic radius smaller than vanadium, can be used to raise the transition temperature [58].

When vanadium samples are doped using transition metals such as Fe, Co and Ni, the critical switching temperature decreases between 10 to 12 °C, while when doping with oxides with the MoO_2-type structure as Mo, Nb and W, the temperature can be lowered from 60 to 70°C [59].

The most studied and effective dopant used to reduce the transition temperature is the tungsten (w^{6+}) with an ionic radius of 0.6 $\AA$. Tungsten doped vanadium dioxide thin films prepared *via* reactive radio frequency (RF) sputtering or sol-gel methods present a diminution of the critical temperature from 68 °C to 25 °C [60] [61]. Doped films are mainly intended to be used for architectural purposes. Other ions as Mo^{6+} and Nb^{5+} with ionic radius of 0.78$\AA$ and 0.73$\AA$ respectively, are also used to reduce the transition temperature.

As mentioned before, a high transition temperature is only one of the problems when using vanadium(IV) oxide for solar control coatings. A low luminous transmittance is another problem, however, studies have used fluorine doped vanadium(IV) oxide films to overcome this problem [62]. The addition of fluorine in films prepared *via* AACVD increases the visible transmittance without compromising the thermochromic properties of the material, this occurs because the absorption band is shifted to the UV region, resulting into a transparent

film in the visible [62].

Other works reported that magnesium doped VO_2 films prepared *via* sputtering showed a low transition temperature and higher visible transmittance. The effect of the magnesium in the films is to enlarge the band gap, therefore to lower the visible absorption. Theoretically, the change in the band gap induced by the magnesium also helps in the improvement of the colour of the film [63].

1.7 VO_2 particles: hysteresis and size-effects

The reversible metal to semiconductor transition in vanadium(IV) oxide presents hysteresis behavior implying a first order transition.

A first order phase transition in a single system means that a discontinuity in one or more state variables exists. In the vanadium dioxide case specifically, the volume and the entropy change discontinuously at the equilibrium transition temperature (68 °C). Tetragonal and monoclinic phases coexist at T_c, therefore their enthalpies are different, suggesting that each phase holds a different structure. In other words, for VO_2, some regions of the material complete the transition before others.

The hysteresis curve in vanadium(IV) oxide is expected to be as narrow as possible in terms of temperature if is meant to be used for architectural purposes. This will reflects a fully phase transition at certain temperature [64].

Experimental studies report that the thermal hysteresis in VO_2(M) / VO_2(R) shows a difference in the transition temperatures for heating and cooling cycles, suggesting that the transformation does not materialize at the point where the free energies of the two phases are the same [65].

In other words, the hysteresis behavior in vanadium(IV) oxide indicates that a phase transformation is taking place in the material but some regions of the material have completed the transition and some others have not, this is because first order transitions involve a latent heat [65] and the energy of the transition can not be transferred right away.

Studies have demonstrated that the particle size and defects in the materials, mainly induced by dopants, affect the features of the hysteretic phase transition [66]. Small VO_2 particles lead to wider hysteresis loops with high transition temperatures for the heating cycle and low transition temperatures for the cooling cycle. On the other hand, in bigger particles the interface between two grains (grain boundary) is reduced thus more number of defects and nucleation sites are produced (more nucleation sites results in faster transition phase), provoking thus narrow hysteresis [64].

According to Li *et al.*, thermochromic nanoparticles provide superior luminous transmittance and solar energy transmittance modulation [67]. This is because the size of the particles alters the effective absorption spectra of VO_2 i.e. some wavelengths may exhibit a higher absorption coefficient (compared to bulk VO_2) due to electromagnetic resonances in the nanosized metallic VO_2 elements of the system .This resonance effect is related to the size of the VO_2 elements and this is why it is possible to induce some sort of blue shift that improve the luminous transmittance and solar energy modulation. Moreover producing nanoparticles of VO_2 has advantages in the optical features. Vanadium dioxide presents a non attractive (for architectural purposes) yellow/brownish colour, however, if the VO_2 particles are smaller than the visible light wavelength, the nanoparticles have lower absorption between 400 to 700 nm of the electromagnetic spectrum, therefore, the obtained particles or films will be optically transparent with low scattering effect.

Particle size is not the only factor that affects the metal to semiconductor transition in VO_2, among them the synthesis and annealing conditions, thickness of the film, dopants and crystallograpic orientation [65] play an important role in the phase transitions in VO_2.

1.8 Synthetic methods for producing VO_2

Vanadium dioxide films can be produced using different methods such as, sol-gel spin coating [68] [69] and dip-coating [70] [71], sputtering [72, 73], chemical vapour deposition [74] [75] [76], whereas powders are produced *via* hydrothermal synthesis [34] [46]. Vanadium dioxide nanoparticles can be incorporated into a polymeric matrix to obtain VO_2 films.

The most studied method to produce VO_2 particles is hydrothermal synthesis, while the most studied thin film deposition method is CVD. In this work hydrothermal synthesis, AACVD and spin-coating methods were used.

1.8.1 Hydrothermal synthesis

Hydrothermal synthesis is a method to produce different chemical compounds and materials which uses a closed-system where physical and chemical processes occur in aqueous solution [77] . There are many different definitions for hydrothermal synthesis in the literature and there is no definite lower limit for the temperature and pressure condition reported, however, the majority of the authors fix the hydrothermal synthesis at temperatures above 100 °C and pressures above 1 atm.. According to these definitions, hydrothermal can be described as any heterogeneous chemical reaction in the presence of water occurring at above room temperature and at pressure higher than 1 atm. in a closed system [78].

The method consists on the dilution of precursors (insoluble under normal conditions) by water or aqueous solutions at high temperature and pressure [79]. Hydrothermal synthesis allows us to access to phases that will not occur spontaneously at room temperature. The advantages of using this method includes the easy formation of crystals of substances that are unstable near their melting point and the ability to synthesise large crystals.

Figure 1.6 shows a drawing of a typical hydrothermal teflon lined

autoclave used in this work. It contains a teflon cup where the water or the aqueous solution is placed together with the precursor material. The teflon cup is inside of a stainless steel shell and closed by a secure lid that has a bursting disc for safety reasons, in case the pressure becomes too high inside the vessel.

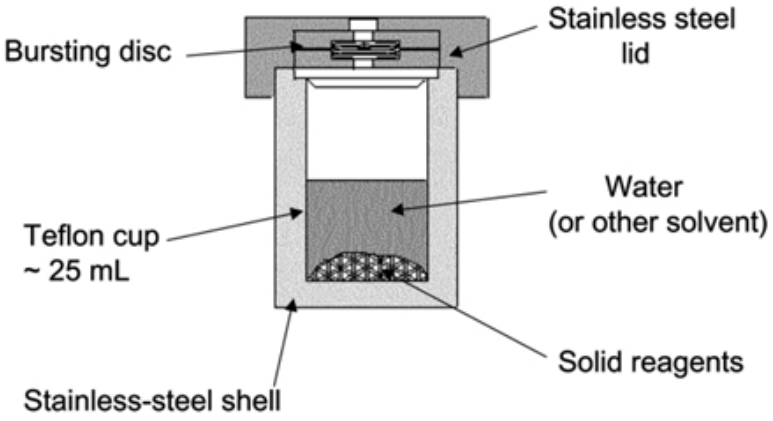

Figure 1.6: Typical hydrothermal synthesis reactor (autoclave)

Hydrothermal synthesis has been widely used for the synthesis of zeolites, ZnO nanorods, MnO_2, lithium iron phosphate cathodes, CdTe nanocrystals, anatase and rutile TiO_2 among others [80][81] [82] [83] [84] [85]. In particular, synthesis of VO_2 leads to the formation of different phases of VO_2 and morphologies like rods [86], star shapes [46], spherical shapes [87], among others, depending on the temperature, precursor and time used for the reaction.

To better understand the hydrothermal synthesis process, it is necessary to explain the nucleation and growth of particle processing.

1.8.1.1 Nucleation and growth of particles

Nucleation is defined as the first step of a process that occurs in the formation of a crystal from a liquid, vapour or a solution, where the ions, atoms, or molecules turn into a characteristic pattern of a crystalline solid [88]. Nucleation is the site where the additional particles accumulate during the crystal growth process.

Nucleation processes are classified into heterogeneous and homo-

geneous. In the heterogeneous nucleation process, the crystallization occurs on the surface of the material while in the homogeneous nucleation process, a few particles fix themselves closely in their way through the bulk of the medium [65].

There are different theories explaining the nucleation and growth process, including the LaMer Mechanism, Ostwald Ripening [89] and Digestive Ripening [90], Finke-Watzky two step Mechanism [91], Coalescence and Oriented Attachment [92] and Intraparticle Growth [93]. For hydrothermal growth of vanadium nanoparticles, the most used is the LaMer mechanism [94]. LaMer divided the nucleation and mechanism process into three steps: (I) a fast increase in the concentration of the reacted species that are dissolved in a solution (called monomers). These monomers are able to adhere to a particle without a significant energy barrier. (II) the concentration of the monomers outpaces the critical point of supersaturation where the nucleation process is energetically favorable and occurs. Stage (III) involves the growth of the particles after nucleation [93].

Figure 1.7 shows the three phases of the LaMer mechanism.

Another way to explain this process is *via* classical nucleation using the Gibbs energy. Moreover, this method also demonstrates that homogeneous nucleation for VO_2 nanoparticles is not possible.

The variation of Gibbs energy for nucleation and growth of nanoparticles consists of two terms: the bulk free energy that releases energy to the system, and the surface free-energy that inputs energy to the system, for spherical nucleus (small unstable region of the product phase) of radius *r*, the change in free energy ΔG is defined as in equation 1.3.

$$\Delta G = -\frac{4}{3}\pi r^3 \Delta G_v + 4\pi r^2 \gamma \tag{1.3}$$

where ΔG is the Gibbs energy variation, ΔG_v is the bulk free energy variation and γ is the surface energy of the nanoparticles [65].

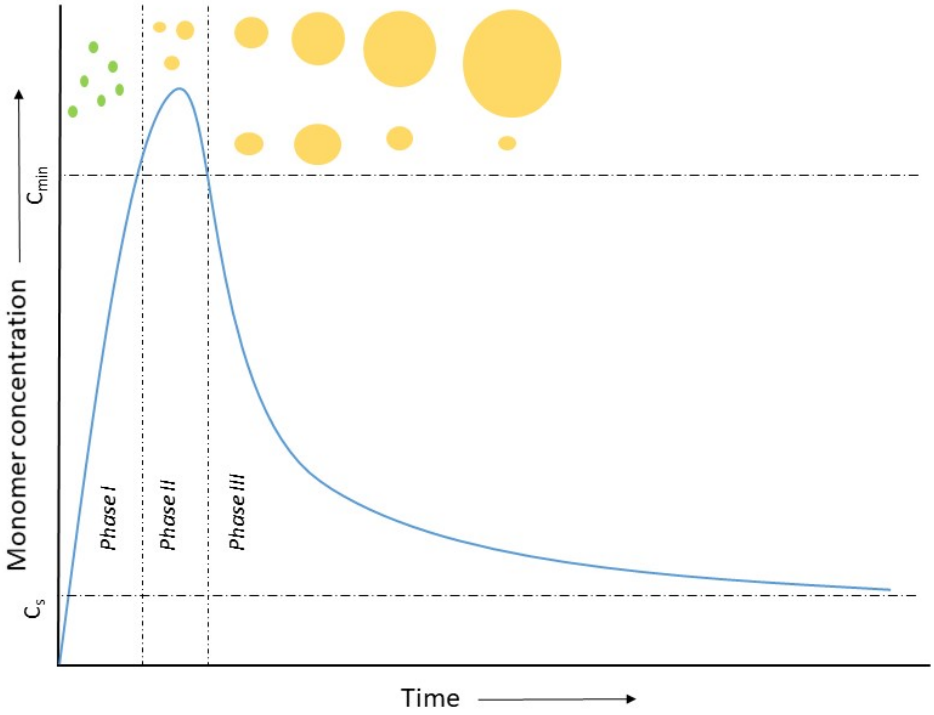

Figure 1.7: LaMer mechanism for nanoparticles growth

The nucleus can only become stable if the change in the free energy is negative, however, as the second term is always positive and dominates over the negative first term for small values of r, therefore nuclei of those sizes are thermodynamically unstable and nucleation cannot occur. If the nucleus has a critical radius (r_c), ΔG decreases and the nucleus growth is thermodynamically favourable.

Figure 1.8 shows the plot of equation 1.3 and in particular shows ΔG as function of the radius, with $\gamma = 10^{-2}$ J $\cdot\, m^{-2}$ and ΔG_v as indicated in equation 1.4, where Δ_s is the entropy difference between the initial and the final phase. Δ_s value for VO_2 is $6.57 \cdot 10^5$ J $\cdot$ K^{-1} $\cdot$ m^{-3} [65].

$$\Delta G_v = \Delta_s |T - T_c| \tag{1.4}$$

For any temperature different to the critical one, the critical nucleous size (r_c) and the critical ΔG_{crit} can be obtained from the maximum of the free energy. Mathematically, it means partial derivation of ΔG as function of the $r = r_c$ equation 1.5 [65].

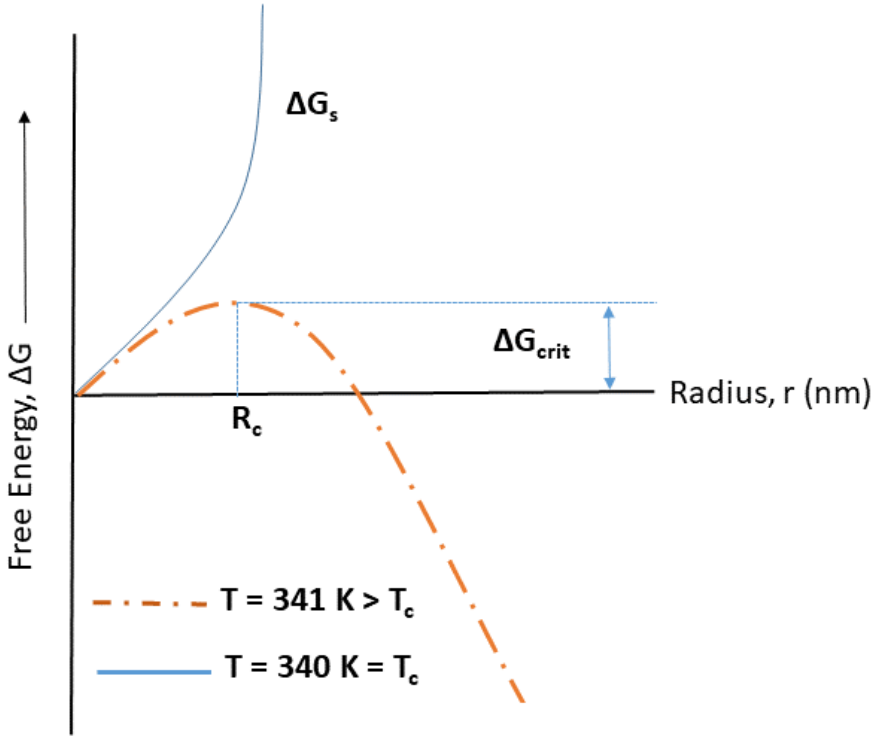

Figure 1.8: Variation of nucleation barrier ΔG as a function of the particle size, at two different temperatures

$$\frac{\partial \triangle G}{\partial r} \mid_{r=r_c} \Rightarrow r_c = \frac{2\gamma}{\triangle G_v} = \frac{2\gamma}{\triangle s \mid T - T_c \mid} \tag{1.5}$$

therefore, ΔG_{crit}

$$\triangle G_{crit} = \frac{16\pi}{3} \frac{\gamma^3}{\triangle G_v^2} = \frac{16\pi}{3} \frac{\gamma^3}{(\triangle_s \mid T - T_c \mid)^2} \tag{1.6}$$

If the temperature is the same as the critical temperature, $\Delta G \longrightarrow \infty$; therefore no nucleation can occur. This means that the phase transformation can not occur at the equilibrium temperature unless extra forces (ΔG_{crit}) are present to promote the transition.

A certain magnitude of ΔG_{crit} is necessary to promote the transition, as can be confirmed schematically in Figure 1.8. It can be concluded that for VO_2 nanoparticles homogeneous nucleation is not possible due to an energy barrier. The energy barrier for this type of nucleation is

$\Delta G_{crit} \approx 250$ eV and the energy involved in this transition at the critical temperature of 340 K is $k_b T_c = (8.61 \cdot 10^{-5}\ \text{eV} \cdot \text{K}^{-1})(340\ \text{K}) \approx 0.03$ eV, thus the nucleation cannot start uniformly all over the material but needs to be initiated at special sites of high potency, indicating a heterogeneous nucleation.

1.8.2 Thin films growth *via* AACVD

CVD is a method used to produce films on a heated surface by a chemical reaction in vapour phase [95] [96]. The precursor used can be in the liquid, solid or gas state. The physical state of the precursor can influence the characteristics of the final film [97].

AACVD, as the name suggests, is a liquid-phase variation of the CVD technique [96] [98]. Precursors (not necessarily volatile, but merely soluble in any solvent) are firstly dissolved in a solvent from which an aerosol is generated by use of an ultrasonic humidifier (nebulizer). This creates a precursor mist, which is transported to the CVD reactor by a carrier gas. Evaporation of the solvent takes place inside the reactor. The precursor reacts to form a film on the top of the substrate positioned inside the reactor [99].

The substrate is placed onto a heated carbon block that serves to maintain the substrate at a temperature suitable for the molecule to be deposited.

Figure 1.9 shows a schematic drawn of a typical AACVD system.

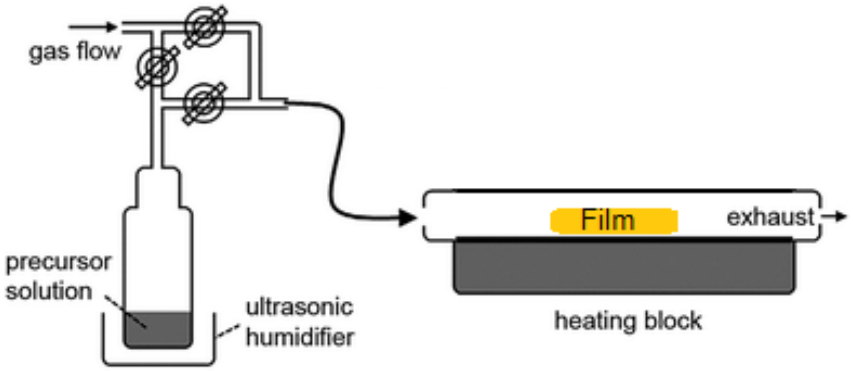

Figure 1.9: Aerosol Assisted Chemical Vapour deposition apparatus [1]

In this work, aerosol assisted chemical vapour deposition was used to prepare VO_2 films onto glass substrates.

1.8.3 Thin films growth *via* sol-gel / spin-coating

Sol-gel is a method used to produce materials from nano-sized particles [100]. A sol-gel process uses a mixture with properties of a solution and fine suspension that contains the precursor of the material that has to be prepared [101] [102]. The process is widely used in industry to fabricate metal oxides due to its simplicity to coat large areas [103] [69].

Figure 1.10 shows schematically the sol-gel process to form a film after calcination of the solution, an aerogel after gelation and extraction of the remaining solvent in the solution, a bulk material after heating the solution and uniform particles after precipitation of the solution.

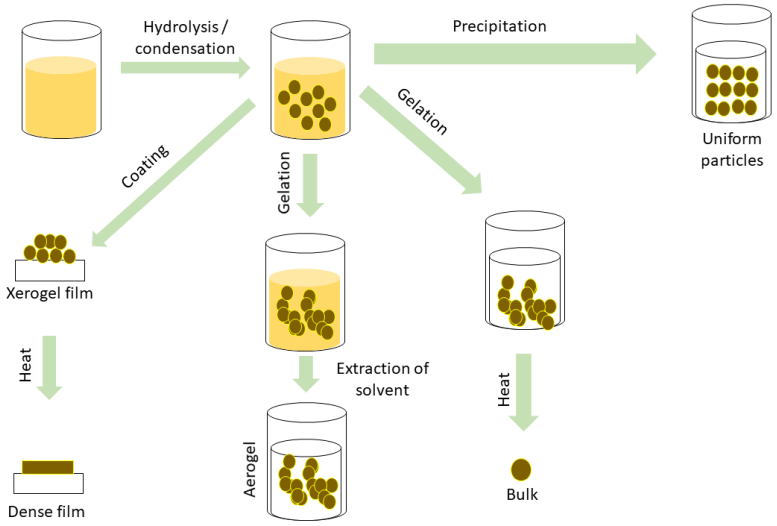

Figure 1.10: Sol-gel process scheme

Spin coating is a sol-gel method used during several decades for the deposition of thin films [104]. The process is very simple and consists of the deposition of a small amount of a fluid solution on the center of a substrate which is spun at high speed [105], as shown in the scheme in Figure 1.11 shows. The thickness of the film depends on several factors such as the spinning speed (typically around 2000 to 3000 rpm), the number of times that the process is repeated, viscosity, drying rate,

percent solids, surface tension, etc.

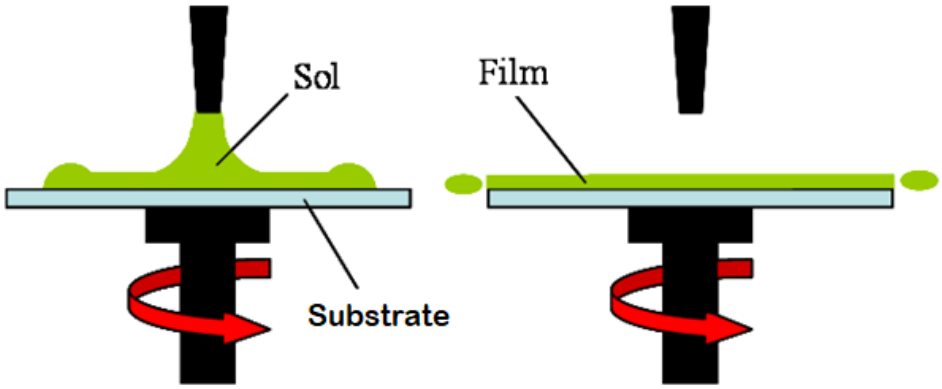

Figure 1.11: Spin coating deposition process scheme

Due to the simplistic nature of the method, sol-gel has been used extensively to prepare vanadium(IV) oxide thin films in both a pure and doped form. The most widely used precursor for the sol-gel preparation of vanadium(IV) oxide is vanadium tri(isopropoxide) -used in the present work-, followed by vanadyl tri(tert-amyloxide). The alkoxide is usually dissolved in the parent alcohol to form the solution. The use of different alcohols causes transesterification and formation of different alkoxides [14].

1.9 Thesis outline

This thesis is focused on the synthesis of VO_2 thin films, microparticles and nanoparticles to be used as thermochromic material mainly for architectural purposes. The first experimental chapter will introduce and discuss the synthesis of thermochromic VO_2 thin films *via* sol-gel/spin-coating and AACVD. The results will be compared to those reported in the literature.

Chapters 3 and 4 will introduce the newly reported D phase of VO_2. Hydrothermal synthesis of microparticles and nanoparticles of VO_2(D) will be discussed and analyzed, as well as applications (easy route to obtain thermochromic VO_2) and morphology of the as-prepared VO_2(D) particles.

In chapter 5 the structure of the VO_2(D) reported in the literature is reviewed and moreover, an approach to a new structure for VO_2(D) is suggested.

Finally, the results discussed in this thesis are summarized and potential future work are suggested.

Chapter 2

Thin films *via* sol-gel/spin coating and Aerosol-Assisted Chemical Vapour Deposition

2.1 Introduction

Vanadium dioxide can be synthesized using different methods to obtain either particles or films. There are several variables that play an important role in the preparation of vanadium dioxide films like: temperature, precursors, solvents and pressure among others factors [106].

The phase diagram of vanadium oxide as a function of the concentration of vanadium and pH of the solution, is shown in Figure 2.1. Another diagram is shown in Figure 2.2 where the different species of vanadium (Magneli phases and pure phases) that can be obtained by changing the temperature are shown [107].

The vanadium oxide phase diagrams show schematically some of the phases/species that can be obtained by just changing some features. It is evident that obtaining the desired phase of vanadium oxide needs controlled conditions over a very narrow window.

Vanadium dioxide films were prepared *via* sol-gel/spin-coating method and aerosol-assisted chemical vapour deposition (AACVD). VO_2 prepared using these two techniques were studied in order to un-

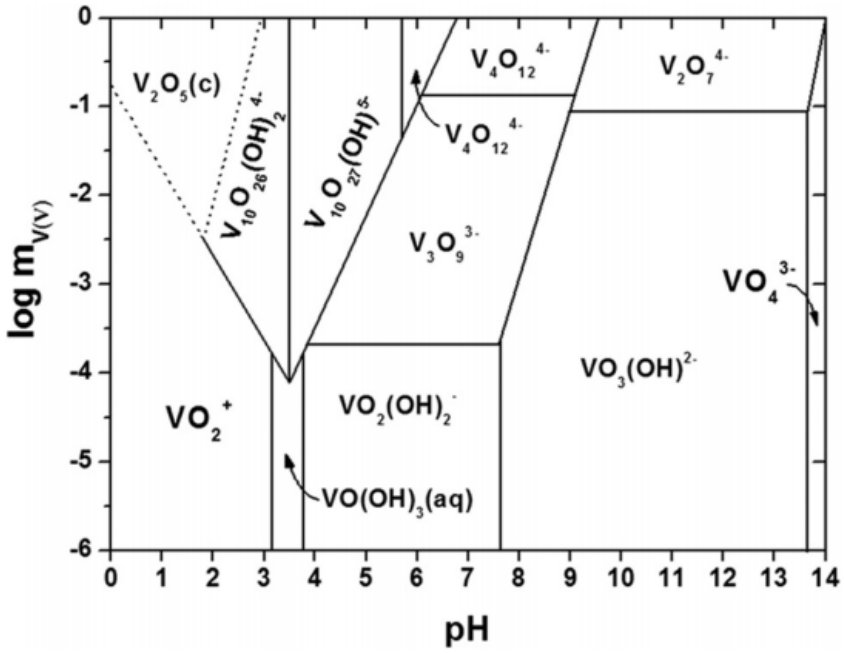

Figure 2.1: Phase diagram of vanadium oxide as function of the volume concentration of vanadium and pH of the solution. Diagram taken from [106] (with permission)

derstand the formation process of vanadium dioxide and its phases, under different conditions. This research was carried out to get familiarized with the VO_2 field, variables that need to be controlled during the process and moreover, the required characterization.

The literature reports that V_2O_5 was spin coated onto indium tin oxide glass by Shimizu et al in 1992 [108] using V_2O_5 powder dissolved into benzyl alcohol and isobutanol. The solution was spin coated to obtain vanadium pentoxide thin films with thermochromic properties. High quality vanadium dioxide films were prepared by Dachuan *et al.* in 1993 [109] with an electrical switching at about 60 °C using V_2O_5 as a precursor materials. The films were calcinated under a reduced atmosphere. In 1998 Beteille and Livage [110] prepared VO_2 thermochromic films with a switching temperature around 70 °C from vanadium alkoxides [$VO(OR)_3$] (where R is the organic substituent). In 2009, Kang *et al.* reported a novel solution process to produce VO_2 thermochromic films [111] *via* spin-coating using vanadium pentoxide and diamide hy-

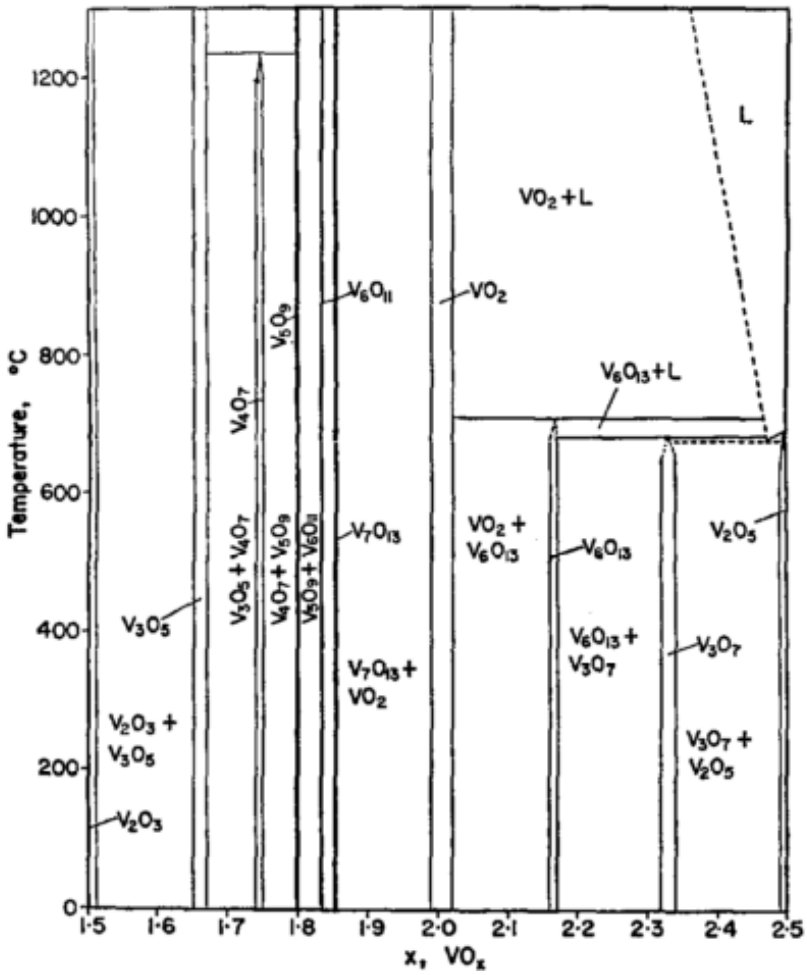

Figure 2.2: Vanadium phase diagram in terms of temperature variation. Diagram taken from [107] (with permission)

drochloride as starting materials. The prepared films had a transmittance of 54.5 % in the visible range and 41.5 % reduction in the near IR.

Thermochromic films were prepared by Parkin *et al.* [112] *via* aerosol assisted chemical vapour deposition using $[VO(acac)_2]$ as a precursor (no need to be volatile) dissolved into a solvent. The precursor does not need to be volatile because AACVD depends in the solubility of the precursor rather than its volatility, in the process a nebulizer is used to form aerosol droplets of precursor solution, rather than evaporation of volatile precursors as in CVD. Tungsten doped VO_2 samples were also prepared by AACVD and exhibited a transition temperature

from rutile to monoclinic at 22 °C by adding only 1 wt% of dopant [113].

In this chapter a detailed methodology will be presented for the preparation of vanadium dioxide films using spin-coating and AACVD technique, as well as characterization of the prepared samples. The experiments performed in this work show similar results to those reported in the literature.

2.2 Aim

The aim of this chapter was to prepare thermochromic thin films *via* sol-gel/spin-coating method and understand the variables that play important roles in the production of thermochromic VO_2 films.

2.3 Experimental

2.3.1 Thin films *via* spin coating

vanadium(IV) oxide by spin-coating two steps were necessary: hydrolysis of the precursor material to form a vanadium(V) oxide amorphous gel, then secondly heating in a reducing atmosphere to obtain a crystalline vanadium(IV) oxide [14].

In a typical synthesis 0.58 g (0.0023 mol) of vanadium oxytriisopropoxide and 0.1 g (0.0016 mol) of acetic acid were dissolved in 15.7 g (0.2612 mol) of isopropyl alcohol. The solution was stirred for 15 minutes at room temperature and aged for 4 days.

All reagents were purchased from Sigma-Aldrich and were used without further purification.

The films were deposited on a 3 X 3 cm square wafer of glass substrate with a barrier layer of silicon dioxide (supplied by Pilkington/NSG). The substrates were cleaned by ultrasonic treatment in acetone and then in deionised water. For each solvent, the ultrasonic treatment lasted for 20 minutes. Finally, the substrates were dried at room temperature.

For the deposition process a Laurell model WS-650-8B spin coater instrument was used. The spin rate was 1500 rpm, acceleration 2,200 rpm/s, for 30 seconds. In a typical procedure 4 drops of the precursor solution were deposited on the glass using a pipette, and then a yellow film of V_2O_5 was formed on the glass surface. After each layer the film was dried in order to evaporate the extra solvent on the sample. The process was repeated 10-20 times to increase the thickness of the resulting film.

The films were dried at room temperature for 1.5 days. Thickness was measured using a Veeco Dektak 8 profilometer.

Samples were annealed under flowing nitrogen atmosphere [2 L min^{-1}] at 550 °C for 4 hours, at a ramp 10 °C/min, in order to obtain monoclinic phase of the vanadium(IV) oxide (VO_2(M)).

From now on the term as-prepared will be used to refer to the samples prepared using the recipe mentioned in the experimental section of each chapter.

2.3.2 Thin films *via* AACVD

To obtain vanadium(IV) oxide *via* AACVD, a green solution made of 0.3 g of vanadyl acetylacetonate ($VO(acac)_2$) was mixed with 40 mL of ethanol and stirred for 20 min.

For the film deposition, a rectangular glass substrate having a SiO_2 barrier layer was placed on top of a carbon block heated at 550 °C inside the CVD reactor (Figure 1.9). Nitrogen was used as carrier gas for delivering the material into the reactor at 1.5 flow rate [L min^{-1}].

2.4 Results and discussion

The preparation of VO_2 thin films *via* spin-coating and AACVD in this work involved optimization and several experiments carried out in the laboratory. In appendix A are listed most of the experiments performed in this chapter, however, only important results, compared to the ones found in the literature will be shown.

2.4.1 Results for thin films obtained *via* spin-coating

A precursor solution made of vanadium oxytriisopropoxide, isopropyl alcohol and acetic acid was spin-coated onto a glass substrate (repeating the process many times - 10 times - to increase the thickness of the film). The film after the spin-coating deposition is amorphous and had a yellow colour which turned into brown colour after annealing the sample under a controlled nitrogen atmosphere at temperatures above 550 °C for 4 hours or more. After calcination the film becomes crystalline and turned to thermochromic VO_2, as will be shown below.

Figure 2.3A shows the film obtained after the spin-coating process. The film is yellow and transparent and evenly deposited on the glass substrate. The obtained film was aged for 4 days at room temperature. Experiments aging the sample from 0 to 7 days were performed concluding that, aging the sample for 4 days at room temperature result in the best films. Best film means that the monoclinic phase was obtained after the calcination process. The aging time of the precursor solution (or the thin film before annealing) played an important role in the formation of the desire phase and even different morphologies [114].

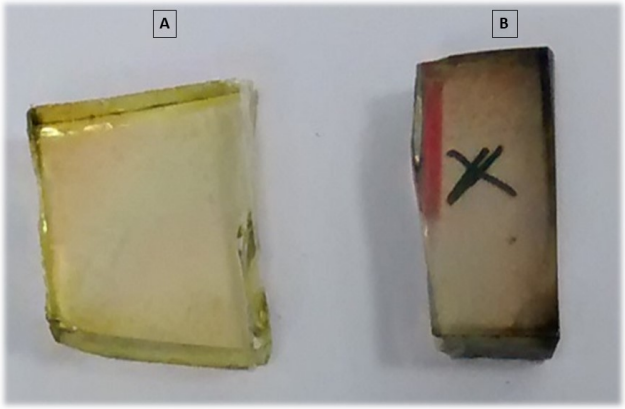

Figure 2.3: (A) Amorphous VO_2 sample prepared by spin-coating before annealing and (B) VO_2 sample prepared by spin coating after annealing at 550 °C for 4 hours

Figure 2.3B presents the film obtained after calcination at 550 °C under nitrogen atmosphere for 4 hours. The film is still transparent,

however, the colour is a darker yellow-brown.

Raman spectroscopy was performed on the samples in order to check if the desired monoclinic phase, with thermochromic properties was obtained. In Figure 2.4 bands at 143, 192, 223, 261, 310, 390, 500, 595 and 612 ($\pm$ 2) cm^{-1} were observed in sample DP57 prepared using vanadium oxytriisopropoxide, isopropyl alcohol and acetic acid. These bands match with vanadium(IV) oxide monoclinic bands reported in the literature by Manning [14], suggesting that, indeed, the VO_2 thin film obtained after calcination is monoclinic.

Typical Raman spectra of VO_2, V_2O_5, VO_x and V_6O_{13} are shown in Figure 2.5.

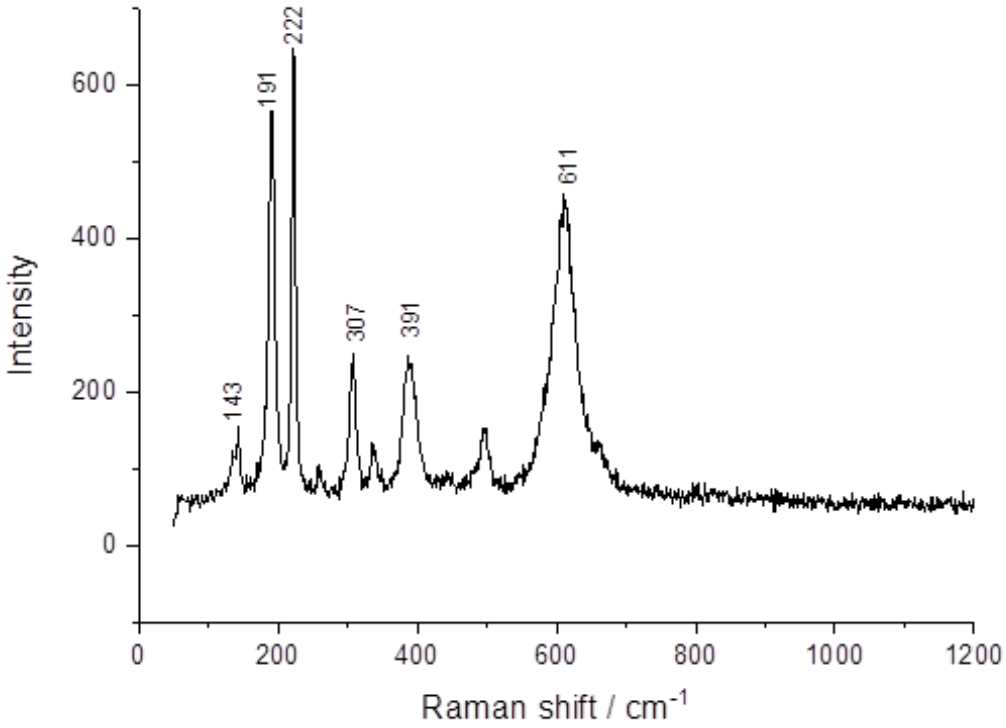

Figure 2.4: Raman spectrum of sample DP57 (vanadium oxytriisopropoxide, isopropyl alcohol and acetic acid) after annealing at 550 °C for 4 hours showing VO_2(M) peaks

Different phases of the vanadium(IV) oxide were encountered during the research (determined by XRD and Raman), mainly thin films showing VO_2(B) phase and mixed vanadium Magneli phases. How-

ever they are not shown here as this work (but summarized later in this chapter) is focused on the production of monoclinic phase with thermochromic properties to be used for architectural purposes.

It is worth mentioning that obtaining the monoclinic phase is challenging, and if the conditions are not suitable, other phases are obtained as was shown before in the vanadium phase diagram; for example, calcinating the films between 400 and 500 °C for 10 hours under nitrogen atmosphere, result in V_2O_5, whereas annealing under nitrogen for more than 12 hours, results in V_2O_3, also, annealing under nitrogen for less than 4 hours results in V_2O_5 or mixed phases, including Magneli phases whilst, temperatures below 400 °C result in a non-crystalline structure, therefore, the annealing temperature and the calcination under an inert atmosphere (nitrogen) are crucial to the process to obtain the desired phase.

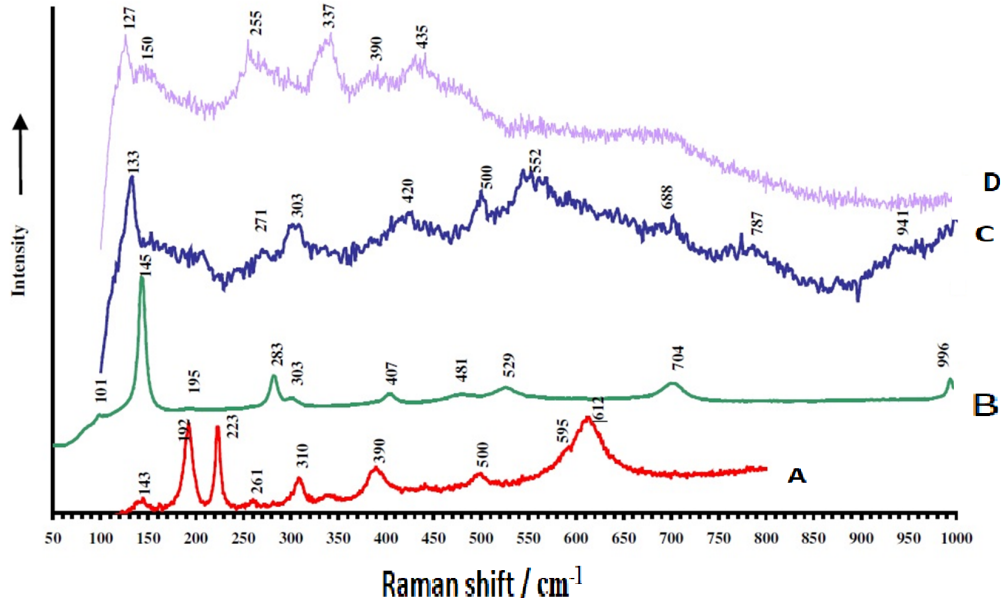

Figure 2.5: Reference Raman spectrum of different phases of Vanadium at λ = 785 nm, taken from [14] used with permission of the author. (A) VO_2(M) (B) V_2O_5 (C) VO_x (D) V_6O_{13}

X-Ray diffraction was performed on the samples to confirm that VO_2 monoclinic phase was obtained *via* spin-coating/sol-gel method. Figure 2.6 shows the obtained XRD pattern of one of the as prepared

thin film. The pattern shows peaks at 2θ 27, 37 and 55 °, these obtained peaks match the vanadium(IV) oxide monoclinic peaks reported in the literature [115] [116] [117] and no other phases of vanadium oxides were detected.

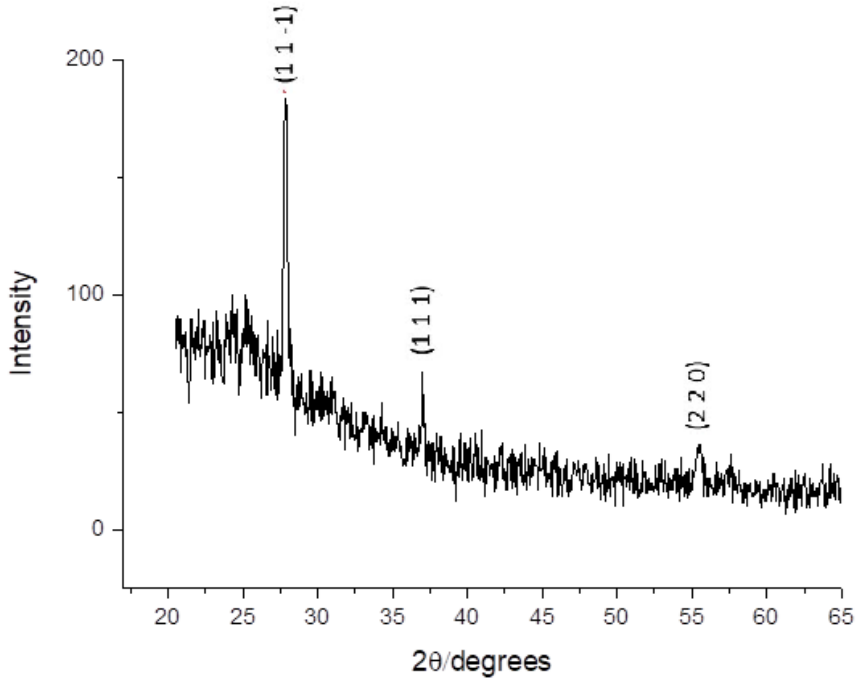

Figure 2.6: XRD pattern of sample DP57 (vanadium oxytriisopropoxide, isopropyl alcohol and acetic acid) showing typical VO_2(M) peaks

The main characteristic diffraction peaks of the vanadium(IV) oxide monoclinic phase are at 2θ 27.88, 37.06, 42.18 and 55.01°and the simulated XRD spectrum is shown in Figure 2.7 for comparison.

For architectural applications, it is important that the samples present thermochromic behavior. When a material presents thermochromic behaviour, optical changes can be observed under temperature variation, in particular for bulk vanadium oxide, the transition phase occurs at 68 °C. To study the thermochromic properties of the as prepared samples, transmittance and reflectance spectra of each sample were measured at room temperature and at 100 °C.

As previously mentioned the final purpose of using VO_2 thin films

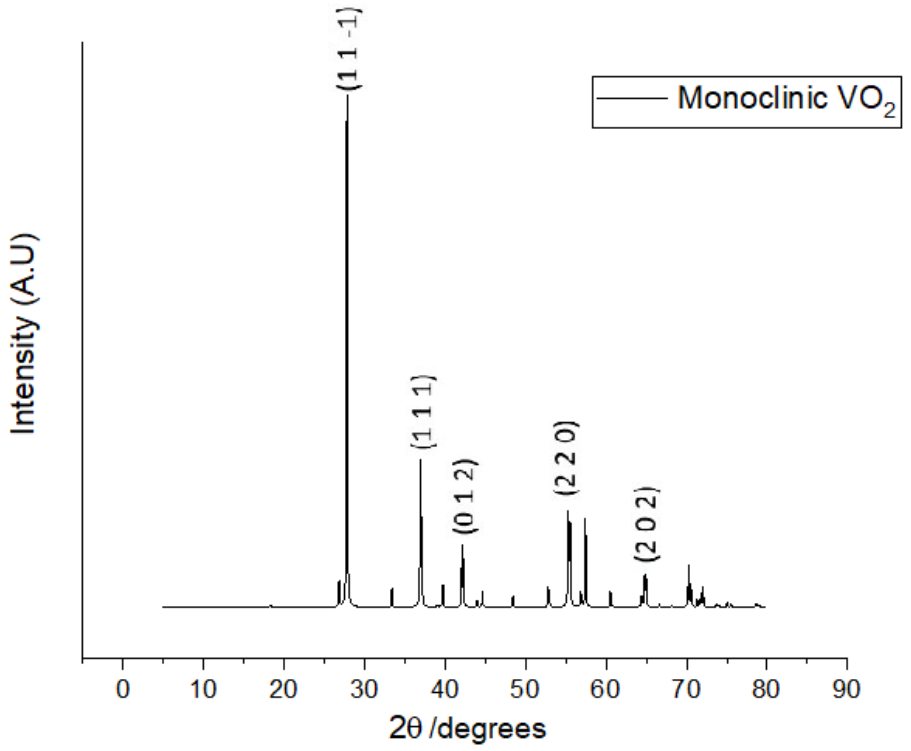

Figure 2.7: Simulated XRD pattern of the VO_2(M) (ICSD 34033)

is to coat the windows of building, producing "smart windows" in order to save energy, this is because recent reports state that energy consumption in buildings represent up to 20-40 % of the total energy consumption in developed countries [118], a considerable high value for energy consumption that wanted to be reduced.

Ideally films prepared to act as smart windows should have maximum transmittance when the environment is below room temperature, and maximum reflectance when the temperature is above room temperature.

In Figure 2.8 the transmittance of the as-prepared thin film *via* spin-coating at room temperature and at 100 °C is shown. As observed, the transmittance decreases when the temperature is above 68 °C ($\approx$ 100 °C in this study), indicating that the material changes its properties to be more reflective, as expected when a phase transition from monoclinic to tetragonal phase at 68 °C occurs.

To measure the transmittance at high temperatures, the sample was heated up to 100 °C to assure a thermodynamical stable temperature in the sample in order to complete phase transformation (that occurs at 68 °C) from VO_2(M) to VO_2(R).

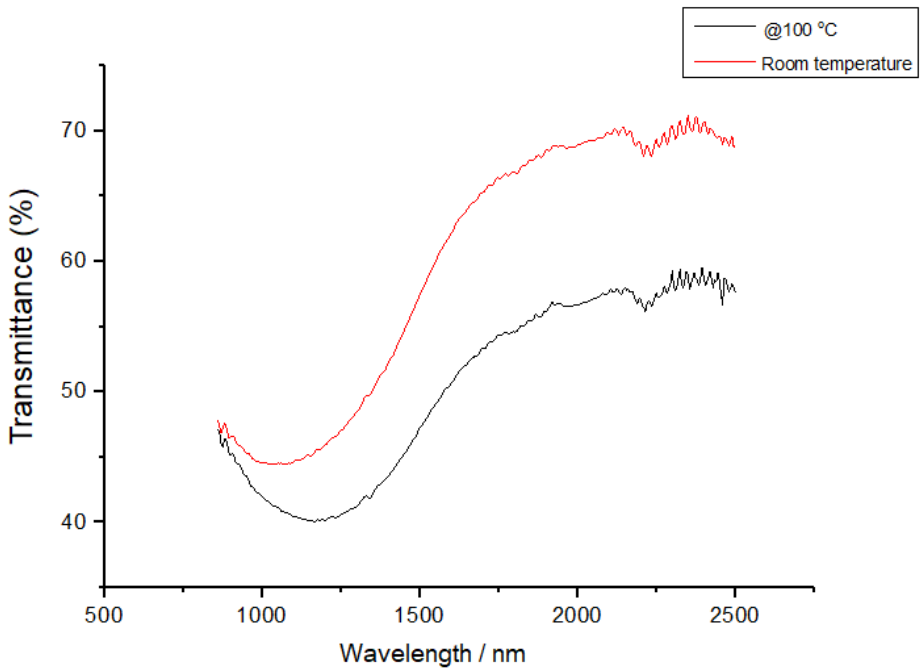

Figure 2.8: Transmittance of sample DP101 (vanadium oxytriisopropoxide, isopropyl alcohol and acetic acid) made by spin-coating

From Figure 2.8 it is evident that the film presents thermochromic behavior because there is a difference in the transmittance at room temperature and at 100 °C, however, it is necessary to calculate the solar modulation of the sample weighting the solar values to the data [17] [119], because the terrestrial atmosphere absorbs in more or less intensity at certain wavelengths. This calculation was done using Equation 1.2.

Table 2.1 shows the T_{lum} values for the films at room temperature ($\approx$ 25 °C) and at 100 °C, the ΔT_{lum} and the ΔT_{sol} values for sample DP101, prepared by spin coating.

Table 2.1: Weighted visible transmission at 25 °C and at 100 °C for thermochromic VO_2 film prepared *via* spin-coating

	T_{lum} 25 °C (%)	T_{lum} 100 °C (%)	ΔT_{lum}	ΔT_{sol}
Sample DP101	48.3	47.6	0.73	-1.83
Kang *et al.*[68]	59.2-11.5	61.1-12.6	N/A	N/A
Zhang *et al.*[115]	83.5-11.7	82.8-7.6	N/A	N/A

The results obtained T_{lum} of 48.3 % at room temperature and T_{lum} of 47.6 % at 100 °C are consistent with the results reported in the literature by Kang *et al.* [68], having T_{lum} values at room temperature between 59.2 % to 11.5 % (depending on the sample thickness) and T_{lum} values at 90 °C between 61.1 % to 12.6 % for thin films and also are in concordance with the results reported by Zhang *et al.* [115] presenting T_{lum} between 83.5 % to 11.7 % (depending on the thickness) at room temperature and T_{lum} between 82.8 % to 7.60 % at 90 °C for thin films prepared *via* spin coating.

In the same way, reflectance analysis were performed on the films to corroborate the previous results.

Figure 2.9 shows the reflectance obtained from the as-prepared film at room temperature and at 100 °C. As expected the reflectance increases at 100 °C, compared to the reflectance at room temperature, this is because the material (VO_2) properties change at temperatures above 68 °C to become reflective (transition from monoclinic phase to tetragonal phase). The observed variation between the room temperature and high temperatures is $\approx$ 4-6 %. Ideally, the reflectance gap between hot and cold temperatures should be as big as possible, taking into account the energy loss and light absorbed by the material.

For architectural applications focused on energy saving solutions, having a high % of reflectance at temperatures above the critical temperature is important, as the IR rays are mainly reflected away, helping to keep the temperature inside the building constant.

Transmittance Figures 2.10 and 2.11 are shown below in order to compare the transmittance profiles obtained in this work and those re-

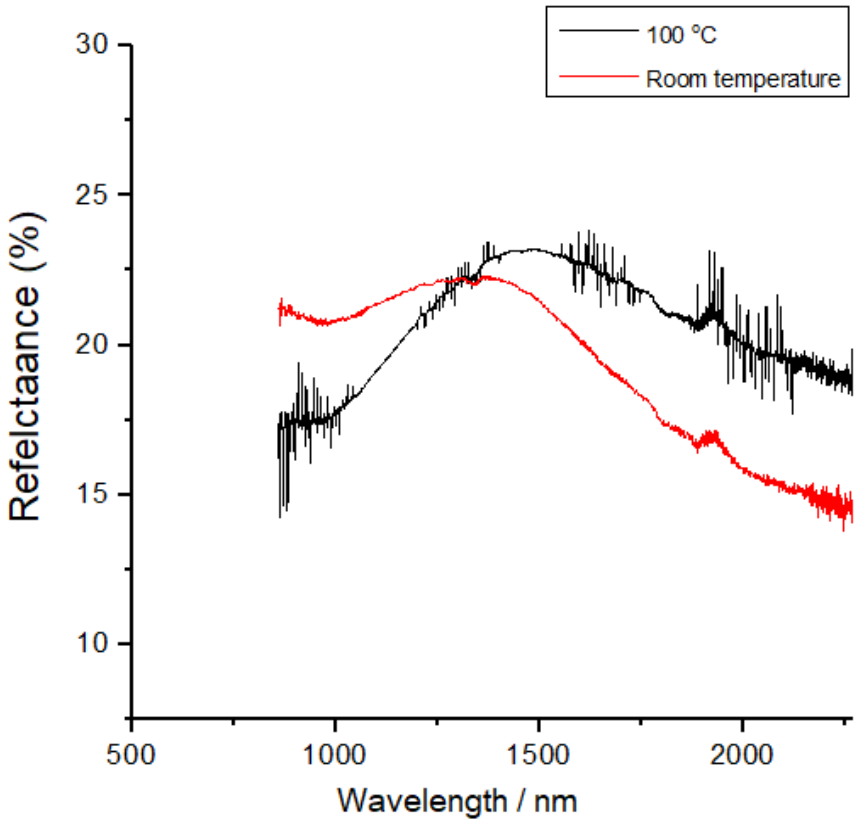

Figure 2.9: Reflectance of a sample DP101 (vanadium oxytriisopropoxide, isopropyl alcohol and acetic acid) prepared by spin-coating (5 layers)

ported in the literature by Zhang *et al.* [115] and by Kang *et al.* [68].

Transmittance and reflectance values (%) change from sample to sample. The variation depends on many factors including thickness of the film, roughness, material composition of the film, imperfections of the glass and annealing conditions.

The obtained results for the VO_2(M) samples reported in this thesis shows that thermochromic films with good properties to be used for smart windows can prepared successfully *via* spin-coating. The properties can be improved by changing the thickness of the samples.

The most important and starting point of the research in the VO_2 field for architectural applications is to have a film that presents thermochromic behavior, once the film is obtained, the properties (such a

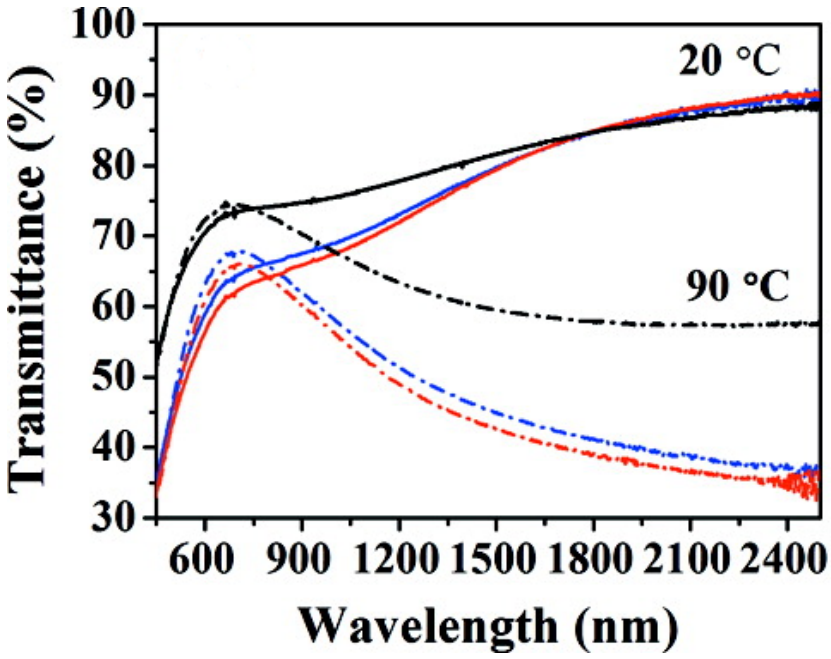

Figure 2.10: Reference of transmittance profiles for VO_2 samples prepared by spin-coating. Blue line: films that were treated at 600 °C for 20 min, red line: 530 °C for 30 min, and black line: 440 °C for 4 h. The solid and dashed lines are for the films at 20 and 90 °C, respectively. Figure taken from [115] with permission of the author.

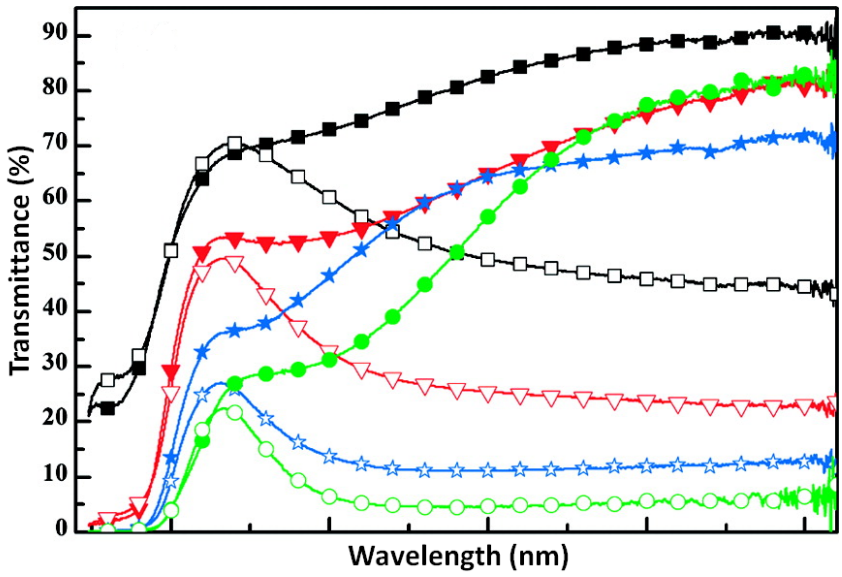

Figure 2.11: Reference of transmittance profiles for VO_2 thin film samples with different thicknesses 43 nm (black squares), 102 nm (red triangles) 215 nm (blue pentagrams) and 428 nm (green circles). Figure taken from [68] with permission of the author.

transparency and transition temperature) needs to be improved.

The results shown before are an example of a successful VO_2 thin film prepared *via* spin-coating with thermochromic properties, however, several experiments were performed in order to obtain the right conditions for a thermochromic film.

Some of the parameters that were changed include:

- Change of the solution concentration.
- Change the annealing atmosphere.
- Change the annealing temperature.
- Change the annealing time.
- Change the precursor.
- Number of layers
- Aging the solution.

In Table 2.2 are listed some samples prepared *via* spin-coating deposition technique annealed for 4 hours under nitrogen atmosphere, where the parameters mentioned above were changed and the final product is different for each case. To determine the final product outcome, in all cases X-Ray diffraction was performed on the thin film.

Table 2.2: List of samples prepared *via* spin-coating deposition technique changing different parameters in order to obtain different results. Samples were annealed for 4 hours under nitrogen atmosphere. In the table precursors A: vanadium(V) oxytriisopropoxide, B: vanadyl acetilacetonate

	DP13	***DP18***	***DP25***	***DP40***	***DP57***	***DP60***	***DP125***
Precursor	A	A	A	A	A	B	A
Precursor Concentration	0.16	0.16	0.16	0.16	0.12	0.12	0.12
Annealing atmosphere	Air	N_2	N_2	N_2	N_2	N_2	N_2
Annealing temperature (°C)	500	500	500	550	550	550	570
Aging time (days)	N/A	N/A	2	N/A	N/A	4	N/A
Result	Amorph	Amorph	Amorph	V_4O_9	VO_2(M)	Mixed	Unknown

Table 2.3 shows the chemical composition of samples DP13, DP18, DP25, DP40, DP57, DP60 and DP125 mentioned in Table 2.2.

Table 2.3: Chemical composition of samples DP13, DP18, DP25, DP40, DP57, DP60 and DP125 (variable % composition)

DP13 ***DP18*** ***DP25*** ***DP40*** ***DP57*** ***DP125***	vanadium oxytriisopropoxide isopropyl alcohol acetic acid
DP60	vanadyl acetilacetonate methanol polyethylene glycol

Figure 2.12 shows the diffraction pattern of the samples DP13, DP18, DP25, DP40, DP57, DP60 and DP125 discussed in Table 2.2.

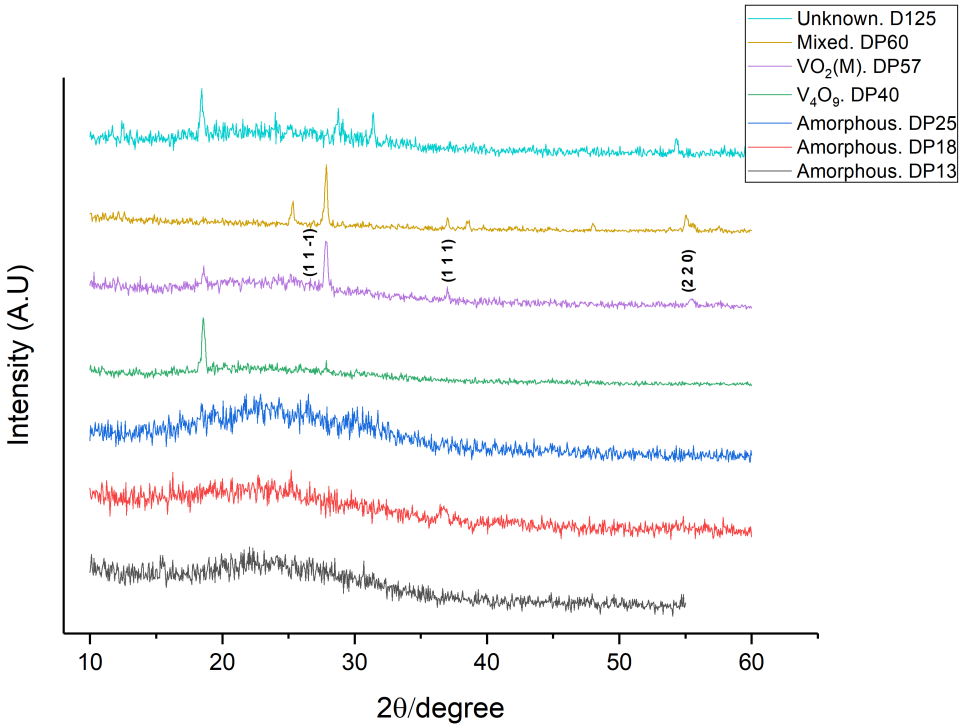

Figure 2.12: X-Ray diffraction pattern of the samples DP13, DP18, DP25, DP40, DP57, DP60 and DP125

As can be seen in Figure 2.12, and mentioned before, slight changes in the parameters can lead to very different result. A crucial parameter in the production of VO_2 thin films *via* spin-coating deposition technique is the annealing and atmosphere temperature. Once the film is deposited in the substrate, the thin film is amorphous and requires it to be annealed in order to crystallize the material. Calcination needs to be carried out in a controlled atmosphere, for example nitrogen atmosphere as performed in this work and also reported in the literature [51] [70]. Vacuum is also often used in VO_2 field to anneal samples [120] [121].

2.4.2 Thin films *via* AACVD

Thin films were prepared *via* AACVD method onto a glass substrate. Several samples were prepared and pure VO_2(M), VO_2(B) and amorphous samples were obtained. In appendix A are listed some of the prepared samples and condition used.

Figure 2.13: Black and non-uniform VO_2 film obtained by AACVD method (10X4cm)

In all cases the resulting film present dark colour, as is shown in Figure 2.13, and the adhesion of the deposited film onto the substrate was not good. The film looked more like fine powder not well attached to the surface. The dark colour of the film is due to carbon species, possibly side products coming from the organic part of the solvent and precursor used.

Figure 2.13 shows a dark film prepared *via* AACVD at 550 °C and a 1.5 N_2 flow rate (L min^{-1}) as mentioned in the experimental section 2.3.2.

Raman spectroscopy were performed on the as-prepared samples in order to determine the phase of material. Figure 2.14 shows the Raman spectrum for the VO_2 sample prepared. The obtained Raman bands for the analyzed film correspond to the thermochormic VO_2 Raman bands reported in the literature [122], suggesting that, even if the film was not deposited uniformly and presents a dark colour, it still shows the correct phase.

X-Ray diffraction was also performed on the sample to corroborate that monoclinic VO_2 was achieved. Figure 2.15 shows the obtained pattern and the peaks match to the main peaks of monoclinic VO_2 from the literature [123].

No further analysis were performed to the sample as they were

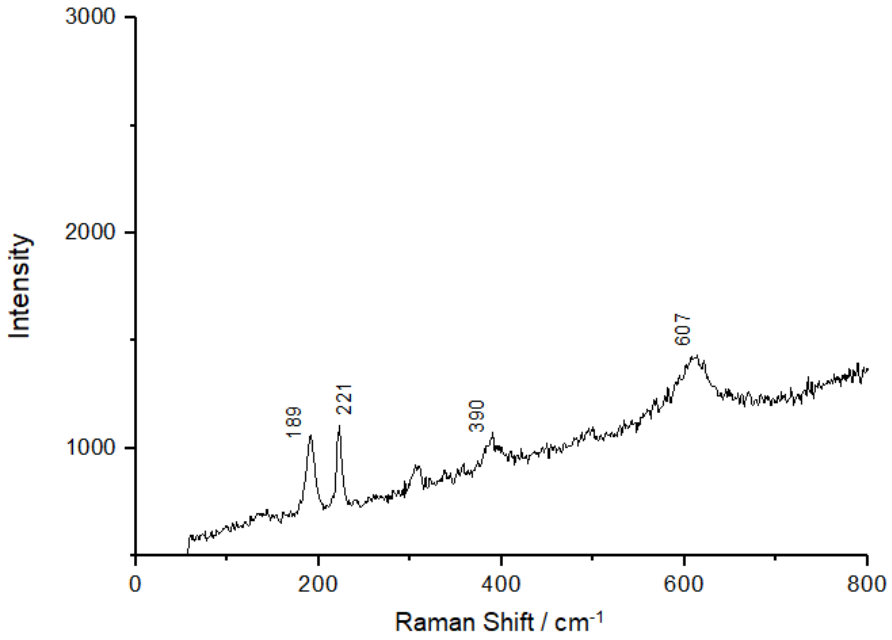

Figure 2.14: Raman spectrum of sample DP138 after calcination prepared *via* aerosol-assisted chemical vapour deposition showing typical VO_2(M) bands

mainly synthesized in order to gain experience on the preparation of VO_2 films using different methods.

The results obtained in this work are in concordance with the results presented in the literature. Piccirillo *et al.* [124] synthesized successfully thermochromic VO_2, V_2O_3 and V_2O_5 onto glass. In other studies Piccirillo *et al.* [113] synthesized tungsten doped thermochromic VO_2 films with a lower transition temperature from monoclinic to rutile phase, Moreover, same authors prepared niobium doped VO_2 films [125] *via* preparing doped thermochromic films with low transition temperature compared to bulk VO_2(68 °C).

Other works reported in the literature induced electric field in the AACVD reaction to prepare different metal oxides (vanadium oxide among them) for gas sensing applications [122] [126].

According to the literature, VO_2 thermochromic films prepared *via* AACVD are suitable to be used for smart windows applications and even for gas sensing applications, however, the thermochromic films

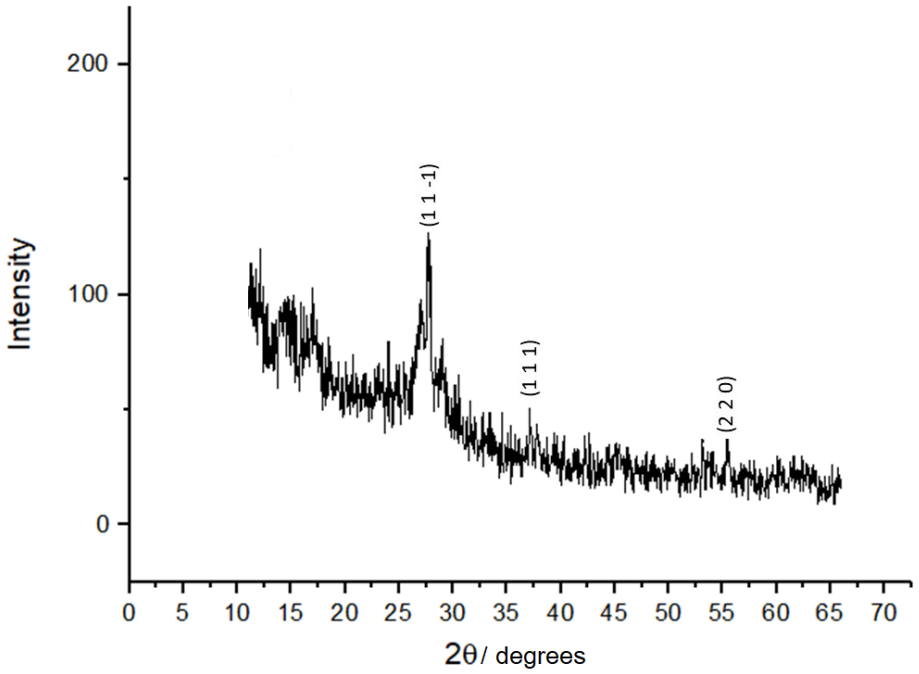

Figure 2.15: XRD pattern of sample DP138 showing typical VO_2(M) peaks

prepared *via* AACVD in this work are not suitable to be used for architectural applications (even if the right phase and properties were obtained) as the film is too dark (due to carbon species, possibly side products coming from the organic part of the solvent and precursor used) and the adhesion needs to be improved. One of the possible reasons to explain why the prepared films in this work are not suitable for architectural applications is the cleaning/preparation of the substrate, therefore the adhesion of the film is not good.

The results shown before represent only a successful VO_2(M) film prepared using aerosol-assisted chemical vapour deposition, however, other results (other VO_2 phases) were obtained by changing certain parameters like:

- Carbon block temperature.
- Nitrogen gas flow.

In Table 2.4 are shown a summarized set of thin film results obtained *via* aerosol-assisted chemica vapour deposition changing carbon

block temperature and nitrogen gas flow.

Table 2.4: Summarized results table of thin film samples prepared *via* AACVD for different temperatures and nitrogen gas flow

	Temperature (°C)	**Nitrogen flow (L min^{-1})**	**Result**
Sample 82	560	1	VO_x
Sample 92	550	1	Amorphous
Sample 104	555	1	Mixed phases
Sample 115	550	1.5	VO_2(M)
Sample 140	545	1	VO_2(B)

Figure 2.16A presents the XRD diffraction pattern of three samples prepared *via* AACVD using different deposition conditions while in Figure 2.16B the Raman spectra of the same three samples are shown. As reported before, the XRD pattern of the VO_2 thin films prepared using AACVD and in general VO_2 thin films do not have very well defined peaks as evidenced in the presented patterns, on the other hand, Raman spectroscopy shows better defined peaks, thus helping on the material characterization.

The XRD patterns and Raman spectra presented below correspond to some of the samples reported in Table 2.4 where sample 115 present typical XRD peaks and Raman bands of VO_2(M), sample 104 presents XRD peaks and Raman bands that can be associated to VO_2 mixed phases and sample 82 presents a well defined XRD peak and a few Raman bands that can not be associated to any known VO_2 phase to our knowledge, even though it contains only VO_2.

During the performance of the experiments, in several cases the system line was blocked due to condensation of the precursor, avoiding the successful deposition of the material onto the substrate.

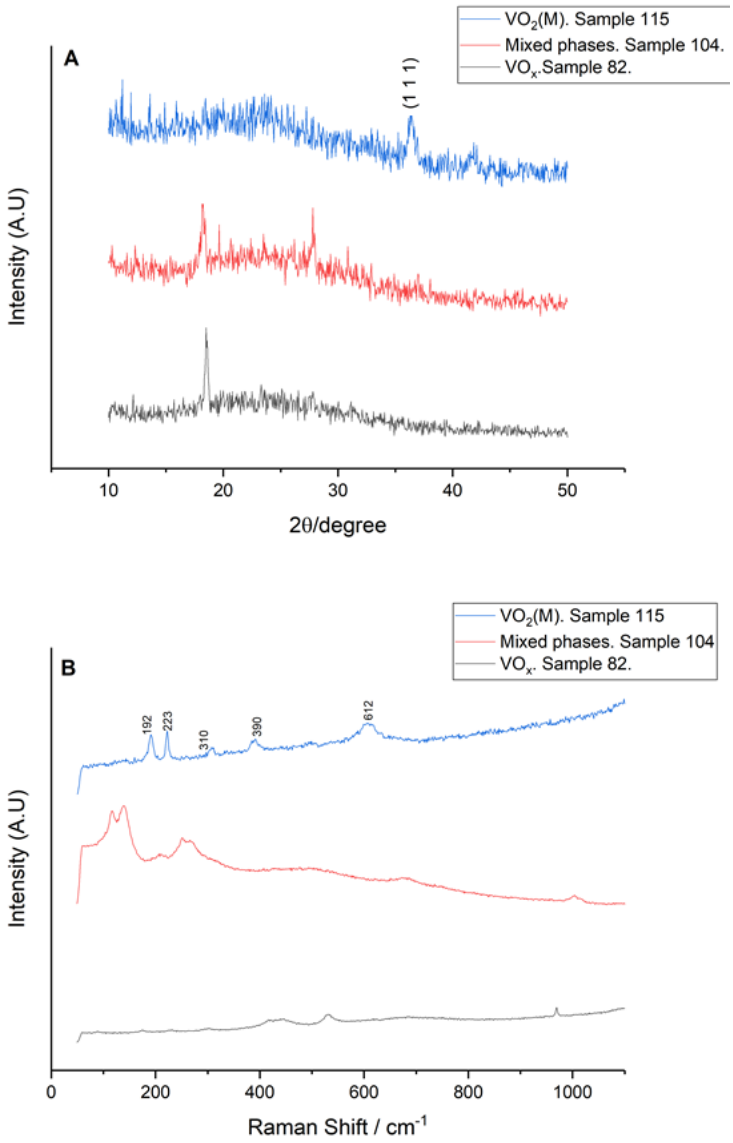

Figure 2.16: (A) XRD of three samples prepared *via* AACVD (B) Raman spectra of three samples prepared *via* AACVD

2.5 Conclusions

Yellow and transparent films were obtained after deposition using the spin-coating method and subsequent annealing in a controlled atmosphere at 550 °C for 4 hours. Films obtained were monoclinic vanadium(IV) oxide which present thermochromic behavior under changes of temperature. Thickness of the films were around 120 nm after depositing 10 layers using the mentioned conditions above.

The spin-coating method was successfully used to produce films of monoclinic vanadium (IV) oxide that present thermochromic properties under variable temperature, and the research done so far on this work was useful to understand the important variables that play a role into the process of obtaining the monoclinic phase of the used material, vanadium oxide. Variables such as temperature and aged solution were found to be fundamental in the process; they give to the system the energy needed to raise a stable level and also help the system to start the polymerization process of the initial solution, respectively.

Dark and non-uniform films were obtained *via* aerosol assisted chemical vapour deposition deposited onto glass substrate. The adhesion between the film and the substrate was poor, moreover, the resultant deposition was like a fine powder instead of a film.

The experiments performed *via* AACVD were very helpful in order to understand the formation process of films and the variables that play an important role in the deposition, as temperature, substrate, gas flow, among others.

As mentioned before, thermochromic VO_2 has been intended to be used for architectural applications in order to reduce the energy use in buildings, the problem with the use of VO_2 thin films for architectural problems can be divided into three as detailed by Li *et al.* [67]: The first one is that the switching temperature at 68 °C is too high, and needs to be lowered close to room temperature, this can be done doping the material with tungsten ions [127] [128] [129], the second problem is that the thermochromic VO_2 films with important thermochromism have to be very thick films, therefore, the T_{lum} is compromised being around 50% and the third problem, is that the thermochromic reflectance modulation in VO_2 films is good enough for architectural applications only in the near infrared and at certain wavelengths where the solar radiation is low.

To overcome the T_{lum} and T_{sol} problems, the luminous transmit-

tance (T_{lum}) and the solar modulation (T_{sol}) of VO_2 have to be optimized [130]. Diverse studies report that VO_2 nanoparticles present an improved luminous transmittance and solar modulation compared to VO_2 thin films [130] [131].

This chapter was focused on the preparation of VO_2 thin films with thermochromic properties and also showed the difficulties in obtaining VO_2(M) thin films deposited *via* sol-gel/spin-coating and AACVD. Due to this obvious difficulties and even more knowing that VO_2 nanoparticles are reported to have a better luminous transmittance and solar modulation to be used for architectural applications, the investigation presented in the next chapters will be focused on the synthesis and analysis of micro and nanoparticles of thermochormic VO_2 instead of VO_2 thin films as presented in this chapter.

Chapter 3

VO_2(D) nanoparticles and thin films

3.1 VO_2(D) nanoparticles

The study of thermochromic VO_2 nanoparticles has gained a lot of interest not only in the VO_2 field, but also in the architecture field due to its applications as an intelligent coating for windows.

Thermochomic VO_2 coatings have a non aesthetically yellow/brownish colour, this is as a result of the absorption of visible wavelengths. Efforts to improve the colour of the coatings have lead to experiments where magnesium is used as a dopant of the VO_2 with the sole aim to synthesize clear films [132] [133].

In other efforts to enhance the colour of the films, some work has demonstrated theoretically [67] [134] and supported with experiments [135] the fact that VO_2 nanoparticles present an improved luminous transmittance and solar modulation compared to films having particle sizes greater 50 nm. Moreover Li *et al.* [67] demonstrate with theoretical calculations that spherical particles on the nanometer order embedded in a dielectric matrix have the highest levels of transmittance reported, being the $T_{lum} \approx 72\%$ for the semi-conductor state and 62% for the metallic state, while the best value obtained for films (regardless of the temperature) is $\approx 38\%$. On the other hand, the calculated ΔT_{sol}

is $\approx 20\%$ while for films is $\approx 7\%$.

Based on these analyses, synthesis of VO_2(M) nanoparticles has become a priority and moreover the production of monoclinic vanadium dioxide in one single step, is a real challenge.

The literature includes a few articles where the authors report the production of VO_2(M) in one step, however, usually the conditions are very hard to reproduce, as there is the need to control temperature, pressure and pH over a very narrow range. In some reported cases, the temperature used exceeds the safe temperature limit for reactions in an autoclave.

An easy and reproducible way to prepare nanoparticles of VO_2(M) is *via* calcination of VO_2(D) nanoparticles at low temperatures for a short time under a controlled atmosphere.

3.1.1 Aim

The main objective of this work was to prepare doped and undoped nanoparticles of VO_2(D) and anneal them under a controlled atmosphere at low temperatures to produce nanoparticles of VO_2(M). Nanoparticles of VO_2(M) present higher luminosity and better performance in terms of solar modulation applications, as discussed previously and reported in the literature [135] [67].

3.1.2 Experimental

VO_2(D) nanoparticles were prepared *via* hydrothermal synthesis. The reaction took place in a 45 mL lined autoclave over 48 hours at 240 ^oC. The samples were prepared by mixing 0.45 g (0.0024 mol) of vanadium pentoxide (V_2O_5) as a vanadium source, 0.75 mL (0.0140 mol) of sulfuric acid (H_2SO_4) as a reducing agent, 0.25 mL (0.0079 mol) of hydrazine (to promote formation of the desired phase) and tungsten(VI) ethoxide as dopant (for the doped samples), into 10 mL of DI water. The solution was strongly stirred for 5 minutes to obtain a green solution.

To obtain the VO_2(D) phase it is very important to control the pH of

the solution. This has to be in range of 6.6 to 6.9; outside of this range, other phases like V_2O_3, VO_2(B) (or mixture of phases) are obtained. The pH of the solution was measured using a pH 211 microprocessor pH meter from Hanna instruments with an error of $\pm$ 0.1.

In order to control the pH, sodium hydroxide (1.0 M) was added to the solution and stirred for 1 minute. Finally, the solution was centrifugated to obtain a grey paste that was finally dissolved in 19 mL of DI water and poured in the autoclave for the reaction.

After the reaction took place, the final solution was centrifugated, washed with DI water and ethanol and dried at 60 °C overnight to obtain the final product.

Table 3.1 shows the name (sample number) and pH of three as-prepared samples that meet the pH requirements to prepare VO_2(D).

Table 3.1: Sample names and descriptions for VO_2(D) powders synthesized by the reaction between V_2O_5 and H_2SO_4 in water. NaOH was used to adjust the pH of the solution. Samples were synthesized *via* hydrothermal synthesis for 48 hours at 240 °C

Sample	pH of starting solution
S16	6.62
S17	6.75
S18	6.82

3.1.3 Characterization

X-Ray diffraction studies were performed using a D8 GADDS Bruker diffractometer, utilizing Cu K_α radiation (λ = 1.541 $\AA$) between 10 to 60 °C, 2θ in order to determine the phase of the vanadium dioxide obtained product. A Renishaw 1000 spectrometer was used to perform Raman spectroscopy analysis. The equipment was coupled to a 633 nm laser and calibrated using a silicon reference.

Morphology and size of the as-prepared samples were obtained using a Field Emission Scanning Electron Microscope (FESEM), JEOL JSM-6700F instrument with an accelerating voltage of 5 KeV and Transmission Electron Microscopy (TEM) analysis were performed us-

ing a Phillips CM300 FED TEM, operated at 300 kV.

Differential scanning calorimetry (DSC) analysis was performed on a DSC 1 instrument from Mettler Toledo. The experiments were carried out between 0 to 300 °C under nitrogen atmosphere with a heating ramp of 5 °C/min.

X-Ray photoelectron spectroscopy (XPS) was conducted on a Thermo Scientific K-alpha spectrometer with monochromated Al K radiation, a dual beam charge compensation system and constant pass energy of 50 eV (spot size 400 μm). Survey scans were collected in the binding energy range 0 - 1200 eV. High-resolution scans were obtained for the principal peaks of V 2p, O 1s and C 1s. Data was calibrated against C 1s (binding energy, 285.0 eV). Data was fitted using Casa XPS software.

The d-space was calculated using the Fast Fourier Transform (FFT) in the image processor software ImageJ, where it is possible to measure the distance between atomic planes in high resolution transmission electron microscopy (TEM) images.

3.1.4 Results and discussion

Vanadium dioxide can exist in different phases, and all of them have different properties. In order to perform a proper study of the obtained phase in the samples, all of them were characterized by X-Ray diffraction to check the crystallographic phase, by SEM and TEM to observe the morphology and size of the particles, and by DSC to study the transition phase of the samples.

3.1.4.1 Scanning Electron Microscopy

Scanning Electron Microscopy was performed in order to determine the size and morphology of the samples and additionally study the growth mechanisms of the samples.

Undoped samples: Figure 3.1 shows the SEM and TEM images of two of the as prepared samples.

Figure 3.1A shows the SEM image of sample S16 made with a pH of 6.62. As can be seen the measure scale is 100 nm and the particles are smaller than that. Using this SEM image, its hard to recognize a specific shape of the particles. Moreover agglomeration of the particles are seen. In Figure 3.1B, C and D, TEM images of the same sample are shown. In Figure 3.1B, an aggregate of particles is observed, but as mentioned before, the particles seem to be smaller than the measure scale used. Figure 3.1C and D show single particles of the same sample with a round and oval shape. The particle is well defined and the size is between 20 to 35 nm.

Figure 3.1E, shows the SEM image of samples S17 with a pH of 6.75. Using this image, its hard to see the morphology and size of the product, nevertheless, agglomeration of particles can be seen in the image. TEM Figure 3.1F, shows an agglomeration of the as-prepared nanoparticles, however, it is easy to see the well defined round morphology of the particles. In Figure 3.1G and H, two nanoparticles of the as prepared VO_2 are shown. Both of them have a mainly round shape morphology and the sizes of these particles are about 20 to 40 nm.

As mentioned before, smaller particle sizes of the thermochormic VO_2, present better performance [66], this is because the size of the particles alters the effective absorption spectra of VO_2. At this point only VO_2(D) nanoparticles are shown. So far, no thermochromic behavior has been reported for this phase, in the nanoscale regime.

Despite the fact that the reaction takes place over 48 hours, and usually longer reactions times produce growth of the particle size, and agglomeration, we do not see this in our product, we attribute this to the presence of hydrazine in the reaction, that not only promotes the formation of the desired phase, but also acts as a surfactant dispersing the nanoparticles [86] [3]. Moreover, experiments without hydrazine were performed (not reported in this work, as the results were not relevant for this work purpose) and different phases of VO_2 were obtained (not

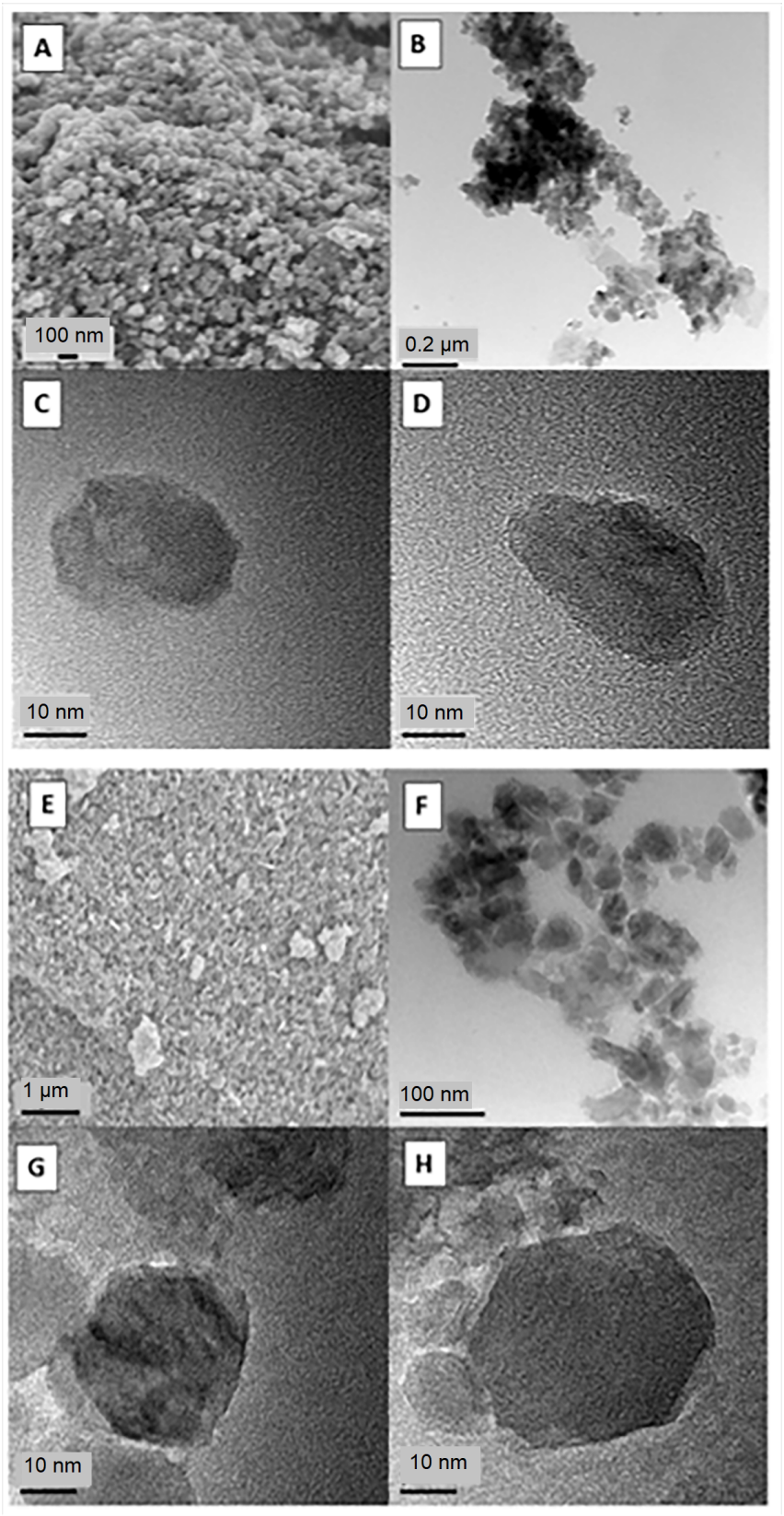

Figure 3.1: (A) SEM image of sample S16 (B, C, D) TEM images of sample 16 (E) SEM image of sample S17 (F, G, H) TEM images of sample S17

VO_2(D)) and bigger particle sizes were encountered.

VO_2(D) nanoparticles were calcinated under nitrogen for 2 hours at 180 °C in order to obtain thermochromic VO_2. TEM analysis was performed on the samples, before and after annealing, to study (by comparison), possible changes in size and morphology before and after annealing the particles.

Figure 3.2A, shows a TEM image of sample S16 with a pH = 6.62 after annealing under nitrogen. The sample have an oval shape and approximate size of 20 nm. It is not evident any crystal growth after calcination (by eye comparison).

Figure 3.2B, shows the TEM of sample S17 with a pH of 6.75. As with sample S16, particles have an oval shape, size is around 20-25 nm and the morphology is round/elongated. By comparing particle size before and after annealing, it can be concluded that there is no growth in the particle size due to calcination.

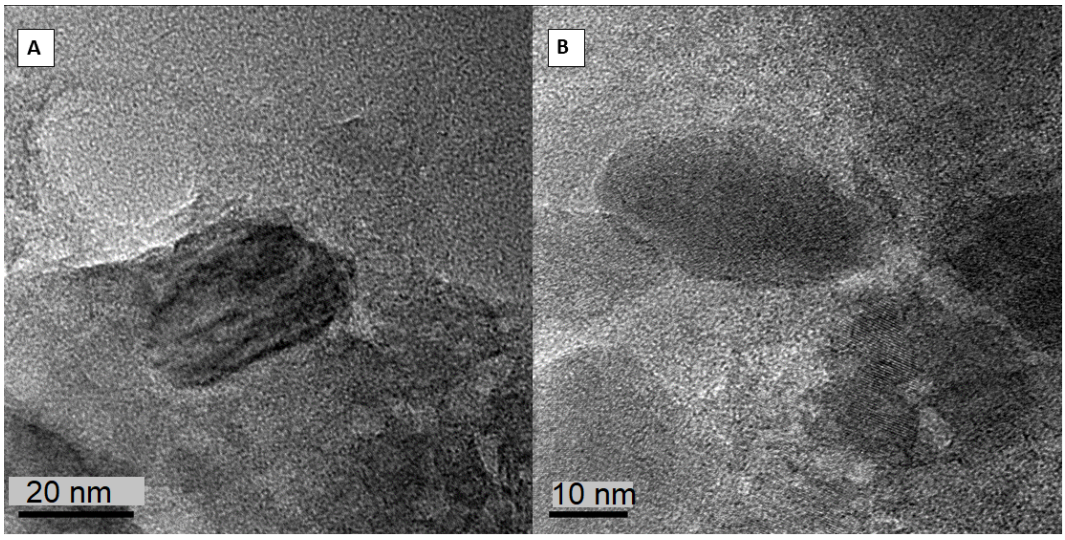

Figure 3.2: (a) TEM image of sample S16 after annealing under nitrogen at 180 °C (b) TEM images of sample S17 after annealing under nitrogen at 180 °C

Obtaining VO_2 nanoparticles is very important for architectural applications because nanoparticles have a better luminosity performance when they are in the nano-scale order. Moreover, preparation of films

its easier with nanoparticles.

Tungsten composite samples: A tungsten doped sample was intended to be prepared in order to study the effect of the tungsten in the diminution of the transition temperature when the sample presents thermochromic behavior. The size of the vanadium particle is very important when it presents thermochromic behavior [67]. Ideally the sample size should be in the nanometer range (smaller than the wavelength), typically smaller gives better performance in terms of luminosity [57].

In Figure 3.3A and B, the TEM of the supposed tungsten doped as-prepared sample is shown. The TEM of the sample show mainly round and oval particles of around 20-30 nanometers. The addition of tungsten ethoxide (VI) to the precursor solution does not seem to affect the morphology or size of the samples compared to the undoped VO_2(D) samples shown before.

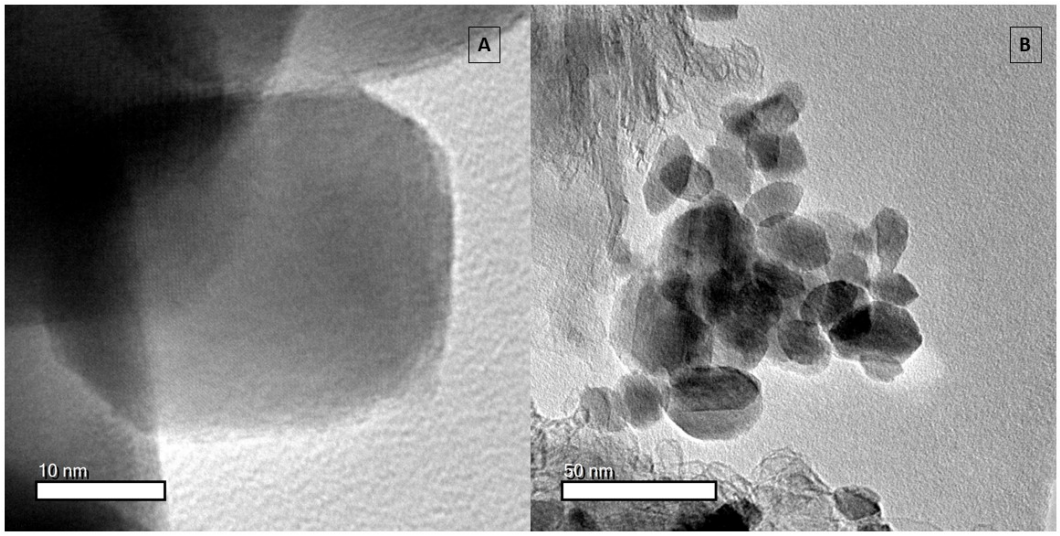

Figure 3.3: TEM of a tungsten composite VO_2(D) sample

The as-prepared sample was intended to be tungsten-doped samples, however, the TEM analysis in Figure 3.4 shows the presence of long rods that correspond to tungsten oxide after study of the composition of the rod *via* EDX and measurement of the corresponding d-space.

These findings confirms the existence of tungsten in the sample, in the form of tungsten oxide, suggesting that at least some tungsten was

not incorporated into the vanadium dioxide lattice.

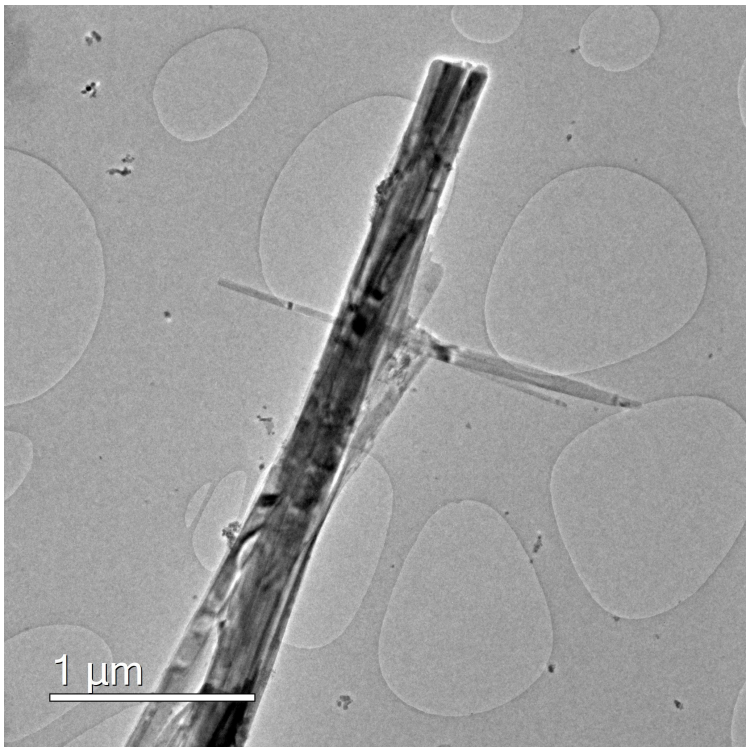

Figure 3.4: TEM of a tungsten oxide rod in a tungsten composite VO_2(D) sample

The composite sample was calcinated under vacuum at 180 °C for 2 hours in order to obtain a thermochromic VO_2 sample (shown in Figure 3.12). The XRD pattern shown in Figure 3.10 of the following section, confirmed the successful phase transition from VO_2(D) to VO_2(M). TEM was peformed on the sample after calcination to study, by comparison, if there was particle size growth after annealing in the tungsten composite sample.

Calcination of VO_2 particles at high temperatures for long time periods have been reported in the literature to cause a growth in the particle size [136], however, as can be seen in Figure 3.5 no particle size growth is observed if compared (by eye) to the particle size of the particles before annealing. The size of the particles remains between 20 to 30 nm in diameter and the morphology is not affected either.

The obtained VO_2(M) nanoparticles present mainly a round and

oval shape and constant size. The addition of tungsten to the as-prepared samples, seems to not affect the size and shape of the nanoparticle product, at least by simple size and shape comparison *via* SEM / TEM images, the difference is imperceptible.

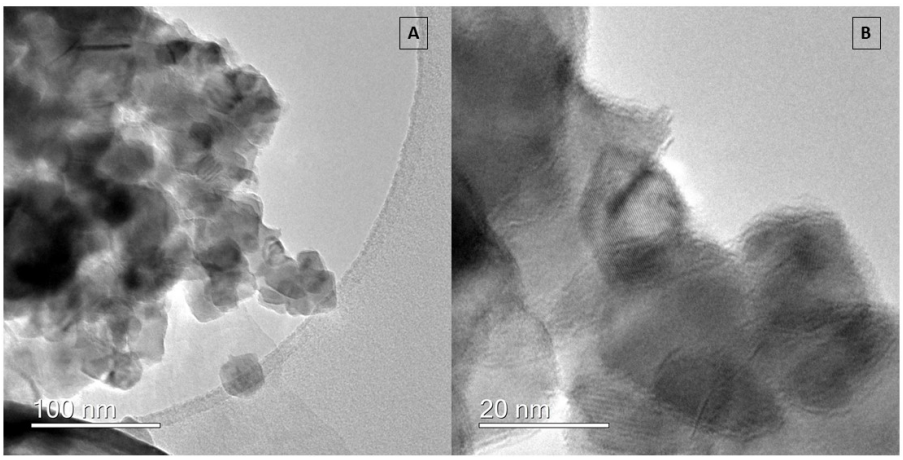

Figure 3.5: TEM of tungsten composite VO_2(D) nanoparticle after calcination under vacuum at 180 °C for 2 hours (A) cloud of nanoparticles (B) closer image of the nanoparticles

3.1.4.2 X-Ray Diffraction

Undoped samples: VO_2(D) nanoparticles were synthesized using vanadium pentoxide mixed in water with sulfuric acid, hydrazine and sodium hydroxide. Figure 3.6 shows the XRD pattern of three as-prepared samples at different pH. Patterns were compared with the VO_2(D) pattern shown in the literature, and the peaks of the obtained samples, match to those in the literature.

Even if the presented data is not fully crystalline, it is easy to see the main peaks at 30.6^o, 36.4^o, 41.7^o and 54.6^o. However, it is not easy, due to the XRD quality, see clearly the peaks at 23.6^o and 57.8^o (2θ, λ = 0.7093 $\AA$).

A pH of the samples between 6.60 to 6.90 is required in order to obtain the D phase of vanadium dioxide. For samples with basic or acidic pH, other phases were obtained like VO_2(A), VO_2(M) or a mixture of phases. Figure 3.7 show some examples of the obtained patterns (VO_2

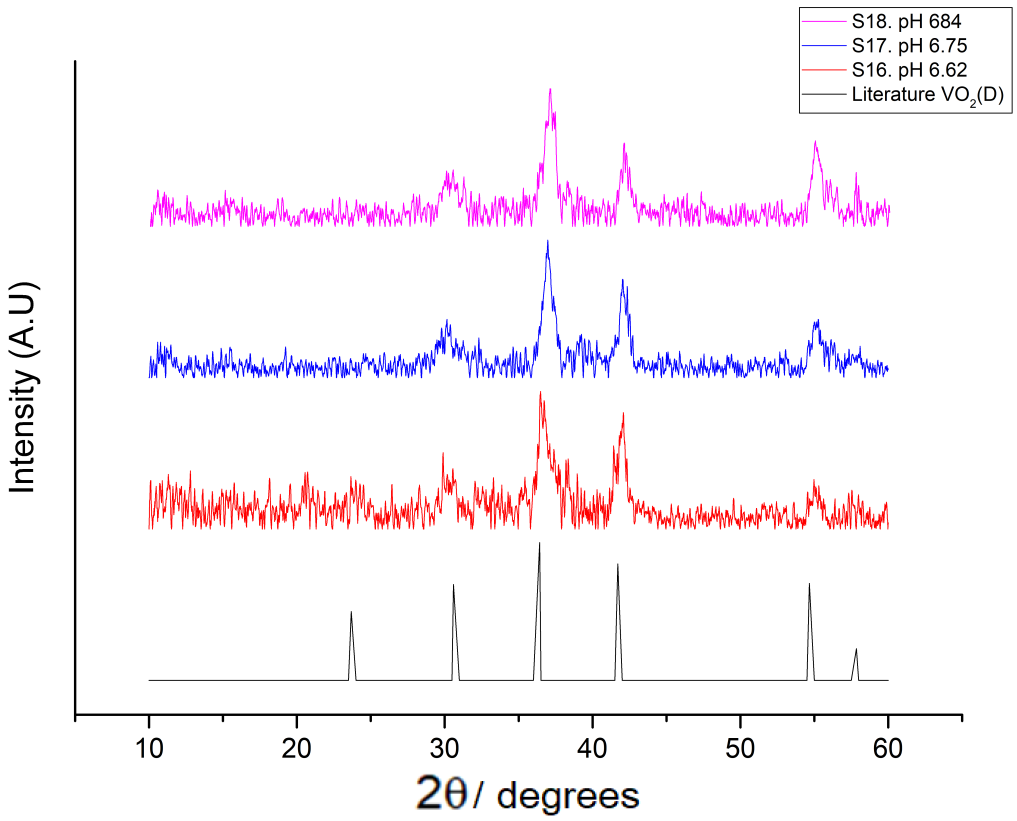

Figure 3.6: XRD pattern of the prepared samples using vanadium pentoxide as a precursor and NaOH to adjust the pH of the solution. All peaks correspond to the VO_2(D) phase shown in the literature

phases) when the pH of the solution is not between 6.60 to 6.90. Figure 3.7A for example shows a VO_2(A) pattern with a sample prepared with a pH of 7.34 and Figure 3.7 D shows a XRD pattern of a mixture of vanadium phases.

The obtained XRD data of the as-prepared samples shows broad peaks, that usually means that either the sample is not crystalline or the particles size is on the order of nanometers. In this case, previous SEM / TEM analysis confirm that the broad XRD peaks means the presence of nanoparticles [135].

On the other hand, when broad peaks are obtained, it is hard to understand if there is more than one phase in the product, as some peaks can be hidden by the broad ones, however, further analysis will show later in this work (Figure 3.15) that the sample composition is mainly

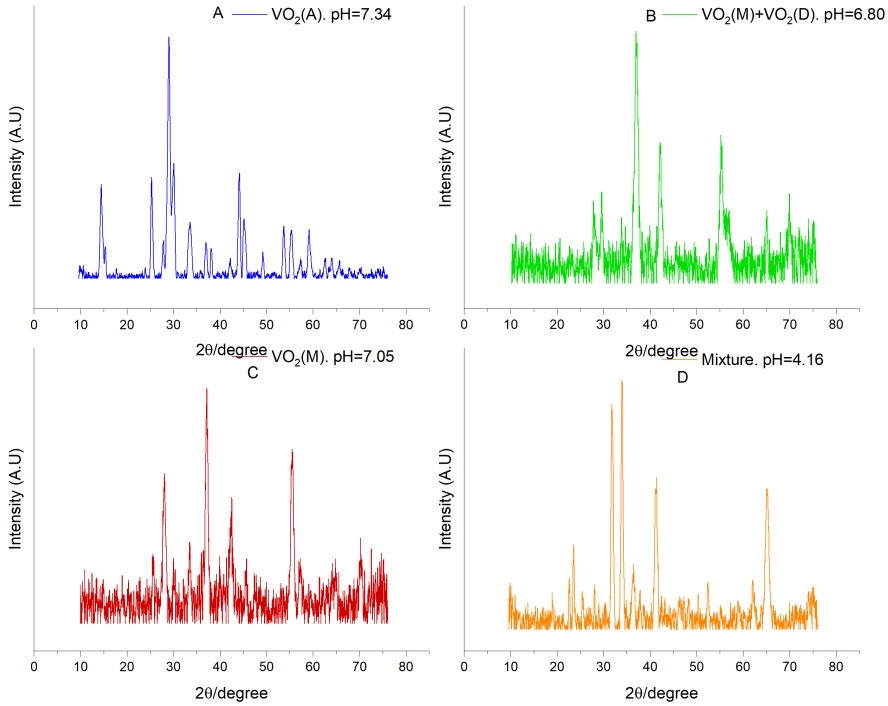

Figure 3.7: XRD pattern of samples prepared *via* hydrothermal synthesis using V_2O_5 as a precursor at different pH (A) VO_2(A) pH = 7.34 (B) VO_2(M) + VO_2(D) pH = 6.80 (C) VO_2(M) 7.05 (D) mixture of phases 4.16

vanadium 4+, corresponding to VO_2(D).

In Figure 3.8 it is shown the XRD pattern of sample 17 with pH of 6.75 after annealing in vacuum at 180 °C, for 2 hours compared to the VO_2(M) pattern obtained from the literature.

As can be seen in Figure 3.8 the obtained pattern of the nano VO_2(D) after annealing matched well to the known pattern of VO_2(M), pointing out that the phase transformation from D to M phase was successful using low temperature annealing under vacuum.

This result is very relevant in the VO_2 field as the usual way to obtain monoclinic VO_2 particles is either annealing VO_2(A,B) phases at high temperatures (550-600 °C) or to obtain it in a one step synthesis under high reaction temperatures (higher that those permitted by the reactor vessel).

To our knowledge, nanoparticles of VO_2(D) have not been reported

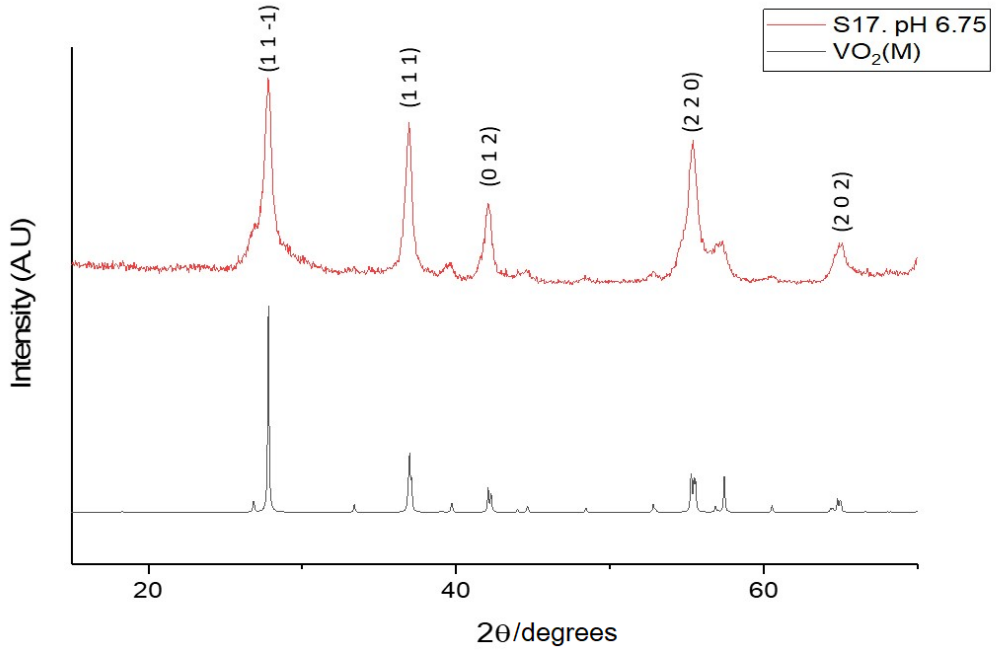

Figure 3.8: XRD pattern of sample S17 with pH of 6.75 after annealing in vacuum at 180 °C for 2 hours compared to the VO_2(M) pattern obtained from the literature

in the literature yet, furthermore a transition from VO_2(D) to VO_2(M) at low temperatures has also not been reported in the literature so far.

One of the advantages of obtaining the desired phase at low calcination temperatures is the fact that there is little growth in the size of the particles. This is very important in the vanadium dioxide field for architectural applications, as has been proved that nanoparticles present better luminosity and performance compared to micro size particles of the same compound [68].

Tungsten composite samples: It is very common to use tungsten to dope VO_2 samples in order to decrease the transition temperature when the samples presents thermochromic behavior, it means a transition from metal to insulator. In this case, nano particles of VO_2(D) were intended to be doped using tungsten(VI) ethoxide as a source of dopant.

Figure 3.9 shows the XRD pattern of the tungsten doped VO_2(D) as-prepared sample, compared to the VO_2(D) XRD pattern obtained from the literature. The XRD peaks obtained by the as-prepared sample,

match the peaks from the literature with no evident peak shift (typical feature after successful doped material), however around $2\theta = 42°$there is low intensity peak, that could not be indexed to the VO_2(D) XRD pattern presented in the literature. It is not possible by this method to confirm that the extra non-intense peak represent other VO_2 phase or compound or if the tungsten was incorporated successfully in the lattice of the sample, however, the VO_2(D) phase was obtained.

The obtained diffraction peaks are broad, this suggests that, either the sample is not fully crystalline or the obtained particles are on the order of the nanometers. Previous analysis showed that the obtained particles are on the order of nanometers and this is the most probable reason of having broad peaks.

The as prepared sample was calcined under vacuum at 180 °C for 2 hours in order to obtain a VO_2(M) with thermochromic properties. In Figure 3.10 the XRD pattern of the sample after calcination is observed compared with the typical VO_2(M) pattern from the literature.

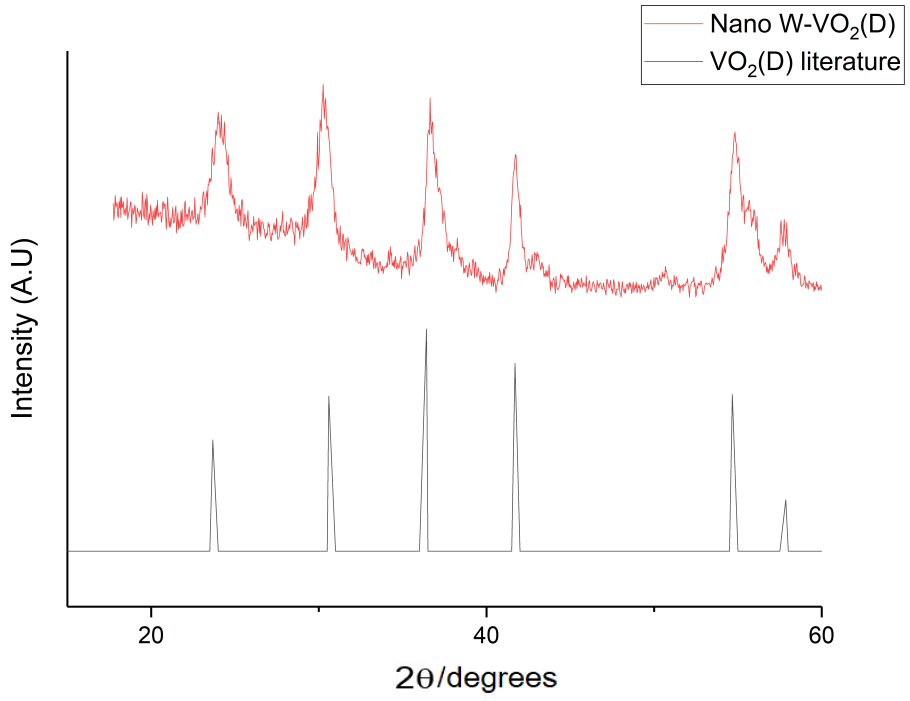

Figure 3.9: XRD pattern of nano composite W-VO_2(D) sample before annealing

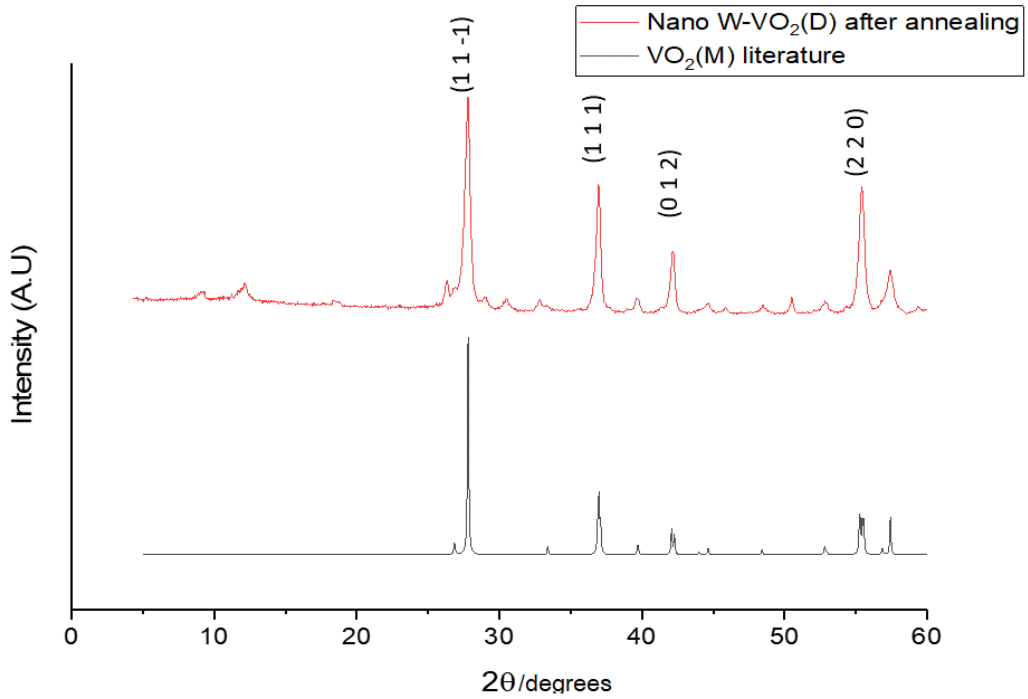

Figure 3.10: XRD pattern of tungsten composite nano-VO_2(D) sample after annealing at 180 °C for 2 hours

As can be seen, the main peaks of the as prepared sample match with the main peaks of the VO_2(M) from the literature, however, extra peaks with low intensity are observed. These peaks can be product of the presence of WO_3, as peaks at low intensity are characteristic of this compound. No shifts in the VO_2(M) peaks are noticed. Usually shifts in the peaks means that the sample was successfully doped, and this is due to the change in size of the atomic radius that is replacing the existing atom [127].

3.1.4.3 Differential scanning calorimetry

Undoped samples: The most common way to obtain VO_2(M) for thermochromic applications is to anneal the samples, typically VO_2(B), in a controlled atmosphere at temperatures between 500 to 700 °C. We have found in this work that the annealing temperature is related to the morphology and particle size. In particular, we discovered that VO_2(D) nanoparticles require less time/temperature to be transformed into ther-

mochromic VO_2(M)

Figure 3.11 shows the differential scanning calorimetry analysis performed on two VO_2(D) nanoparticle samples. In both cases it can be observed that in the first heating cycle, there is an endothermic peak around 165 °C. This peak represents a first transition phase from the D to R phase. The sample is heated up until 300 °C without presenting any other phase transition. Continuing with the analysis, the sample is cooled down and no peaks at 165 °C are shown, this means that the transition phase is not reversible. Furthermore an exothermic peak appears at around 42 °C, this peak represents the transition of VO_2(R) to VO_2(M).

On the second heating cycle (same sample) an endothermic peak around 59 °C provides evidence of the widely known transition from VO_2(M) to VO_2(R) representing a typical thermochromic behavior in the sample. No further signals are obtained up to 300 °C. In the second cooling cycle, it is observed again that an exothermic peak is seen at 42 °C and no further peaks are present up 0 °C.

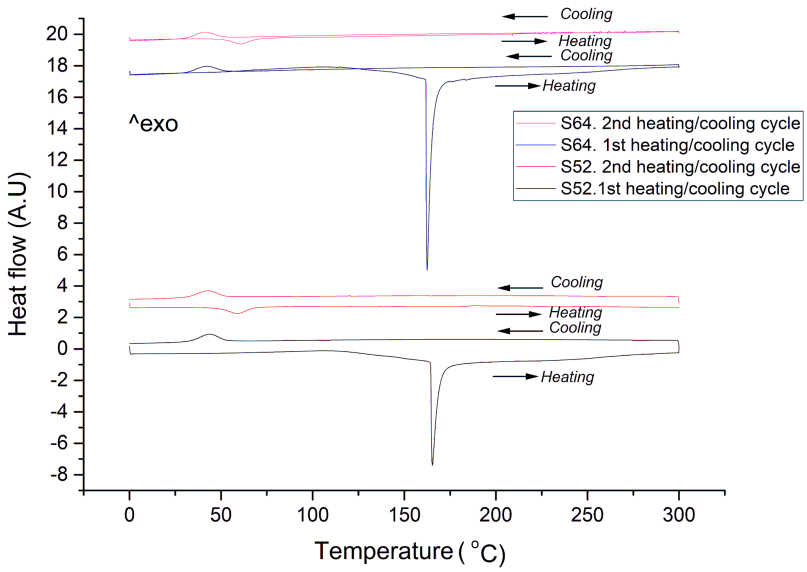

Figure 3.11: DSC curves of VO_2(M) obtained *via* nano-VO_2(D) samples showing: the transition from D to M phase and then, the reversible thermochromic behaviour of VO_2(M)

An important point to note is the fact that the transition from VO_2(D) to VO_2(R) is noticeable at 165 °C, being this the lowest reported temperature in the literature (by us) for this transition [87]. We attribute this to the nanoparticle size and phase. Moreover, the produced thermochromic material has a MST temperature at 42 °C for the cooling cycle and 59 °C for the heating cycle; this is 9 °C less than the MST temperature reported in the literature for bulk undoped samples of VO_2(M).

Tungsten composite samples: Literature reports on the lowering of the transition temperature of the thermochomic VO_2 when tungsten is incorporated into the lattice [43]. The as prepared samples, according to the results presented above, have tungsten oxide that was not incorporated into the VO_2 lattice (no shift in the XRD pattern).

Differential scanning calorimetry was performed to the as prepared sample with tungsten(VI) ethoxide. The black line in Figure 3.12 represent the first heating cycle performed to the sample, where one endothermic main peak is observed at 185 °C and two small peaks are present at 142 °C and at 153 °C. The main endothermic peak is suspected to be the transition from VO_2(D) to VO_2(R) that was also observed in the undoped samples, however, the transition temperature is higher than expected and reported for undoped samples in the previous section, this difference in the transition temperature is attributed to the presence of tungsten oxide in the sample that was not incorporated into the lattice. As the sample is not pure VO_2(D), but a tungsten-vanadium composite, the transition phase takes longer, as the sample needs more energy (in this case energy in the form of temperature) to complete the phase transition.

The first cooling cycle, red line in Figure 3.12 does not show any exothermic peak evidencing the complete transformation from VO_2(D) to thermochromic VO_2(R). The sample was heated up to 200 °C, while the undoped sample was heated up to 300 °C (different instruments

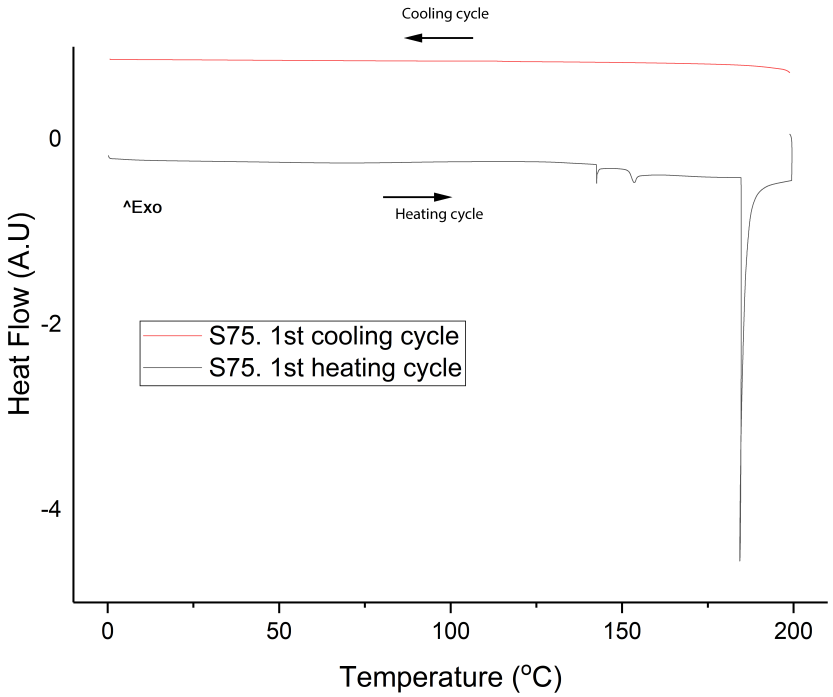

Figure 3.12: Differential calorimetry of the tungsten/VO_2 composite sample

and laboratory conditions were used), therefore it is possible that even if an endothermic peak is observed as evidence of a phase transition, the transformation has not occurred entirely, therefore, no detectable exothermic peaks are observed.

The presence of tungsten oxide particles in the sample could also explain the fact that the transformation did not occur. If the sample presents impurities (a significant amount, not incorporated into the lattice), it will require more energy (temperature) and time to achieve the total transformation of the material.

In order to obtain a complete phase transformation from VO_2(D) to thermochromic VO_2(M) the sample was calcinated at 180 °C for 2 hours under vacuum atmosphere. Figure 3.13 shows the differential scanning calorimetry analysis performed to the sample after annealing. In the heating cycle there is a broad peak at $\approx$ 75 °C accompanied by another small peak at $\approx$ 88 °C. This is an unusual behavior for thermochormic VO_2 during the heating cycle as only one peak is expected at around

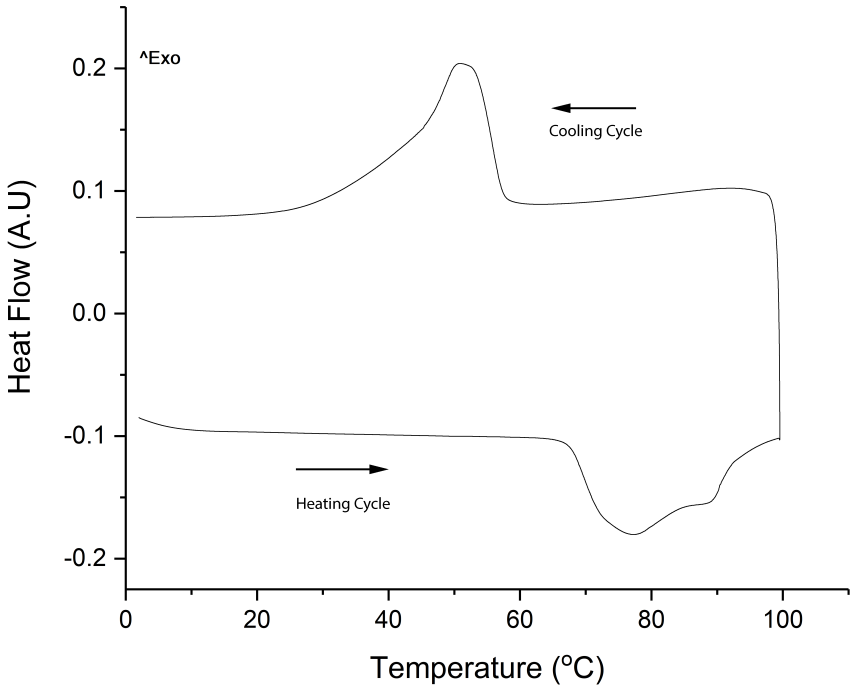

Figure 3.13: Differential calorimetry of the tungsten/VO_2 composite sample after annealing at 180 °C

68 °C for bulk VO_2. However, when the thermochromic VO_2 is not a pure phase (like in this case) broad peaks are expected; this is because the material requires longer time and temperature to switch to the rutile phase. Moreover, as the prepared sample is a composite and tungsten oxide is not thermochromic, this explains the anomalous (broad) peak obtained in the heating cycle. As the sample is not pure VO_2, it requires more energy input for the transition

On the other hand, in the cooling cycle an exothermic peak is observed at around 50 °C. The peak is broad and does not present any abnormality.

3.1.4.4 Raman Spectroscopy

Raman spectroscopy is a surface analysis technique used to study the vibrational and rotational modes of a system, in this particular case, the studied system is the vanadium dioxide compound prepared (VO_2(D)).

In chemistry, Raman analysis can be used for phase identification for vanadium species as every phase has a different set of typical bands.

Undoped samples: Raman spectroscopy was performed on the as prepared VO_2(D) nanoparticles powder samples (placed in a silica glass substrate) in order to study the phase of the VO_2 samples. VO_2(D) Raman spectra have not been reported in the literature so far.

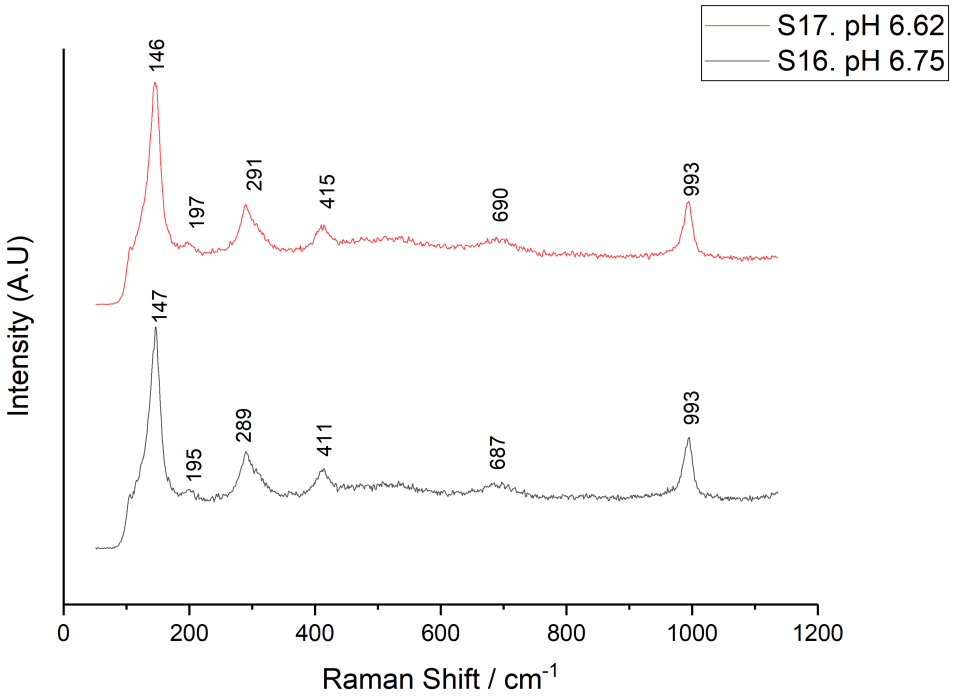

Figure 3.14: (A) Raman spectra of Sample S16 with pH of 6.62 (B) Raman spectra of sample 17 with pH of 6.75

Figure 3.14 shows the Raman spectroscopy of two VO_2(D) nanoparticles samples prepared at (A) 6.62 and (B) 6.75 pH. The obtained spectra represent the bands of the well known V_2O_5 compound [14] however, Raman bands of V_2O_3 and V_6O_13 compounds are very similar to V_2O_5 Raman bands as reported by Chen *et al.* [137] and Troy [75], therefore, if the band are not well defined it is impossible to determine if it is a mixture of phases, the V_2O_5, V_6O_13 or the V_2O_3 compound. Besides that, no other bands are present that can be indexed to the newly reported VO_2(D) phase. However, as Raman spectroscopy

is a surface analysis technique and VO_2 gets oxidized easily in presence of air, if the compound is not protected, it is very common to obtain V_2O_5 spectra, so it can be speculated by this analysis that it is the characteristic Raman spectra of the V_2O_5 compound due to the oxidation of the VO_2(D).

Different laser intensities (10 to 100 %) as well as different laser wavelength (633 nm and 785 nm) were used to compare the results, however the same outcomes were obtained.

3.1.4.5 X-Ray photoelectron spectroscopy

Undoped samples: In order to determine the oxidation state of the obtained VO_2(D) particles, X-Ray Photoelectron Spectroscopy (XPS) measurements were performed. XPS is a surface analysis, and will determine only the oxidation in the surface of the particle, not into the bulk material [138]. The binding energies for vanadium and oxygen were measured against carbon C1s (285.0 eV).

Figure 3.15 shows the surface oxidation state of one as-prepared VO_2(D) nanoparticles. It is evident that the $V2p_{3/2}$ peak is not symmetric which means it can be composed for two or more chemical environments at different binding. Vanadium oxidation state binding energies have very similar values and that is the reason why the peak was decomposed, therefore it can be concluded that the surface oxidation state of the as-prepared and analyzed sample was a mixture of V^{4+} (516.1 eV) and V^{3+} (514.6 eV). Similar values has been reported before in the literature ($\pm$ 0.2 eV) for V^{4+} by Demeter *et al.* [139] and by Sawatzky *et al.* [140]. For V^{3+} similar values ($\pm$ 0.2 eV) have been reported in the literature by Horvath *et al.* [141].

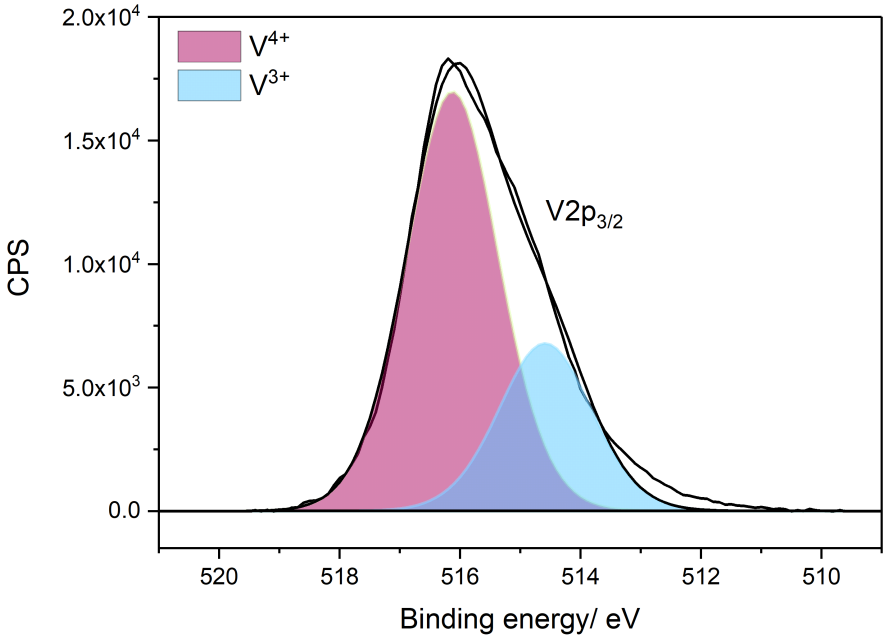

Figure 3.15: Surface XPS spectrum for vanadium binding energy from VO_2(D) nanoparticles prepared *via* hydrothermal synthesis

This is a remarkable result as the surface is mainly V^{4+} and it is well known that vanadium dioxide species oxidize easily in presence of air [126]. This means that the prepared samples are stable in the presence of air for periods of at least 6 months. This is an advantage for the application of the material (VO_2(D) nanoparticles) as a VO_2(M) precursor after calcination of the nanoparticles at low temperatures. This analysis was performed 6 months after the preparation of the sample and it remains (mainly) in the V^{4+} state. On the other hand, the presence of V^{3+} seems to indicate reduced VO_2 during the hydrothermal reaction.

The XPS results are consistent with the Raman results. Both are surface sensitive analysis, even though XPS is more surface sensitive. Raman results were not conclusive initially as V_2O_5, V_6O_{13} and V_2O_3 have very similar Raman spectra [75] [137], however, with XPS results showing V_2O_3 content, we can conclude that the VO_2(D) sample

present vanadium 3+ on the surface. The whole set of results (XRD, Raman and XPS) confirms that the as-prepared VO_2(D) samples are vanadium 4+ with some vanadium 3+ content.

XPS results of VO_2(D) samples reported in the literature [44] shows the peak of $V2p_{3/2}$ at 515.4 eV and assigned this to V^{4+}. Our results does not match to this findings in the literature, but they coincide with similar vanadium 3+ and vanadium 4+ values reported in other articles [139] [140] [141].

On the other hand, VO_2(D) XRD analysis, as a bulk analysis, match perfectly with the results obtained in the literature for VO_2(D), this being vanadium 4+.

3.2 Polymeric thin films using VO_2 nanoparticles

Polymeric films with thermochromic properties are prepared and reported in this chapter. The films are synthesized using VO_2(M) nanoparticles (coated with SiO_2 to protect the nanoparticles from the oxidation) incorporated into PVP (polyvinylpyrrolidone) as polymer matrix.

3.2.1 Aim

The objective is to prepare polymeric films of VO_2(M) with thermochromic properties using the previously as-prepared VO_2(D) nanoparticles transformed already into thermochromic VO_2(M) after mild calcination.

3.2.2 Experimental

The VO_2(D) nanoparticles were prepared *via* hydrothermal synthesis and calcinated at 180 °C for 2 hours in order to obtain thermochromic VO_2(M) nanoparticles to be used in the film preparation.

VO_2(M) thermochromic nanoparticles are very sensitive and are oxidized easily in the presence of air [131]. The prepared films will be exposed to air, water, dust, among others and it is important to protect

the nanoparticles in order to retain thermochromic properties. To do so a SiO_2 coating is added to the VO_2 nanoparticles surface, therefore 0.1 g of the as prepared VO_2(M) nanoparticles were dispersed into 5 mL of ethanol and subsequently added to a solution of 280 mL of absolute ethanol, 70 mL of DI water and 5 mL of ammonia solution at 28 wt %. The solution was stirred for 30 minutes and then 0.5 mL of tetraethylorthosilicate was added dropwise to the solution and stirred vigorously for 4 hours. The product was collected *via* centrifugation and washed with water and ethanol. Finally, the obtained paste was dried overnight at 80 °C.

For the preparation of the polymeric solution, 0.02 g of the coated VO_2(M) nanoparticles were added to 2 mL of methanol and placed into an ultrasonic bath at room temperature for 30 minutes in order to obtain a good dispersion of the nanoparticles into the methanol.

After 30 minutes, 1 g of Polyvinylpyrrolidone (PVP) of 44,000 molecular weight were added into the solution slowly and stirred until the solution was homogeneous. The obtained solution presents an homogeneous dark green colour.

Soda lime glass substrate of 2 x 2 cm was used. Substrates were submerged on acetone with ultrasonic treatment during 20 min in order to clean them, then; the glasses were rinsed with DI water in an ultrasonic bath for 20 min. Substrates were finally dried at room temperature.

For the deposition process a Laurell model WS-650-8B spin coater instrument was used. The spin rate was varied between 500 - 1000 rpm, acceleration 100 rpm/s, for 30 seconds. Four drops were deposited on the glass using a chemical dropper, a yellow polymeric film was formed on the glass surface. Process was carried out 5 times to increase the thickness of the resulting film. The film was dried overnight at 80 °C to get rid of the solvent.

The obtained film is uniform and evenly deposited on the substrate.

3.2.3 Characterization

X-Ray diffraction studies were carried out using a D8 GADDS Bruker diffractometer, utilizing CuKα radiation between 10 °to 60 °2θ in order to determine the phase of the vanadium dioxide product obtained. Raman spectroscopy analysis were carried out using a Renishaw 1000 spectrometer coupled with a 633 nm laser. The calibration of the equipment was done using a silicon reference.

Morphology and size of the as-prepared samples was studied using a Field Emission Scanning Electron Microscope (FESEM), JEOL JSM-6700F instrument with an accelerating voltage of 5 KeV.

UV/Vis spectroscopy was performed using a double monochromatic Perkin Elmer lambda 950 UV/Vis/NIR spectrophotometer in the 860 - 2600 nm range in order to study the thermochromic behavior of the prepared thin films. The information obtained with the UV-Vis is valuable for the present research as it is possible to check the transition phase of the vanadium oxide on the studied samples just measuring the transmittance of the sample at room temperature and at 90 °C.

3.2.4 Results and discussion

Polymeric films deposited on glass substrates were prepared using SiO_2 coated thermochromic VO_2(M) nanoparticles obtained *via* mild calcination of VO_2(D) nanoparticles (180 °C for 2 hours under vacuum atmosphere). The obtained results from X-Ray diffraction, scanning electron microscopy, UV-Vis and Raman are show later in order to study and understand the performance of the as prepared films.

The SiO_2 coating does not affect negatively the thermochromic properties of the nanoparticles, moreover, the SiO_2 coating has been reported to enhance the solar modulation efficiency up to 13.6%, the highest reported in the literature [131]. Figure 3.16 shows the coated nanoparticles. As is evident in Figure 3.16B, the SiO_2 coating is between 30-50 nm.

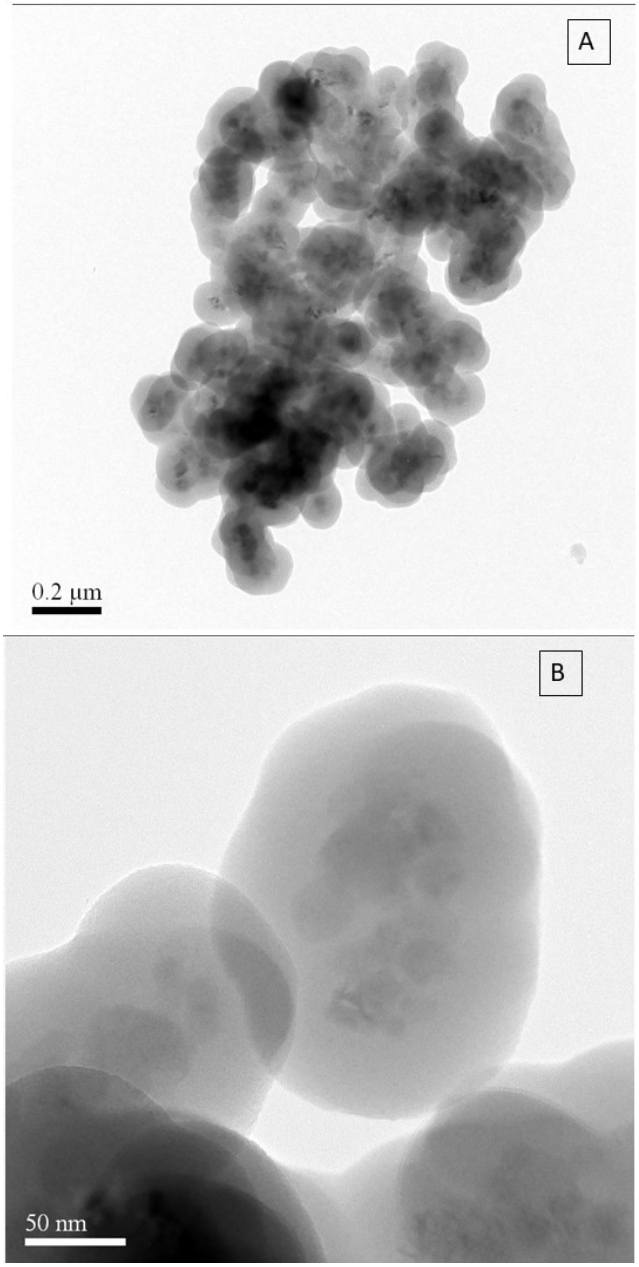

Figure 3.16: SiO_2 coated VO_2(M) nanoparticles (A) set of coated nanoparticles (B) few particles coated

Figure 3.17A and B, shows the obtained polymeric film of 4 and 5 layers, respectively, deposited onto sodalime substrate and dried overnight at 80 °C.

The film is uniform and does not present nanoparticles agglomeration, the yellow-brownish colour is the expected for VO_2(M) based films. The film is transparent enough to see clearly through it. The ad-

hesion between the PVP/nanoparticles solution and the glass was tested using the scratch test, that consist of use scotch tape to check the adhesion. The adhesion was good and no film was removed after the test.

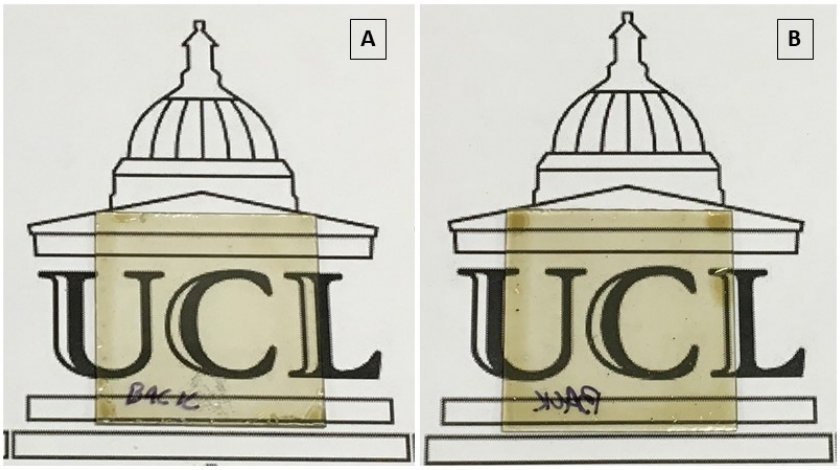

Figure 3.17: Polymeric VO_2 thin film prepared using VO_2(D) calcinated nanoparticles. (A) 4 layers (B) 5 layers

3.2.4.1 Ultraviolet-visible spectroscopy (UV-Vis)

UV-Vis was performed on the samples in order to probe the thermochromic properties of the as prepared samples. The UV-Vis analysis in this case measure transmittance of the samples at room temperature (25 °C) and at 90 °C for each sample. In this way it is possible to study the thermochromic behavior of the VO_2 samples under temperature. For thermochromic VO_2 samples, the samples should have maximum transmittance at temperatures below 68 °C, and lower transmittance (the material becomes semi-metallic), at temperatures above 68 °C.

To measure the transmittance at high temperatures, the sample was heated up to 90 °C to assure a thermodynamical stable temperature in the sample in order to complete phase transformation (that occurs at 68 °C) from VO_2(M) to VO_2(R). In chapter 2, samples were heated up to 100 °C because a different heater that support higher temperatures was used.

Figure 3.18 presents the transmittance obtained for three different samples, with 3, 4 and 5 layers of the nanoparticle/PVP solution de-

posited onto the substrate and, as can be noted, the samples have thermochromic behavior since there is a decrease in the transmittance when the sample is at temperatures above 68 °C.

Even though the transmittance data showed the thermochromic behavior of the samples, it is important to calculate the solar modulation of each sample weighting the solar values to the data [17] [119], this is because the terrestrial atmosphere absorbs in more or less intensity certain wavelengths. This calculation was done using Equation 1.2.

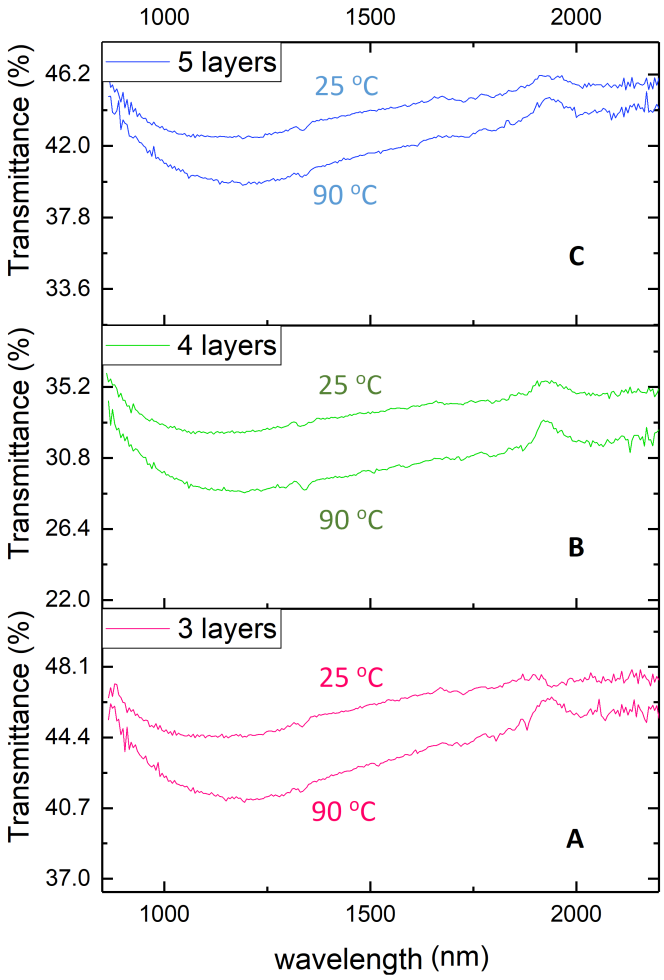

Figure 3.18: Transmittance of samples prepared using VO_2(D) nanoparticles after calcination with (A) 3 layers (B) 4 layers (C) 5 layers

Table 3.2 presents the solar modulation of the three films analyzed

Table 3.2: Weighted visible transmission at 25 °C and at 90 °C for thermochromic VO_2 film prepared using VO_2(D) nanoparticles after calcination and comparison with the results obtained in chapter 2

	T_{lum} **25 °C (%)**	T_{lum} **90 °C (%)**	ΔT_{lum}	ΔT_{sol}	ΔT_{IR}
3 layers	44.75	44.55	0.20	1.15	1.92
4 layers	32.78	31.09	1.69	2.33	2.84
5 layers	43.57	43.45	0.12	0.98	1.68
		Chapter 2			
Sample DP101	48.3	47.6	0.73	-1.83	NA
Kang *et al.*[68]	59.2-11.5	61.1-12.6	NA	NA	NA
Zhang *et al.*[115]	83.5-11.7	82.8-7.6	NA	NA	NA

with, 3, 4 and 5 layers.

As can be seen in Table 3.2 the best film in terms of the visible light transmission is the film with 4 layers, also this film presents the best performance for the solar modulation. On the other hand, the thickest film, with 5 layers, is the one having the worst solar modulation and visible light transmission, contrary to what is expected, as usually thicker films present better solar modulation compared to thinner films, it means that the thermochromic properties of the material have a better performance [142], however, the transmission in the visible range gets compromised. In the case of vanadium(IV) oxide samples, darker and not transparent films are obtained if the film is thick.

The obtained results for T_{lum} and T_{sol} of nanoparticles incorporated into a polymeric matrix and the results for T_{lum} and T_{sol} of a thin film prepared *via* sol-gel (chapter 2) are comparables and no big improvements are noted for thin films prepared using nanoparticles, as reported in the literature [67]. However, further analysis needs to be done for thin films using VO_2(M) nanoparticles obtained *via* VO_2(D) nanoparticles with different concentrations in the polymeric matrix.

3.3 Conclusions

In this work, nanoparticles of the newly reported VO_2(D) were successfully obtained *via* hydrothermal synthesis using V_2O_5 as a precursor.

The obtained nanoparticles of VO_2(D) does not present ther-

mochromic behavior itself, it means, they don't have a critical switching temperature (between 0 to 300 °C) where a metal to insulator transition is evident, however, they do present a transition phase from VO_2(D) to VO_2(M) at 165 °C. The phase transition from VO_2(D) to VO_2(M) phase is evident in the DSC analysis where an endothermic peak appears in the first heating cycle. Subsequently the typical performance of a thermochromic material is observed with an exothermic peak in the cooling cycle and an endothermic peak in the heating cycle. The thermochromism of the VO_2 sample was corroborated by XRD where a pure crystalline VO_2(M) pattern was obtained.

Tungsten(VI) ethoxide was used as a precursor in order to prepare tungsten doped VO_2(D) nanoparticles. The XRD analysis of the tungsten doped prepared samples show a clear VO_2(D) pattern, no shifts in the peak position was noticed, indicating that probably the tungsten was not incorporated into the vanadium dioxide lattice. However, when the sample was annealed at low temperature in order to obtain thermochromic VO_2, the XRD pattern shows several extra peaks, apart from the main peaks representing VO_2(M). This means, a mixed phase was obtained forming tungsten oxide particles.

The DSC analysis for the vanadium-tungsten composite samples shows a transition temperature from VO_2(D) to VO_2(M) phase at 185 °C, 20 degrees Celsius higher than the undoped samples, however, no complete transition is observed in the DSC analysis. The sample presents thermochromic behavior after annealing the sample under nitrogen for 2 hours at 180 °C.

Scanning electron microscope images and transmission electron microscope images show that the size of the as prepared nanoparticles samples, with and without tungsten included in the preparation, have a diameter size of around 20-30 nm and a homogeneous round/oval morphology. The size and morphology of the samples, with and without tungsten, after 2 hours of calcination at 180 °C, remain similar, these

being 20-30 nanometers with round/oval shape.

Nanoparticles of VO_2(D) were prepared for the first time and the transition to VO_2(M) at low temperature (165 °C) and for short time is very important and novel in the VO_2 field. It represents a very easy and reproducible way to obtain thermochromic VO_2 nanoparticles with better performance for architectural applications.

Thermochromic films with a solar modulation as good as 2.33 %, and transmittance in the visible light at 1.69 % were prepared using VO_2(M) nanoparticles, obtained *via* mild calcination of VO_2(D) nanoparticles, mixed with PVP and ethanol deposited onto a glass substrate.

The preparation of VO_2(D) nanoparticles and their easy transition into VO_2(M) gives the idea of use different precursors in order to obtain the same VO_2(D) phase, and moreover to prepare this newly reported phase tuning the size and the morphology.

Chapter 4

VO_2(D) and W composite VO_2(D) microparticles

4.1 Introduction

Vanadium dioxide has been widely reported and has a range of studied phases. There are the stable phases (VO_2(M) and VO_2(R)), the metastable phases, VO_2(A), VO_2(B) and VO_2(C) [45] [50] and the so called Magneli phases, that goes from VO_2 to V_2O_3, following the general formula V_nO_{2n-1} [41].

As already stated, there is a recently reported phase called VO_2(D) [44] [46] that has gained attention in the VO_2 field, as from this phase it is very easy to obtain thermochromic VO_2 at low temperatures (250 - 400 °C) for VO_2(D) microparticles [45] [46]. The mentioned phase does not present thermochromic behavior (which means does not have a reversible transition from semiconductor to insulator at a fixed temperature), which is one of the most studied topics of VO_2, however, once the monoclinic phase is obtained after mild calcination, the MST temperature of the product is around 61 °C, lower than reported in the literature for bulk VO_2(M) [34].

VO_2(D) has not been fully characterized yet. Microparticles of VO_2(D) have been synthesised in the past, however, a range of different morphologies are prepared in this work. Different morphologies of VO_2

can be useful for different applications, for example VO_2 nanorods have been used for Li-Ion batteries [143], VO_2 nanobelts have been used for supercapacitor [144] and nanofibers of VO_2 have been used for degradation of pollutant from wastewater [145].

Doping VO_2 particles is very common in the VO_2 field, as it improves the performance of the films/particles.

Tungsten has been widely used as a dopant to decrease the transition temperature. Manning *et al.* showed that doping only 2 wt% of tungsten to the samples, a transition temperature of 25 °C can be obtained [75].

4.2 Aim

Vanadium dioxide has been largely used for batteries, super capacitors and catalysis [**?**]. It has been widely reported that the morphology of VO_2 samples plays an important role in their performance, for example VO_2(A) flower like microspheres are used for lithion ion batteries [54]. So, changing the morphology, it is possible to enhance the properties and widen the application market, therefore the aim of the preparation of VO_2(D) microparticles with different morphologies is to study the final product for different applications.

Monoclinic VO_2 is obtained *via* VO_2(D) after mild annealing. The properties of the VO_2(D) and the obtained VO_2(M) are reported in this chapter.

As tungsten has been largely used as a dopant to decrease the switching temperature of the VO_2(M) closer to room temperature, in this work, tungsten chloride (IV) was used as a precursor with the intent to dope the VO_2(D) microparticles.

4.3 Experimental

All VO_2(D) and tungsten composite VO_2(D) microparticles were synthesised *via* hydrothermal synthesis using a 45 mL reactor.

In a typical synthesis to form VO_2(D) microparticles, 0.6250 g (0.0215 mol) of ammonium metavanadate (NH_4VO_3) used as a vana-

dium source, 2.52 g (0.027 mol) of oxalic acid ($C_2H_2O_4$) used as a reducing agent and 0.5 g of polyvinylpyrrolidone (PVP) 40,000 wt were mixed (at room temperature) into 50 mL of deionized water with continuous stirring until a green solution was obtained.

The pH of the solution was adjusted (Table 4.1) using sodium hydroxide (NaOH) at 1.0 M concentration, in order to obtain different morphologies of the VO_2(D) microparticles. pH of the solution was measured using a pH 211 microprocessor pH meter from Hanna Instruments with an error or $\pm$ 0.1.

For the tungsten composite samples, 2-7 at % of WCl_4 (relative to the vanadium precursor) used as a dopant, was added to the solution. The selection of this dopant was constrained as only a limited range of chemicals was available in Singapore.

The pH of the tungsten - vanadium composite samples was not adjusted and the pH of the samples conditions of the prepared samples can be seen in table 4.2.

Dopant amount calculation is shown in equation 4.1

$$Mass_d = Dopant[\%] \times Mass_p[g] \times \frac{MolarMass_d}{MolarMass_p} \tag{4.1}$$

where:

$Mass_d$**:** Amount of dopant in grams

$Dopant$**:** Molar percentage of dopant required

$Mass_p$**:** Amount of precursor used in the reaction

$MolarMass_d$**:** Molar mass of dopant

$MolarMass_p$**:** Molar mass of precursor

The hydrothermal treatment was carried out using 27 mL of the prepared solution poured into a 45 mL Teflon lined autoclave and heated

Table 4.1: Sample names and descriptions for VO_2(D) powders synthesized by the reaction between NH_4VO_3 and $C_2H_2O_4$ in water. NaOH was used to adjust the pH of the starting solution. All samples were synthesized *via* hydrothermal treatment for 24 hours at 220 °C

Sample	pH of the starting solution
S01	0.65
S02	0.98
S03	1.05
S04	1.52
S05	2.50
S06	3.51
S07	4.60
S08	5.50
S09	6.91

Table 4.2: Sample names and descriptions for VO_2 powders synthesized by the reaction between NH_4VO_3 and $C_2H_2O_4$ in water. WCl_4 was used as the tungsten dopant. All samples were synthesized via hydrothermal treatment for 24 hours at 220 °C

Sample	*pH of the starting solution*	*Dopant (wt%)*
S10	0.96	2
S11	0.93	3
S12	0.99	4
S13	1.00	5
S14	0.94	6
S15	1.00	7

at 220 ^{o}C for 24 hours. After 24 hours of reaction, the autoclaves were cooled down to room temperature and the obtained product was collected by centrifugation, washed with deionized water and ethanol and dried overnight at 60 ^{o}C.

4.4 Characterization

In order to study the VO_2(D) as prepared, undoped samples and the effect of the tungsten in the prepared VO_2(D) microparticles, a series of analyses were performed to the samples.

X-ray diffraction studies were carried out using a D8 GADDS Bruker diffractometer, utilising CuKα radiation between 10 °to 60 °2θ in order to determine the phase of the vanadium dioxide product obtained. Raman spectroscopy analysis were carried out using a Renishaw

1000 spectrometer coupled with a 633 nm laser. The calibration of the equipment was done using a silicon reference.

Morphology and size of the as-prepared samples was studied using a Field Emission Scanning Electron Microscope (FESEM), JEOL JSM-6700F instrument with an accelerating voltage of 5 keV.

Differential scanning calorimetry (DSC) analysis was performed on a DSC 1 instrument from Mettler Toledo. The experiments were carried out between 0 to 300 °C under vacuum with a heating ramp of 5 °C/min. This analysis was performed in order to see if the samples presented a phase transition.

X-Ray photoelectron spectroscopy (XPS) was conducted on a Thermo Scientific K-alpha spectrometer with monochromated Al Kα radiation, a dual beam charge compensation system and constant pass energy of 50 eV (spot size 400 μm). Survey scans were collected in the binding energy range 0 to 1200 eV. High-resolution scans were obtained for the principal peaks of V 2p, O 1s and C 1s. Data was calibrated against C 1s (binding energy, 285.0 eV). Data was fitted using Casa XPS software.

4.5 Results and discussion

VO_2(D) microparticle powders were produced *via* hydrothermal synthesis using ammonium metavanadate (NH_4VO_3) as a vanadium source reacting with oxalic acid to produce vanadium(IV) oxide, carbon monoxide and carbon dioxide as shown in equations 4.2, 4.3, 4.4 suggested by Phoempoon *et al.*[146]. The solution had acidic pH which results in small particle size, good homogeneity and low agglomeration.

$$2NH_4VO_3 + 4C_2H_2O_4 \rightarrow (NH_4)_2[(VO)_2(C_2O_4)_3] + 2CO_2 + 4H_2O \quad (4.2)$$

$$(NH_4)_2[(VO_2)(C_2O_4)_3] \rightarrow 2VOC_2O_4 + 2NH_3 + CO + CO_2 + H_2O \tag{4.3}$$

$$VOC_2O_4 \rightarrow VO_2 + CO + CO_2 \tag{4.4}$$

When adding the sodium hydroxide to the preparation in order to adjust the pH of the solution, orthovanadate, ammonia and water (equation 4.5) are also produced; this affects the homogeneity of the particles, producing agglomeration and therefore growth of the particle size. Moreover, the production of gas during the reaction (NH_3, CO and CO_2) contribute to increase the pressure inside the hydrothermal reactor, thus helping to obtain the required conditions for the formation of the desired phase.

$$NH_4VO_3 + 3NaOH \rightarrow Na_3VO_4 + NH_3 + 2H_2 \tag{4.5}$$

4.5.1 Undoped samples

4.5.1.1 Field emission scanning electron microscope

Field Emission Scanning Electron Microscope images were taken in order to study variation of the morphology and the size of the obtained VO_2(D) by comparison, when the pH of the solution become basic. The pH of the solution is changed from strongly acidic pH (0.65) to acid pH at 6.90.

In Figure 4.1 eight different SEM images from samples with different pH are shown. It is clear that the morphology of the samples changes when the pH of the solution becomes less acidic. When the pH is strongly acidic (0.65) a star/flower shape is observed (Figure 4.1A), this kind of morphology has been reported before in other hydrothermally produced materials and it resembles the desert rose formation of minerals [143] [147]. In Figure 4.2 is shown a typical desert rose

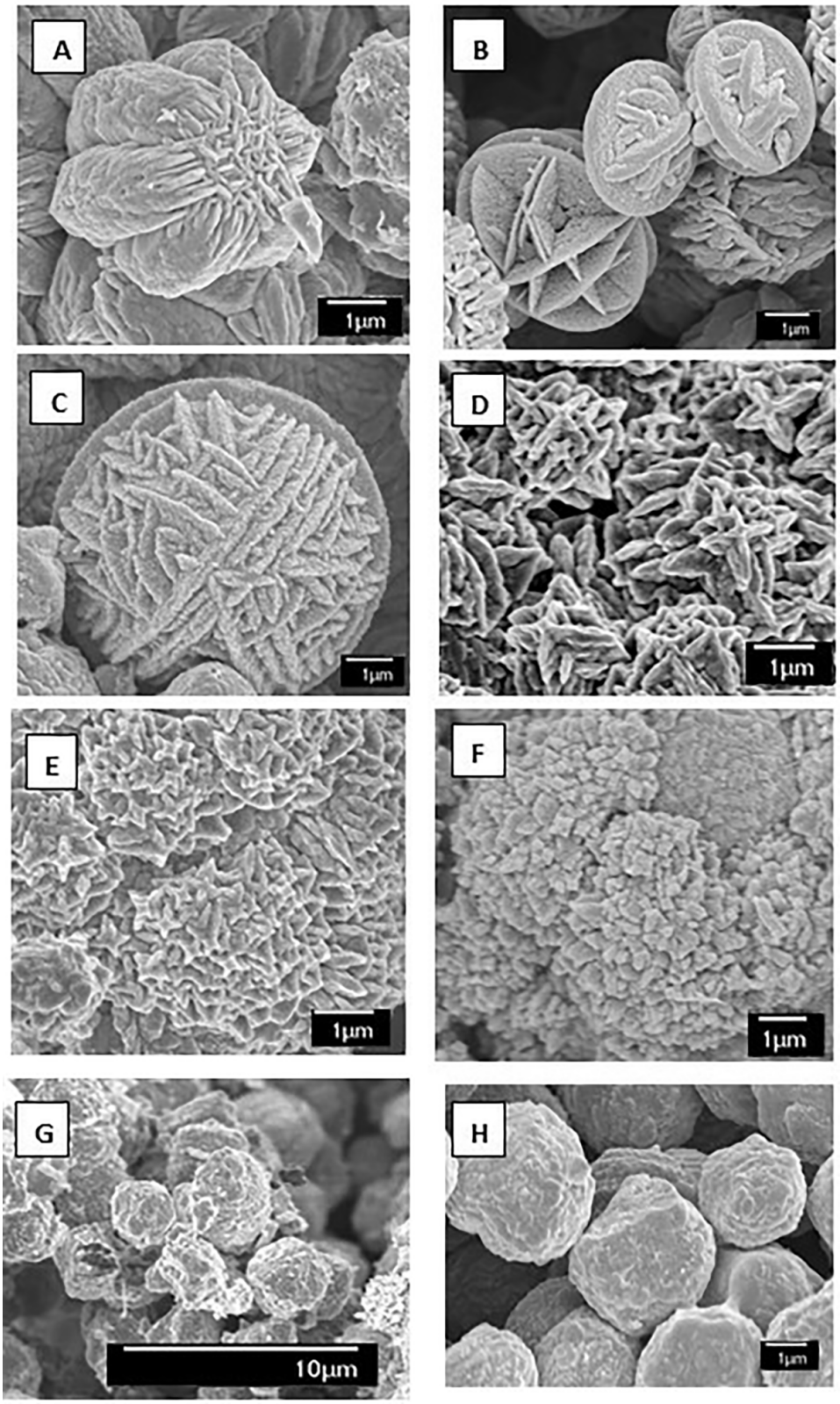

Figure 4.1: SEM of the prepared samples using ammonium metavanadate as a precursor with different pH: (A) 0.65 (B) 0.98 (C) 1.05 (D) 1.52 (E) 2.50 (F) 3.51 (G) 4.60 (H) 6.91

formation reported in the literature [147]. At 0.98 pH, Figure 4.1B, circular fused plates with long coupled particles $\approx$ 1.5 to 2 μm are formed. There is no evidence of remaining star/flower structures at this pH. Making the pH of the solution less acidic to 1.05 in Figure 4.1C we observe a full sphere formed by attached small particles being the smallest around $\approx$ 1 μm and the largest $\approx$ 3 μm, simulating a rubber ball. Further increasing the pH to 1.52 in Figure 4.1D a completely different structure is shown, looking like cross-shape structures between 0.5 to 1 μm overlapping each other to form a bigger structure. In Figure 4.1E with a pH of 1.52, well defined structures such as a cross-shape of around 0.25 to 0.5 μm mentioned before are observed, however it seems that the growth rate has being retarded. At pH 3.51 shows in Figure 4.1F a more homogeneous structure is seen and the attached particles seem to be more close to round shape than to elongated particles, of $\approx$ 0.25 to 0.50 μm. The particles are not elongated anymore, they look like a small robust cross coupled forming a ball. For less acidic pH from 4.60 to 6.91 4.1F, G a complete homogeneous round structure is obtained. It seems like all the small particle structures seen before combined to form a complete massive homogeneous sphere, it is not possible to distinguish small particles forming larger agglomerates.

The formation of these structures is due to the presence of NaOH in the samples [86]. When the NaOH is added to the precursor solution to prepare the samples, the solution becomes less acidic, therefore there is a diminution of the precursor solution solubility, consequently particle agglomeration is expected. See nucleation and growth of particles in chapter 1.

Annealing of the VO_2(D) samples was performed at 350 °C for 3 hours under nitrogen atmosphere in order to study the phase transition from VO_2(D) to VO_2(M) and to control the grain size growth.

In Figure 4.3 it is shown the SEM images of three VO_2(D) microparticles at pH 0.98, 1.52 and 6.91 after annealing. In Figure 4.3A

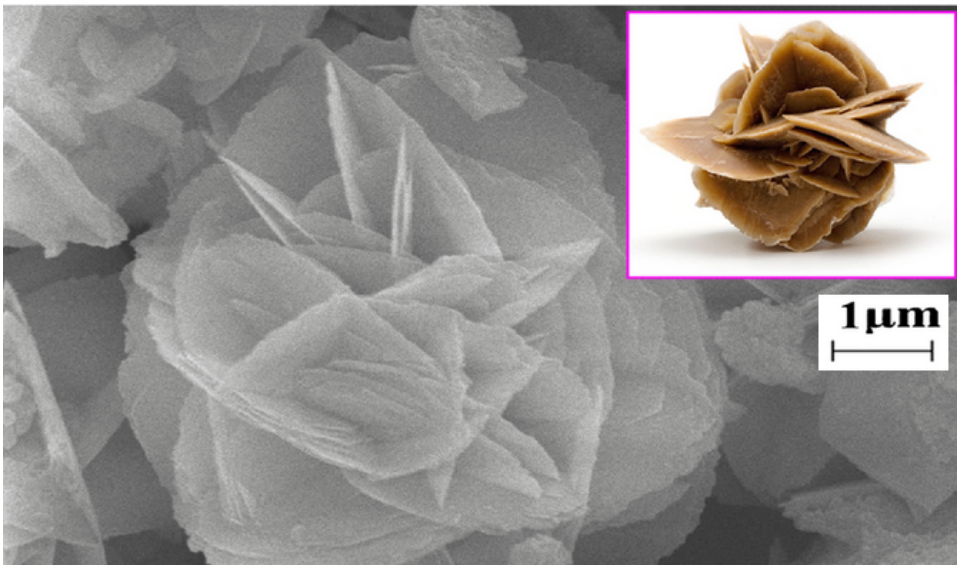

Figure 4.2: Desert rose shaped prepared by Lei *et al.* [147] using zircon dioxide as a precursor (SEM scale: 1 μm). Top-right image is an actual desert rose (formation of crystal clusters of gypsum or baryte) of 6.0 cm in size. Figure used with permission of the author

it is observed that sample S02 at pH 0.98 where thin plates seems to be attached forming a sort of ball and small rods attached forming balls also, no growth in the size particle is observed compared to the same sample before annealing.

In Figure 4.3B, small rods are seen attached to each other, this Figure represents sample S04 with pH of 1.52 after annealing, as in the previous case, no growth in the particle size is shown. Sample 09 with pH of 6.91 is also presented in Figure 4.3C, a series of balls are observed with a diameter of 1.5 to 3 μm, there is no increase in the particle size that can be noted in this samples by comparison with the SEM performed before annealing.

The growth of VO_2 particle size after annealing at high temperatures for longer times have been reported several times in the literature [148] [149]. The advantage of annealing VO_2 samples at low temperatures ($\approx$ 350 °C) is that no growth (or very small increase) in the particle size is shown, as was proved in this work. The results discussed above confirm that it is easy to obtain thermochromic VO_2(M) *via* VO_2(D)

with different morphologies (to be used for different applications) without altering the particle size or morphology initially obtained after thermal treatment at 350 °C.

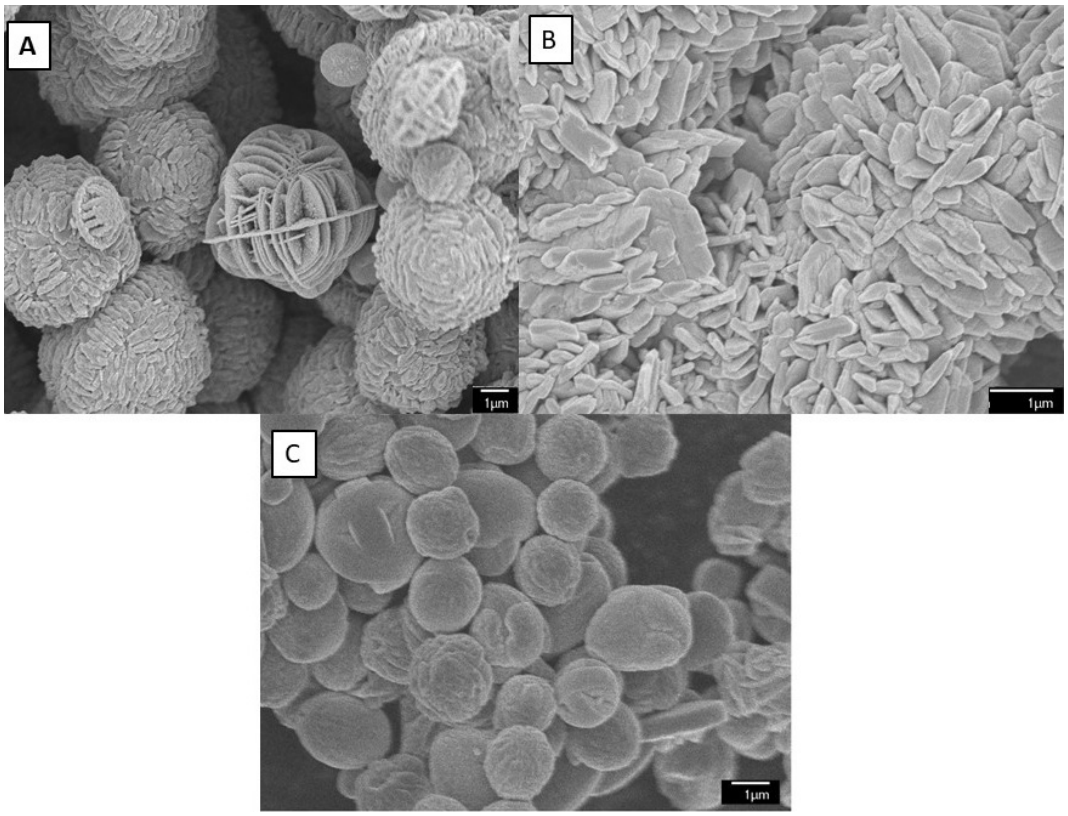

Figure 4.3: SEM of the prepared samples using ammonium metavanadate as a precursor with different pH: (A) 0.98 (B) 1.52 (H) 6.91 after vacuum annealing at 350 °C

4.5.1.2 X-Ray diffraction

XRD patterns of all prepared powders were obtained. The presence of polyvinylpyrrolidone (PVP) in the reaction (0.5 g) is required for the formation of the desired phase VO_2(D), as PVP is well-known as crystal growth modifier and as reducing agent [44] [87] [111]. When PVP is not added, other phases like VO_2(B), VO_2(A) or a mixture of vanadium dioxide phases are obtained as was reported in the literature [44] [131].

Figure 4.4 shows the XRD pattern obtained for six samples with different pH compared to the VO_2(D) pattern from the literature. The range of the pH used is from 0.65 to 6.90, however, previous work in the

literature restrict the pH of the solution between 1.5 to 2.5 as another phase, VO_2(B) phase, is formed in their experiments [46], nevertheless, in this case, VO_2(D) is formed for all pH values used as can be seen in the XRD pattern Figure 4.4.

As NaOH was added to the solution to adjust the pH of the solution, it is possible to think that sodium orthovanadates were formed (instead of VO_2(D)), however Song *et al.* study the effect of sodium on the phase transition of tungsten doped vanadium dioxide [**?**] and reported that the sodium added to the solution used for hydrothermal synthesis is generally removed during the washing step, therefore, it is unlikely the presence of sodium orthovanadates.

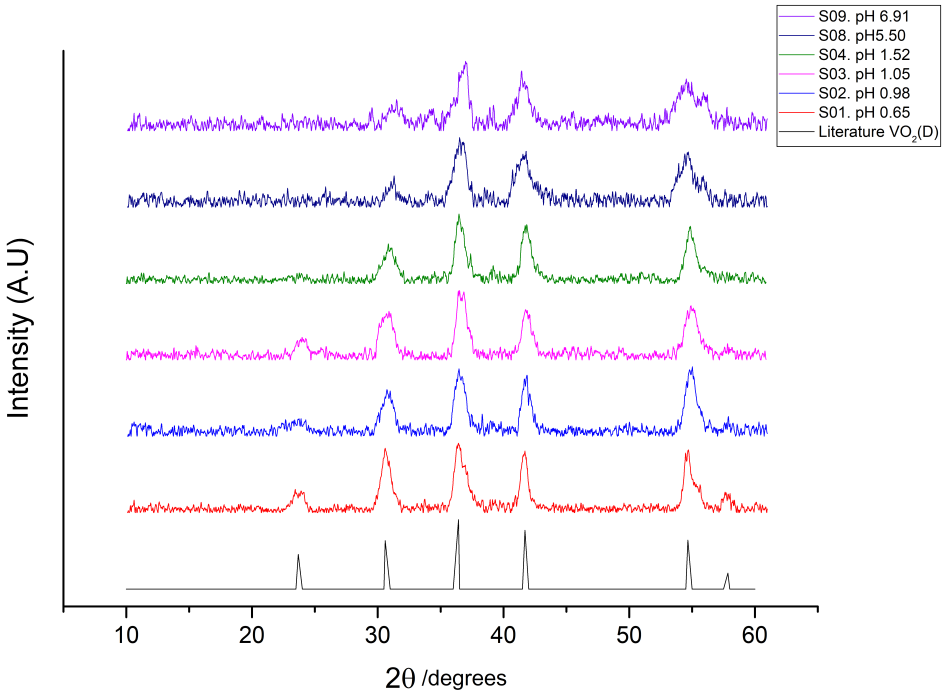

Figure 4.4: XRD pattern of six VO_2(D) microparticle samples, with different pH obtained *via* hydrothermal synthesis compared with the VO_2(D) reference pattern from the literature

The as-prepared samples of VO_2(D) microparticles were calcinated in a vacuum furnace at 350 °C for 2 hours in order to obtain thermochromic VO_2(M). Annealed powder samples of different phases of vanadium oxide are regularly reported in the literature, however, the cal-

cination temperatures needs to be as high as 500 - 600 °C to transform other phases, like VO_2(A,B) into VO_2(M) [44] [43]. In terms of VO_2(D) to VO_2(M) transformation, Liu *et al.* performed a heat treatment at 320 °C for 2 hours under pure nitrogen atmosphere [44] while Song *et al.* calcined VO_2(D) product between 250 to 600 °C for 3 hours. However only samples calcined at temperatures higher than 500 °C show thermochromic behavior [45].

Figure 4.5 shows the XRD pattern of the microparticles of VO_2(D) after vacuum annealing at 350 °C for 1 hour; as can be seen, all the peaks correspond to thermochromic VO_2(M), meaning the conversion was successful and this proves the fact that the monoclinic phase can be obtained via VO_2(D) at low temperature and for a short calcination time.

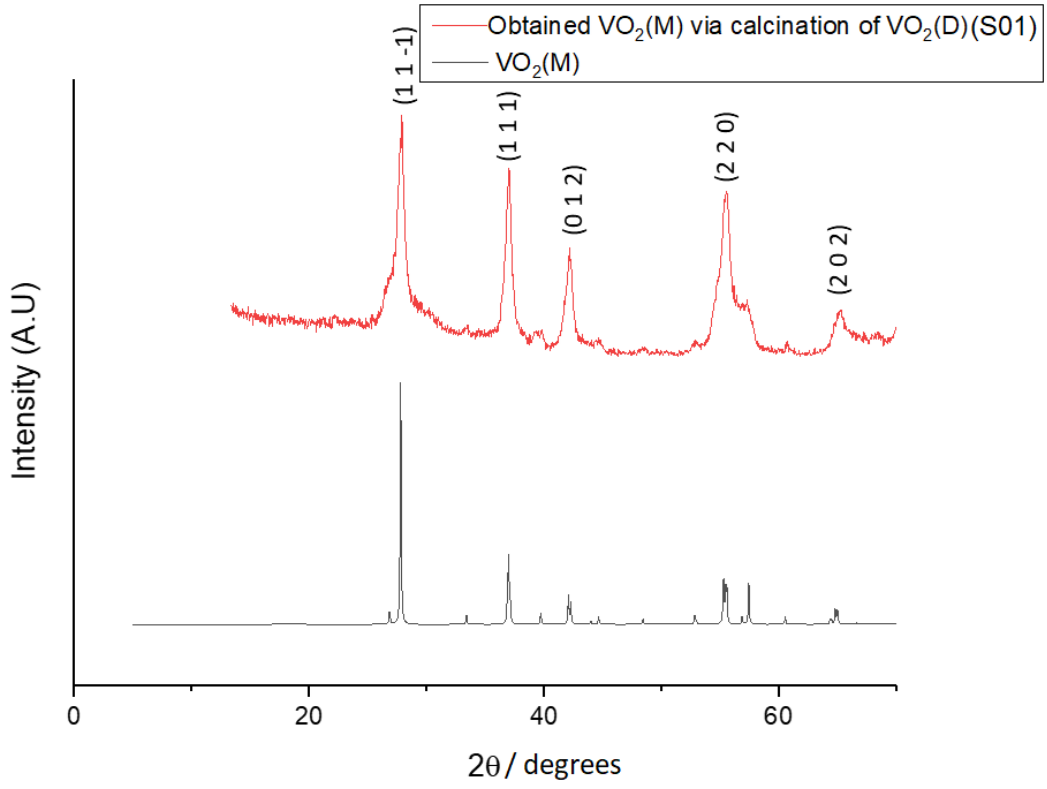

Figure 4.5: XRD pattern of the sample S01 VO_2(D) microparticles annealed under vacuum at 350 °C for 2 hours converted into VO_2(M) compared with the monoclinic VO_2 in the literature

This represents an improvement in the VO_2 field, as there is always

the need to reduce the working/annealing temperatures in a process to make it easy/safer for reproduction or industrial processes.

4.5.1.3 Differential scanning calorimetry

Differential scanning calorimetry was performed to one VO_2(D) microparticles powder sample (S03) in order to study if this phase presents a transition phase. The result of the analysis it is presented in Figure 4.6 and as shown, no phase transition is present from 0 to 300 °C, which means that the sample does not have thermochromic behavior in the range temperature studied.

In Figure 4.6 it can be observed a slope in the heating cycle around 200 to 300 °C, this can be explained as the starting transformation of the sample from VO_2(D) to VO_2(M). We suspect that our sample is composed of particles of different sizes, and it is possible that the nano-size particles are facing the transformation that, for the whole microparticle system takes places at 350 °C.

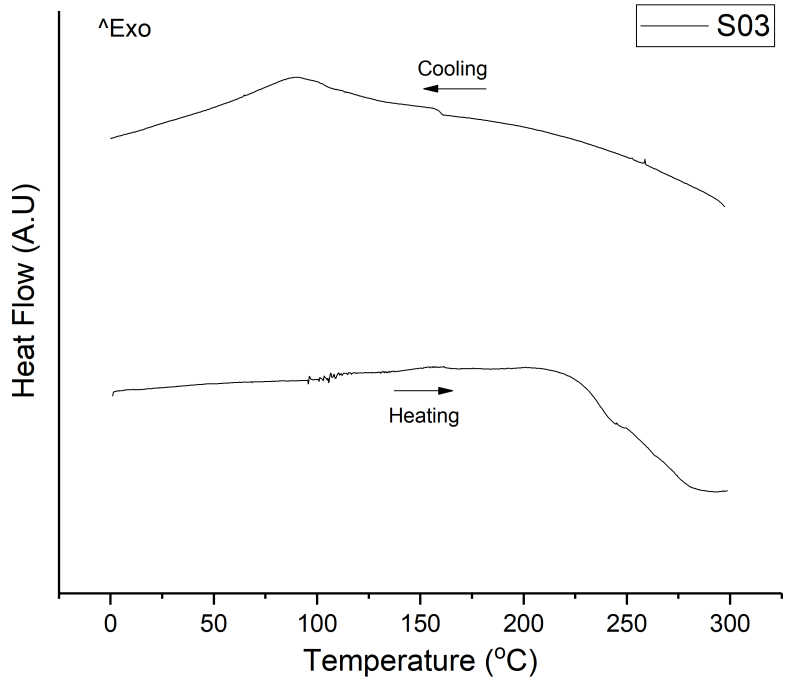

Figure 4.6: DSC curves of VO_2(D) microparticles from 0 to 300 °C

The usual route to obtain thermochromic VO_2(M) is annealing the samples of VO_2(A,B) at 550 - 600 °C under a controlled atmosphere for a few hours. For example Popurri *et al.* reported that is necessary to anneal VO_2(B) particles under vacuum at 550 °C for 1 hour to obtain VO_2(M) [150] and Sahana *et al.* reported the VO_2(B) to VO_2(M) transition after annealing under argon atmosphere between 400 to 500 °C [151]. Annealing at high temperatures is not recommended as the grain size of the particles increase and this is not ideal for vanadium dioxide as it has been demonstrated that small particle size often represents better thermochromic performance [67].

In this work, the synthesized samples of VO_2(D) microparticles were annealed at 350 °C under vacuum for 2 hours in order to obtain thermochromic VO_2(M).

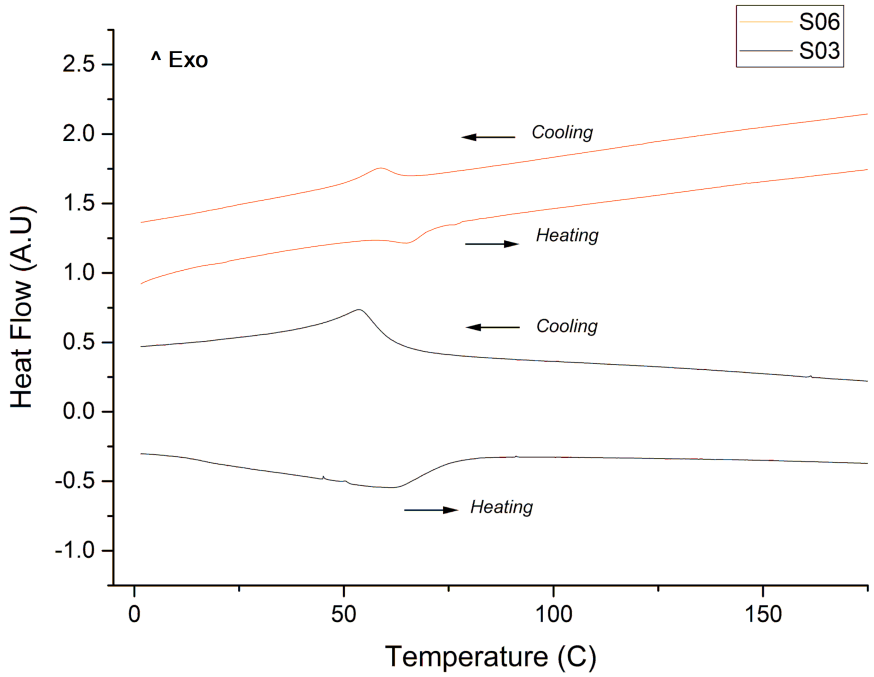

Figure 4.7: DSC curves of VO_2(M) obtained via micro-VO_2(D) after heat treatment

The required temperature to transform the D phase to the M phase is much lower than that reported in the literature to obtain thermochromic

VO_2(M) *via* VO_2(B) [150] [151]. The transition from VO_2(D) to VO_2(M) has been reported in the literature during calcination of samples at 300 °C to 600 °C [44] [87] [45].

Figure 4.7 shows the DSC analysis of the VO_2(D) samples after vacuum annealing at 350 °C. In the Figure it can be observed the typical behavior of a thermochromic VO_2 sample where an endothermic peak appears in the heating cycle around 62 $\pm$ 2 °C, no further peaks are shown up to 200 °C, then an exothermic peak is present in the cooling cycle around 55 °C. Two samples are shown in this Figure, and in both cases the samples present an endothermic peak in the heating cycle and an exothermic peak in the cooling sample, representing the transition from VO_2(M) to VO_2(R) and VO_2(R) to VO_2(M) respectively.

The metal-semiconductor transition (MST) temperature for this thermochromic sample obtained via VO_2(D) is lower than reported in the literature for bulk VO_2(M) which is 68 °C [34] [102], this represents an improvement, as for architectural applications a temperature close to 25 °C is desired.

4.5.1.4 Raman Spectroscopy

Raman spectroscopy analysis was performed on the VO_2(D) samples in order to study the vibrational properties of the samples, the result of two samples with different pH is shown in Figure 4.8.

The spectra in Figure 4.8 could be the spectra of V_2O_5 [14], however, Raman bands of V_2O_3 and V_6O_{13} compounds are very similar to V_2O_5 Raman band as reported in the literature by Chen *et al.* [137] and Troy [75], therefore, if the band are not well defined it is impossible to determine if it is a mixture of phases, the V_2O_5, V_6O_{13} or the V_2O_3 compound.

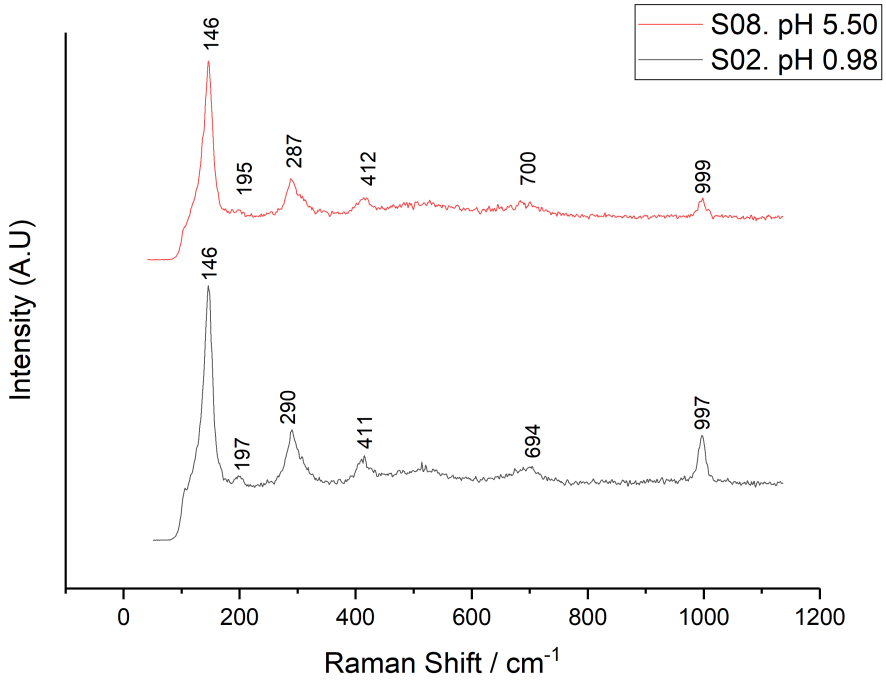

Figure 4.8: Raman spectra of Sample S08 with pH of 5.50 and Raman spectra of sample S02 with pH of 0.98

4.5.1.5 X-Ray photoelectron spectroscopy

Figure 4.9 shows the surface oxidation state of as-prepared VO_2(D) microparticles. The surface oxidation state of the as-prepared sample was a mixture of V^{4+} (516.5 eV) and V^{3+} (515.3 eV). Similar values has been reported before in the literature ($\pm$ 0.2 eV) for V^{4+} by Gracia *et al.* [152], Mendialdua *et al.* [153] and by Colton *et al.* [154]. For V^{3+} these values have been reported in the literature ($\pm$ 0.2 eV) by Silversmit *et al.* [39] and by Mendialdua *et al.* [153].

The XPS analysis shows mainly presence of vanadium 3+ and vanadium 4+. The surface analysis result indicates that there is bigger proportion of vanadium 3+ in the sample, this is probably because during the hydrothermal synthesis some parts of the sample over reduce the vanadium 4+, resulting in vanadium 3+.

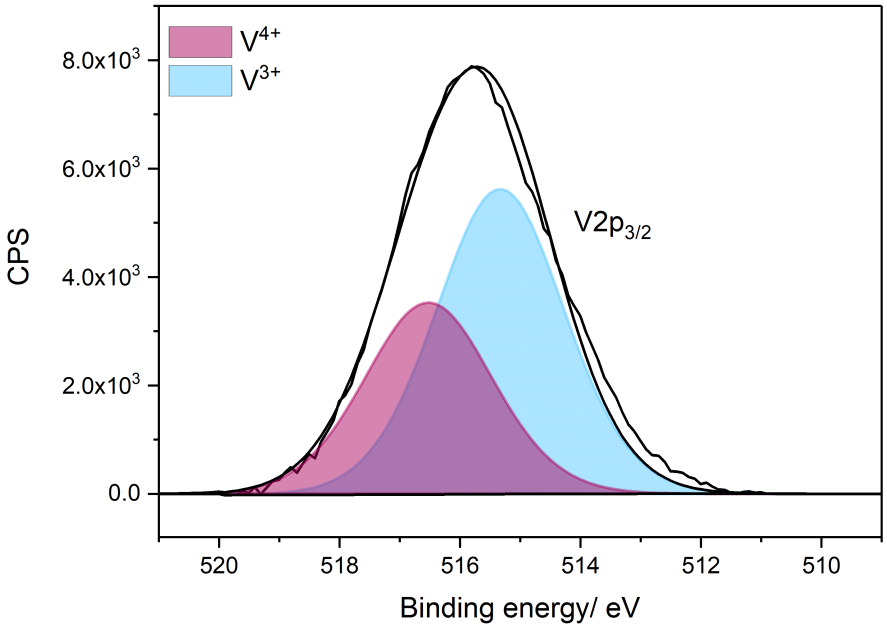

Figure 4.9: Surface XPS spectrum for vanadium binding energy from VO_2(D) microparticles prepared *via* hydrothermal synthesis

On the other hand, with these results it can be concluded that there is no oxidation of the surface (as expected as result of exposure of vanadium 4+ to air) and of the sample due to the absence of detectable vanadium 5+.

The analysis were performed 6 months after the preparation of the samples and stored at room temperature. This is an important result as the samples are meant to be used because of its thermochromic properties after calcination of VO_2(D) microparticles at low temperatures and is very important that the samples stay in 4+ oxidation state, so no long and high annealing temperatures are needed. It is well known that vanadium species tends to oxidize in presence of air, however, the as prepared microparticles samples shows stability over the time (6 months).

The XPS results reported in the literature for VO_2(D) samples [44], shows the peak of $2p_{3/2}$ at 515.4 eV affirming this is vanadium 4+ bulk value, however, our analysis shows same value 515.4 eV ($\pm$ 0.1 eV)

for vanadium 3+ in concordance with other literature works cited previously.

The XPS results suggests that the as-prepared VO_2(D) sample is composed on the surface by vanadium 4+ and vanadium 3+, while Raman spectroscopy, also a surface analysis technique, suggest that the surface of the sample is composed by vanadium 5+, however, it is important to mention that Raman bands of V_2O_5 [14] and V_2O_3 [137] are very similar and is hard to distinguish between them if the band are not strong enough.

The surface analysis is not conclusive in terms of the surface oxidation state composition of the as-prepared VO_2(D) microparticle sample as XPS analysis shows a mixture of vanadium 4+ and vanadium 3+ while Raman spectroscopy analysis shows Raman bands than can be addressed either to V_2O_5 or V_2O_3, but no sign of the presence of vanadium 4+ in the surface by Raman, however, combining the two surface analysis it can assumed that the surface of the sample has in its composition vanadium 3+ and it can be a mixture of different oxidations states of vanadium.

On the other hand, XRD of the VO_2(D) sample shows the typical VO_2(D) pattern reported in the literature, and this result suggest that the bulk of the sample is composed by vanadium 4+.

4.5.2 Vanadium-Tungsten composite samples

4.5.2.1 Field emission scanning electron microscope

SEM images of samples with 2, 3, 4 and 5 wt% were taken to study the effect of the tungsten in the morphology of the samples. pH of the solution of the as-prepared doped samples was not altered, which means that no agglomeration due to the effect of the NaOH is expected.

The morphology observed in the W-VO_2(D) (Figure 4.10) is composed of long rods attached to each other forming, in some cases, star like structures. The obtained morphology is homogeneous and similar in all doped samples. Adding different amounts of tungsten to the

samples does not affect the morphology of the product.

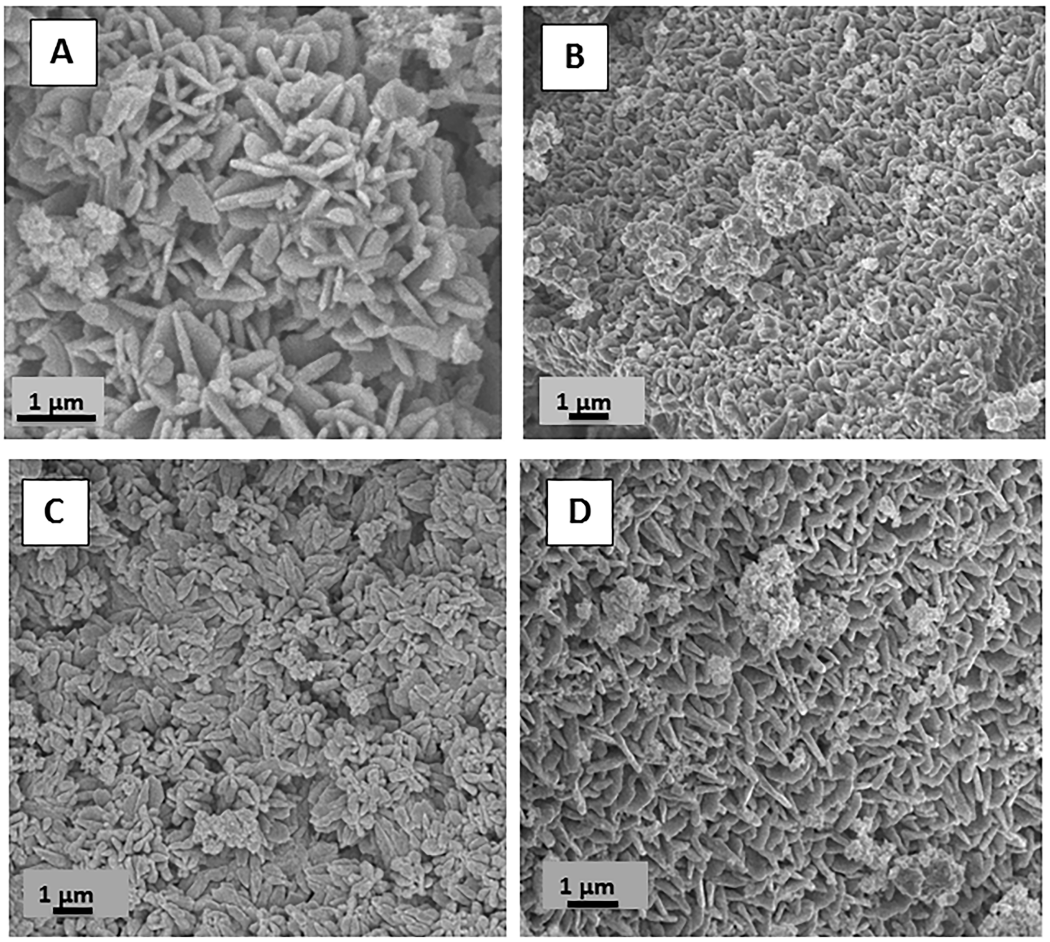

Figure 4.10: SEM of the tungsten composite VO_2(D) prepared samples with (A) 2 wt% (B) 3 wt% (C) 4 wt% (D) 5 wt% of W

The morphology of the tungsten doped samples is different to the morphology presented by the undoped samples at the same pH, which means that addition of tungsten acts as a morphology director producing in all cases star shape long rods.

The pH of the precursor solution used for the doped samples range between 0.93 to 1.00. Morphology of the un-doped VO_2(D) samples in the mentioned pH range are composed by attached rods in a plate, forming a sort of spherical structure, while the doped samples, as mentioned before, are long rod attached structures forming in some cases star shape morphology.

Scanning electron microscopy was performed on the tungsten doped microparticles VO_2(D) samples after vacuum annealing at 350 °C. Figure 4.11 shows the particles morphology of three samples (4.11 A: 2 wt% 4.11 B: 3 wt% and 4.11 C: 4 wt%) after calcination.

The obtained samples after calcination present not only star/elongated shaped particles, but also round structures. This could be due to the calcination process that provokes the growth of the particle size or due to the presence of VO_2(D) undoped particles, as the morphology obtained resembles undoped VO_2(D).

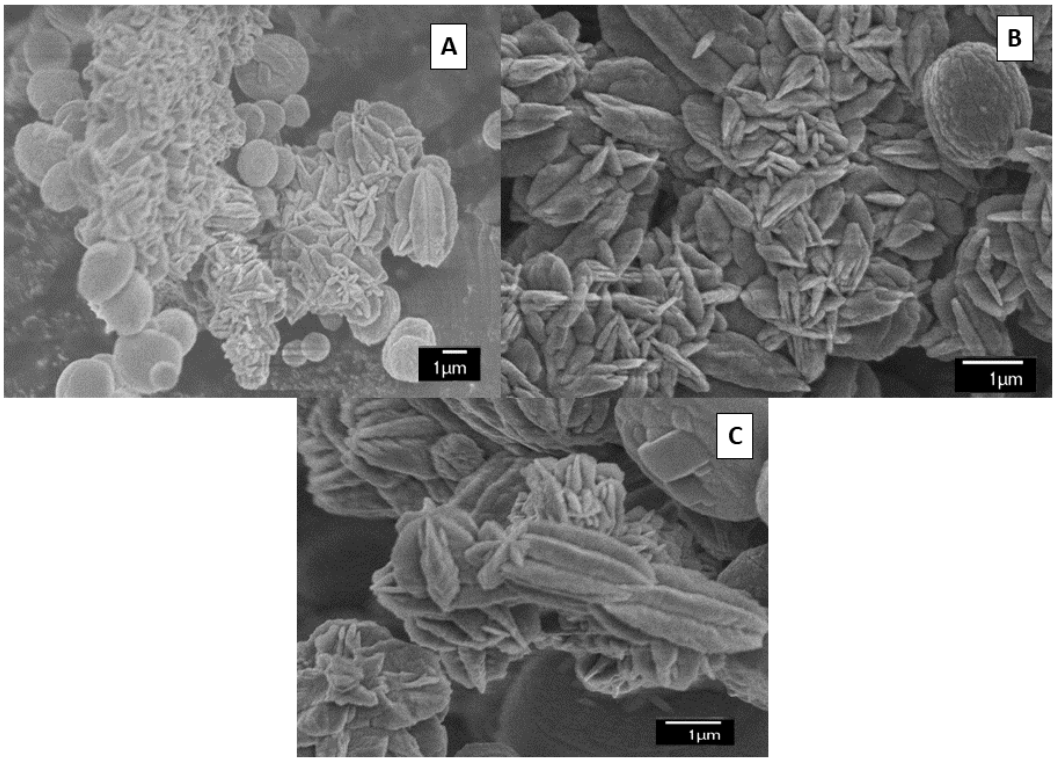

Figure 4.11: SEM of the W-VO_2(D) prepared samples with (A) 2 wt% (B) 3 wt% (C) 4 wt% of W after vacuum calcination at 350 °C

4.5.2.2 X-Ray diffraction

X-Ray diffraction was performed in order to study the phase of the as-prepared W-VO_2(D) particles.

In Figure 4.12 is shown the XRD pattern of the samples intended to be doped with 2-7 wt% of tungsten compared with the VO_2(D) pattern

from the literature. As can be seen, the peaks are very broad suggesting that either the particles are on the order of nanometers or that the produced particles are not fully crystalline. In this case, it is considered that the as-prepared W-VO_2(D) microparticles are composed of agglomerated nanoparticles and this is the reason for the broad peaks.

A common concern that can not be solved *via* XRD analysis when broad peaks are shown, is the fact that other phases/compounds are formed in the product, however, XPS suggests that, only V^{4+} is present

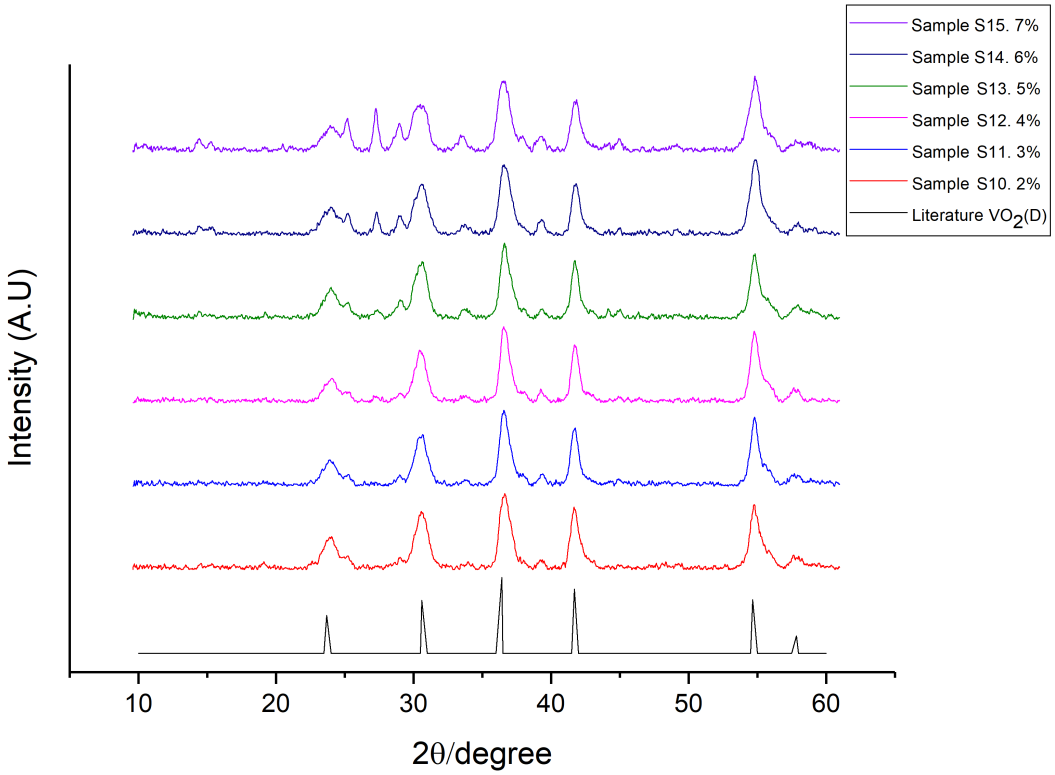

Figure 4.12: XRD patterns of the obtained VO_2(D) doped with 2, 3, 4, 5, 6 and 7 wt% of tungsten compared with the VO_2(D) pattern presented in the literature

The extra peaks that are shown in samples with 5, 6 and 7 wt% of dopant can be indexed to WO_3, this means that the tungsten is not being incorporated into the VO_2 lattice but is actually forming tungsten trioxide. In this case the obtained samples were not tungsten doped but tungsten-vanadium composite VO_2(D).

Tungsten doped samples (2 and 3 wt%) were annealed in vacuum at

350 °C to produce thermochromic VO_2(M). Figure 4.13 shows the obtained pattern for a sample doped with 3 wt% of tungsten relative to the amount of vanadium. VO_2(D) samples with high dopant concentration (4%, 5% and 6%) were not annealed in this work. The obtained peaks at 2θ = 27.9°, 36.9°, 42.1°and 55.5°correspond to monoclinic VO_2 without shift (for tungsten doped VO_2 samples, a slight shift towards big angles is expected, this is because the atomic radius of tungsten is bigger than the atomic radius of vanadium). This can indicate that the tungsten was not incorporated to the lattice, furthermore, the samples are not doped but are a WO_3-VO_2 composite.

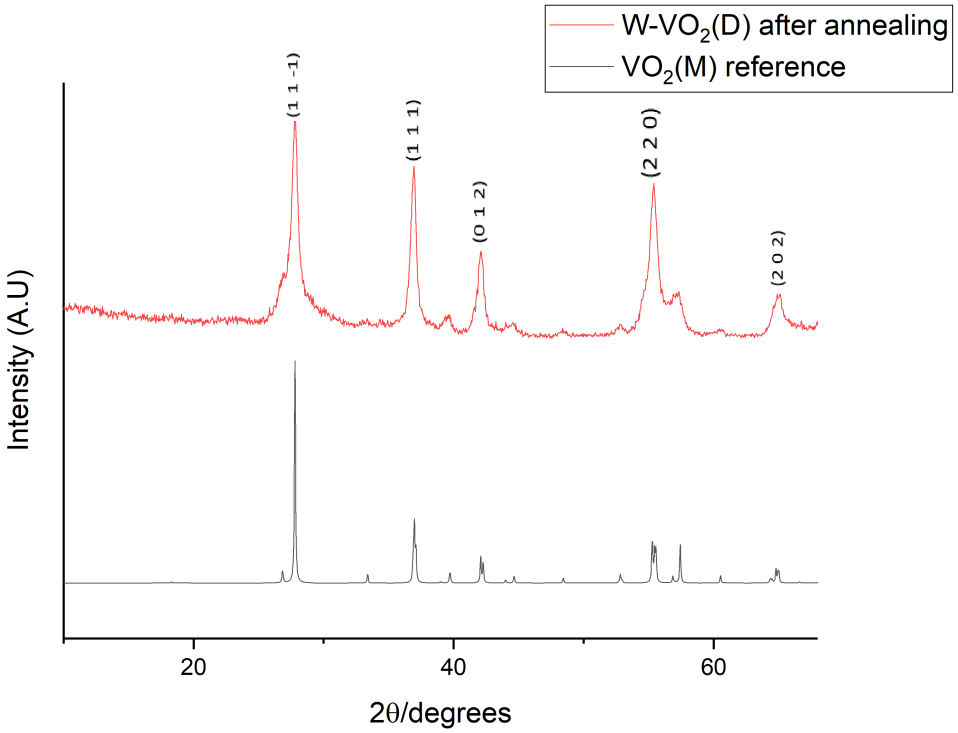

Figure 4.13: XRD patterns of the obtained VO_2(D) doped with 3 wt% of tungsten compared with the VO_2(D) pattern presented in the literature after vacuum annealing at 350 °C

Energy-dispersive X-Ray spectroscopy (EDX) was performed on the samples doped with 2, 3 and 4 wt% to compare the added and the actual amount of tungsten present in the prepared material. Despite the fact that there is the presence of tungsten in the samples, as shown in table 4.3, the added and the measured amount of tungsten in the sam-

ple does not match. Even more, for sample S11, where the amount of tungsten was increased compared to sample S10, the measured amount of tungsten is lower, this could be due to different factors as the error of the instrument and measurements, uncertainty, non homogeneous distribution of the tungsten in the sample, among others.

This means that not only the tungsten was not incorporated into the VO_2(D) lattice (but formed tungsten oxide) but also part of it was washed away. Further experiments have to be done to understand if the dopant precursor is not the adequate or if the VO_2(D) does not allow dopants,for example, using a different tungsten precursor.

Table 4.3: Results of added and measured (by EDX) tungsten in the as-prepared samples

Sample	*Added W (wt%)*	*Measure W (wt%)*
S10	2	1.6
S11	3	1.3
S12	4	2.8

4.5.2.3 Differential scanning calorimetry

Differential scanning calorimetry was performed on the samples in order to study the transition phase in the samples.

The analysis was performed before and after annealing to understand if the tungsten composite VO_2(D) itself presents any change in phase transition.

As shown in Figure 4.14, differential scanning calorimetry to a 3 wt% tungsten composite sample was performed from 0 to 300 °C under a nitrogen atmosphere, no phase transition is shown, as can be seen in the Figure 4.14, at least not in the range studied. The same analysis was performed to all doped samples and the same result was obtained, for simplicity purposes, only one result is shown here.

Differential scanning calorimetry was performed on the tungsten doped samples after annealing them under vacuum at 350 °C for 2 hours. After annealing the samples, the thermochromic VO_2(M) phase was obtained. It is well known that tungsten is widely used in VO_2 to

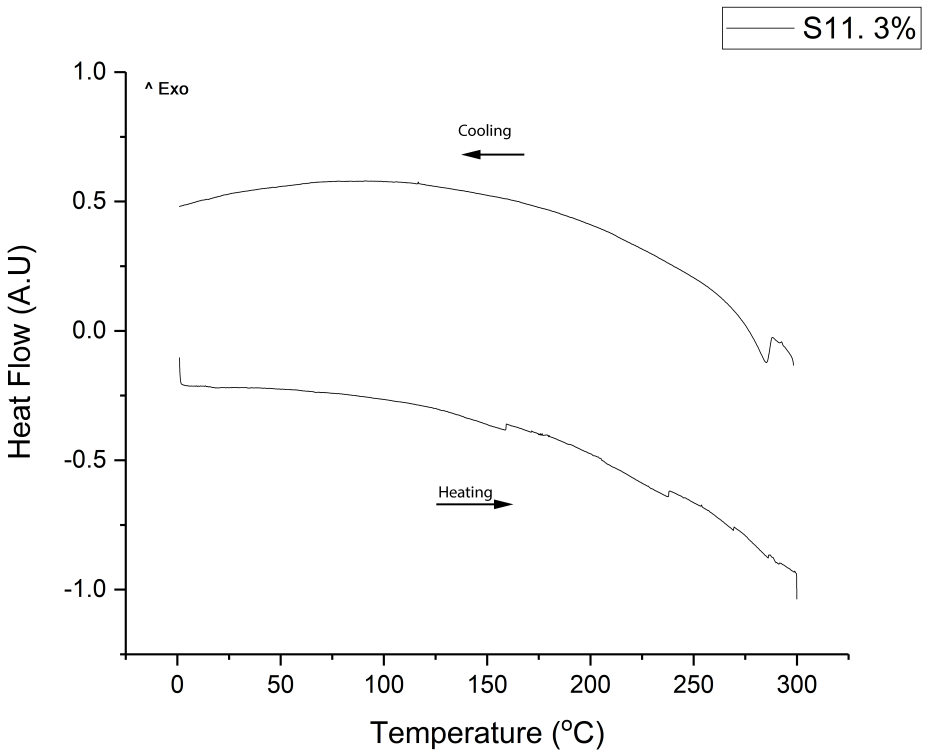

Figure 4.14: DSC curves performed to tungsten vanadium composite VO_2(D) with 3 at% of W before annealing

lower the transition temperature, however, as demonstrated in Figure 4.15, the transition temperature does not decrease as expected. Actually, it is the same transition temperature (61 °C) reported for VO_2(D) undoped samples after annealing. The transition temperature value was obtained using the integral tool of the DSC analysis software from Mettler Toledo.

This result is interpreted as no tungsten was incorporated into the VO_2 lattice (but formed tungsten oxide), corroborating the results discussed before in the X-Ray diffraction analysis section in this chapter for doped samples. This can be either because the tungsten precursor used is not suitable for doping the samples or because the VO_2(D) phase does not allow dopants into the lattice.

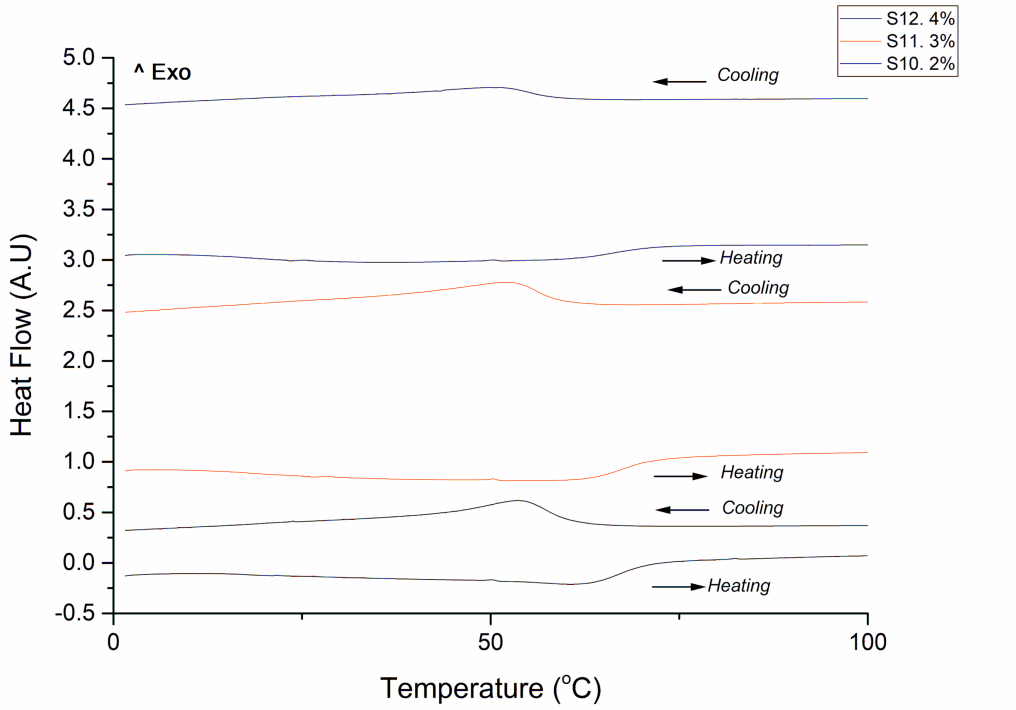

Figure 4.15: DSC curves of tungsten doped VO_2(M) obtained *via* tungsten doped micro- VO_2(D) after heat treatment

4.5.2.4 Raman Spectroscopy

Raman spectra of two tungsten doped samples was performed in order to study the phase of the as prepared samples. Results are shown in Figure 4.16. The obtained spectrum is seems to be the V_2O_5 compound however, as mentioned before, the V_2O_3 compound has similar Raman bands, therefore no conclusions can be drawn if the peaks are not very well defined. There are no extra peaks that suggests the presence of tungsten compound in the sample.

As Raman is a surface analysis, it is very common to obtain V_2O_5 in the samples as the surface gets oxidized, however, XPS results for undoped samples shows a mixture in the composition of vanadium 3+ and vanadium 4+, this can suggests that actually the surface can be a mixture of vanadium oxide in different oxidations states.

No Raman analysis for tungsten dope VO_2(D) microparticles is reported in the literature so far.

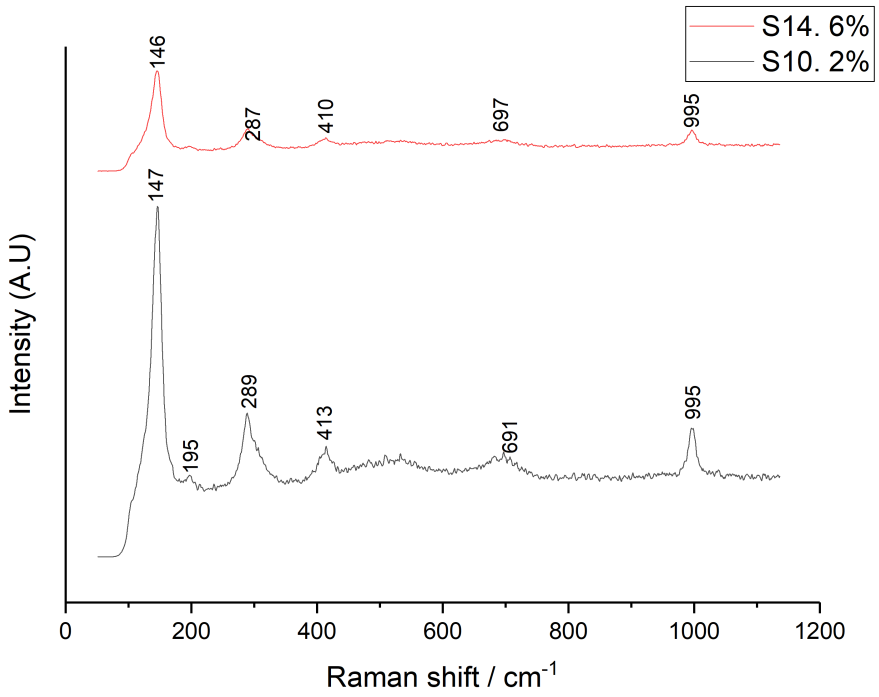

Figure 4.16: Typical V_2O_5 Raman spectra obtained from two tungsten vanadium composite VO_2(D) samples with 2 and 6 wt%

4.6 Conclusion

Different morphologies and sizes of microparticles of VO_2(D) were synthesized in this work using oxalic acid as a reducing agent and NH_4VO_3 as a precursor *via* hydrothermal synthesis. The as prepared samples present different morphologies like a star/flower shape at 0.65 pH with a size of around 1.5-2.5 μm to a big round ball shape at 6.91 pH of 3-4.5 μm.

The studied XRD of the as prepared VO_2(D) samples match the XRD pattern shown in the literature [44]. The obtained peaks are broad, which advise that the big particles obtained are composed by nanoparticles agglomeration as other analysis suggests that the obtained phase is pure.

VO_2(D) itself does not present thermochromic behavior in the studied range from 0 to 300 °C, however, thermochromic VO_2 is successfully produced by annealing the samples under vacuum at 350 °C for 2

hours. The monoclinic samples present thermochromic behavior with a MST transition at 61 °C (studied using differential scanning calorimetry analysis), lower than the bulk VO_2 reported in the literature.

Raman spectroscopy was performed and the typical V_2O_5 spectra was obtained. This result only can prove that the surface of the samples were oxidized due to the exposition of the samples to the air. Bulk analysis can not be performed using this method.

As the obtained particles are in the micron size, preparation of composite thin films using the microparticles without further treatment it is not easy due to its size.

Tungsten doped VO_2(D) were intended to be prepared for the first time in this work. The XRD pattern obtained for these samples match the literature VO_2(D) for samples doped with 2, 3 and 4 wt%. For samples with higher quantity of the dopant, the XRD pattern obtained present extra peaks, indexed to WO_3, suggesting that the VO_2(D) lattices does not allow higher quantities of dopants.

EDX was performed to the samples in order to check the quantity of tungsten present in the samples and compare it with the added amount. Tungsten was found in the samples, however, the amount does not match to the added quantity. This results propose that the tungsten was not incorporated properly to the lattice and moreover, it was probably washed during the process.

Tungsten is a widely used dopant in vanadium dioxide film to reduce the transition temperature of the thermochomic VO_2. The W-VO_2(D) does not present thermochromic behavior itself in the studied range from 0 to 300 °C, however, after annealing the sample under vacuum at 350 °C for 2 hours, VO_2(M) is obtained. This product presents thermochromic behavior and a MST transition at 61 °C. This result represents an improvement compare to the typical MST transition temperature of bulk VO_2(M) at 68 °C, however, no reduction of the MST was observed for tungsten doped samples.

Addition of tungsten to the VO_2(D) samples results in a star/long rod shape morphology, meaning that the tungsten is actually acting as a morphology director in this case. All the studies samples present this long rod/star shape morphology with an approximate size of 1 μm.

Raman spectroscopy was performed to the tungsten vanadium composite samples, however no bands can be indexed to VO_2(D). The obtained spectra correspond to the well known V_2O_5 Raman spectra [155].

Chapter 5

VO_2(D) structure

5.1 Introduction

Vanadium(IV) oxide has different polymorphic forms; VO_2(A), VO_2(B), VO_2(C) and the recently reported VO_2(D). Vanadium(IV) oxide has been widely studied since it was reported back in the late 1950s. Different phases and the so called Magneli phases have been identified, studied and reported in the literature.

The last reported phase, VO_2(D), have gained interest in the field because it can be transformed into thermochromic VO_2 after mild calcination (around 180 °C in our published work [87]) under a controlled atmosphere during short periods of time. Moreover, nanoparticles and microparticles of VO_2(M) obtained *via* VO_2(D) have a phase transition from monoclinic to tetragonal phase at lower temperatures ($\approx$ 61 °C) than the bulk VO_2(M) (68 °C).

The VO_2(D) phase has not been studied extensively, however, it can gain even more importance in the field as it is possible to obtain pure VO_2(D) microparticles with different morphologies that can be used for diverse applications such as sensors, batteries among others.

5.2 Aim

The main objective of this chapter is to demonstrate experimentally that the recently reported VO_2(D) phase is indeed, a new phase of vanadium(IV) oxide and not a mixture of vanadium dioxide phases, and also

to discuss in detail the VO_2(D) crystal structure proposed in the literature compared with the results obtained in this work.

5.3 Important definitions

Crystallinity: periodic array in large atomic distances [156].

Crystal structures: description of the ordered arrangement of atoms, ions or molecules in a crystalline material [156].

Unit Cell: small repeating entity of the atomic structure. It defines the crystal structure with the atom position [156].

Lattice parameter: physical dimension of unit cells in a crystal lattice. For 3-D arrays there are usually three lattice constants, named a, b and c [156]. Table 5.1 shows some crystal systems with its respective lattice constants [156].

Table 5.1: Crystal systems parameters

System	Lattice constant and angles
Cubic	a = b = c, α=β=γ = 90°
Tetragonal	a = b $\neq$ c, α = β = γ = 90°
Orthorhombic	a $\neq$ b $\neq$ c, α = β = γ = 90°
Rhombohedral	a = b = c, α = β = γ $\neq$ 90°
Hexagonal	a = b $\neq$ c, α = β = 90°, γ = 120°
Monoclinic	a $\neq$ b $\neq$ c, α = γ = 90°, $\neq$ β
Triclinic	a $\neq$ b $\neq$ c, α $\neq$ β $\neq$ γ $\neq$ = 90°

Indexing: assigning the correct Miller indices to each peak of a diffraction pattern.

Phase ID or pattern matching: match an experimental diffraction pattern with a database of diverse diffraction patterns until finding a similar one.

Dicvol: Program written in Fortran 77 and used to index new structures from powder diffraction pattern [157]. Dicvol requires, among others, the input of the number of peaks that the new pattern has, the type of crystallographic system that wants to be examined, the 2θ peak position and also information about the wavelength used to collect the data. The program offers as a result a series of lattice parameters corre-

sponding to different crystal systems such as cubic, tetragonal, hexagonal, orthorhombic, monoclinic and triclinic.

Rietveld: Rietveld refinement is a very well known technique described by Hugo Rietveld used to characterize crystalline materials [158]. The Rietveld method uses the least squares of a refined theoretical powder pattern lines until it matches with the experimental powder XRD pattern [159].

5.4 Experimental and characterization

All VO_2(D) products were synthesized *via* hydrothermal synthesis using a 45 mL reactor.

In a typical synthesis to form VO_2(D) microparticles (samples M1 and M3 in this chapter), 0.625 g (0.0215 mol) of ammonium metavanadate (NH_4VO_3) was used as a vanadium source, 2.52 g of oxalic acid (0.0279 mol) ($C_2H_2O_4$) was used as a reducing agent and 0.5 g of polyvinylpyrrolidone (PVP) were mixed into 50 mL (at room temperature) of deionized water with continuous stirring until a green solution was obtained.

In a typical synthesis to form VO_2(D) nanoparticles (samples N1 and N2 in this chapter) the reaction took place in a 45 mL lined autoclave over 48 hours at 240^{o}C. The samples were prepared by mixing 0.45 g (0.0024 mol) of vanadium pentoxide (V_2O_5) as a vanadium source, 0.75 mL (0.0140 mol) of sulfuric acid (H_2SO_4) as a reducing agent and 0.25 mL (0.0079 mol) of hydrazine (to promote formation of the desired phase) into 10 mL of DI water. The solution was vigorously stirred for 3-5 minutes to obtain a green solution.

To obtain VO_2(D) nanoparticles it is very important to control the pH of the solution. This has to be in range of 6.6 to 6.9; outside of this range, other phases like V_2O_3, VO_2(B) (or mixture of phases) are obtained.

The pH of the starting solution for microparticles and nanoparticles was adjusted using sodium hydroxide (NaOH) at 1.0 M concentration.

X-Ray diffraction studies were carried out using a D8 GADDS Bruker diffractometer, utilising CuKα radiation between 10°to 60°2θ. Raman spectroscopy analysis were carried out using a Renishaw 1000 spectrometer coupled with a 633 nm laser. The calibration of the equipment was done using a silicon reference.

For the X-Ray absorption near edge structure the VO_2(D) samples were measured on XAFCA beamline (beamline features [160]) at the Singapore synchrotron light source. A Si(111) double crystal monochromator was equipped to filter the X-Rays. The samples were pressed to pellets with 10 mm diameter and data were recorded under transmission mode. Analysis of the obtained data was performed by Dr. Ian Godfrey using Athena 0.9.25 [**?**]; multiple scans from each film were merged to improve signal-to-noise ratio, followed by an edge-jump normalization.

To suggest a new VO_2(D) crystal structure, the pattern matching technique, Dicvol program and Rietveld refinement, explained before, were used.

5.5 VO_2(D) in the literature

VO_2(D) was presented in the literature for the first time by B.Y. Qu et al [161] in 2011 publishing the "theoretical study of the new compound VO_2(D)" where the authors presents a proposed crystallographic structure for the new phase and compare the simulations with the experimental results obtained by L. Liu and Y. Xie in an articled submitted for publication in the New Journal of Physics.

In B.Y. Qu *et al.* [**?**] work it is suggested that the VO_2(D) unit cell have a parallelepiped shape and furthermore in the work is proposed that the transition from VO_2(D) to VO_2(R) at 320 °C is mainly induced by the thermal motions of vanadium atoms, and the thermal motion of vanadium atoms are provoked by three vibrational modes at different temperatures [161].

In 2012, Liang Liu's published a work titled: New-Phase VO_2 mi-

cro / nanostructures: investigation of phase transformation and magnetic properties in the New Journal of Chemistry [44] where the new vanadium(IV) oxide phase is reported experimentally for the first time in the literature. The authors suggest that the VO_2(D) structure is isostructural with monoclinic nickel tungstate compound with the replacement of Ni and W atoms by V atoms. Their experiments shows a transition from VO_2(D) to VO_2(R) at 320 °C after 2 hours calcination under a pure nitrogen atmosphere. Furthemore, a band gap of 0.33 eV was reported in this work after temperature-dependent DC electrical conductivity measurements [44].

By 2016, Zhengdong Song *et al.* published their work: Controllable synthesis of VO_2(D) and their conversion to VO_2(M) nanostructures with thermochromic phase transition properties where ammonium metavanadate and oxalic acid dihydrate were used as precursor and reducing agent respectively to produce VO_2(D) by hydrothermal synthesis at temperatures ranging 160 to 220 °C. It was determined that temperatures from 160 to 180 °C promote the formation of VO_2(B), while temperatures from 180 to 220 °C favours the production of VO_2(D). The effect of the precursor content and reaction times were studied to determine different sizes and morphologies of the VO_2(D) product [45].

In the literature its also reported in two different works from Li Zhong *et al.* [46] and Ming li *et al.* [162] the use of VO_2(D) as a prior step to obtain thermochromic VO_2.

5.6 VO_2(D) structure

VO_2(D) is a recently reported phase of vanadium. New phases, as new compounds, have a characteristic structure. Solving the structure of a new compound or phase can be difficult. In this section, general methods for solving new structures will be mentioned. VO_2(D) phase structure presented in the literature will be reviewed.

5.6.1 General solving structure strategy

There are different techniques to solve the structure of an unknown material, in this section a general solving structure strategy (according to different authors) is presented for data obtained by X-Ray powder diffraction [163] [164] [165]. However, following these steps do not guarantee the structure solution, the nature of the data (crystalline, noisy, etc.) and the complexity of the compound will determine the best way to solve a new structure. The steps mentioned below are only a general guide, but not a definitive way for solving unknown structures.

1. Collect high resolution and high quality X-Ray powder data
2. Inspect the data and identify the peak position
3. Index peaks to obtain the lattice parameters
4. Determine space group
5. Solve the crystal structure (pattern matching for example)
6. Structure refinement by Rietveld Method

In our particular case, these guidelines did not work, probably because the experimental data presented broad peaks. The methods used were:

- The pattern matching, using the National Chemical Database Service looking for similar binary and ternary oxides patterns that match the experimental one
- The Dicvol indexing program used to obtain a series of suggested lattice parameters to narrow the search of matching patterns using the National Chemical Database Service.
- The Rietveld technique used to refine the obtained data from Dicvol program in order to propose a possible structure for VO_2(D).

However, later in this chapter a more accurate approach to the new VO_2(D) phase structure is proposed by us (following the mentioned methods) as the VO_2(D) structure reported in the literature, in our opinion, is incorrect.

5.6.2 VO_2(D) proposed crystal structure reported in the literature

B.Y. Qu *et al.* presented in 2011 a VO_2(D) calculated structure using computational approach [161]. In Figure 5.1 is shown the structure suggested by the authors. Where the green balls represent the Vanadium atoms and the red ones represent oxygen. The unit cell is enclosed by a black line in a form of a parallelepiped.

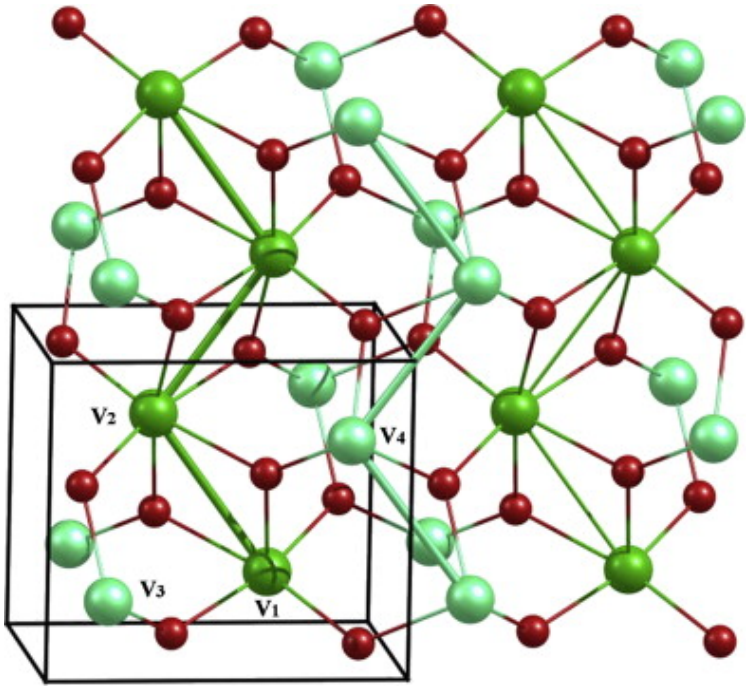

Figure 5.1: The structure of VO_2(D) suggested by B.Y. Qu *et al.* The green balls represent the vanadium while the red balls represent the oxygen ions. The unit cell is enclosed by a black line in a form of a parallelepiped. Figure used with permission of the authors. [161]

In Table 5.2 are presented the lattice parameters proposed by B.Y. Qu *et al.* for VO_2(D).

Table 5.2: Suggested lattice parameters by B.Y. Qu et al for VO_2(D) [161]

Lattice	**a**	**b**	**c**	β
parameters	4.584	5.5580	4.956	89.82

The authors correlated this model prediction with those of Liu *et al.*

On the other hand, Liang Liu *et al.* present in their work a experimental and calculated XRD pattern for the new phase VO_2(D) [44]. Their results are shown in Figure 5.2

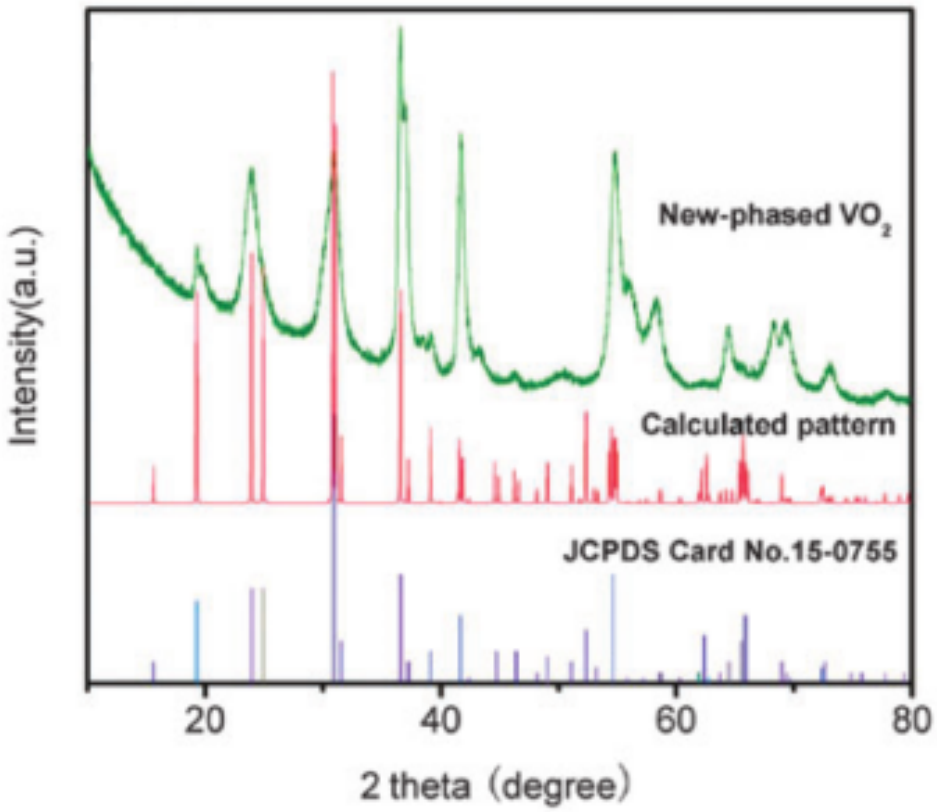

Figure 5.2: Experimental and calculated XRD pattern by Liang Liu *et al.* Figure used with permission of the authors [44]

In their work, the authors start from the premise that the VO_2(D) obtained pattern resembles nickel tungstate. As tungsten, nickel and vanadium have similar ionic radii, Liang Liu et al [44] shows a calculated VO_2(D) pattern replacing nickel(II) (0.69 Å) and tungsten(VI) (0.74 Å) ions of nickel tungstate by vanadium(IV) (0.72 Å) ions [44].

In appendix D are shown the structural and crystallographic parameters suggested by Liang Liu *et al.* for the VO_2(D) phase.

5.7 Results and discussion

In this section some experiments were performed in order to prove that VO_2(D) is indeed a new phase of vanadium(IV) oxide and also a new structure for the new phase VO_2(D) is proposed and discussed.

5.7.1 VO_2(D), a new vanadium(IV) oxide phase

In order to better understand the so called new phase and investigate if it is actually a new phase, some experiments were performed.

Figure 5.3 shows the VO_2(D) microparticles and nanoparticles XRD pattern of two samples prepared in this work (presented in chapters 3 and 4) compared to the VO_2(D) XRD pattern presented in the literature [44].

As can be seen in Figure 5.3 the results presented in this work match to the results reported in the literature. This confirms that, indeed, VO_2(D) newly reported phase can be prepared *via* hydrothermal synthesis using two different precursors (NH_4VO_3 and V_2O_5) obtaining the same results.

As the product does not seem to be fully crystalline and since the obtained pattern has been compared in the literature with the nickel tungstate XRD pattern, it was hypothesized that addition of $NiWO_4$ (as a template) to the reaction mixture might act to improve the crystallinity, this is because the addition of $NiWO_4$ will act as a seed [166] [167] and will promote the formation of the desire phase (reported phase) with improved crystallinity, therefore, VO_2(D) microparticles were synthesized *via* hydrothermal synthesis adding 2wt% of pure $NiWO_4$ to the reaction. The addition of $NiWO_4$ can act as structure template, as it resembles to VO_2(D) (according to the literature) and possibly produce a crystalline product easier to analyze, or, it is also possible that the product shows a crystalline $NiWO_4$ pattern and extra peaks corresponding to VO_2(D).

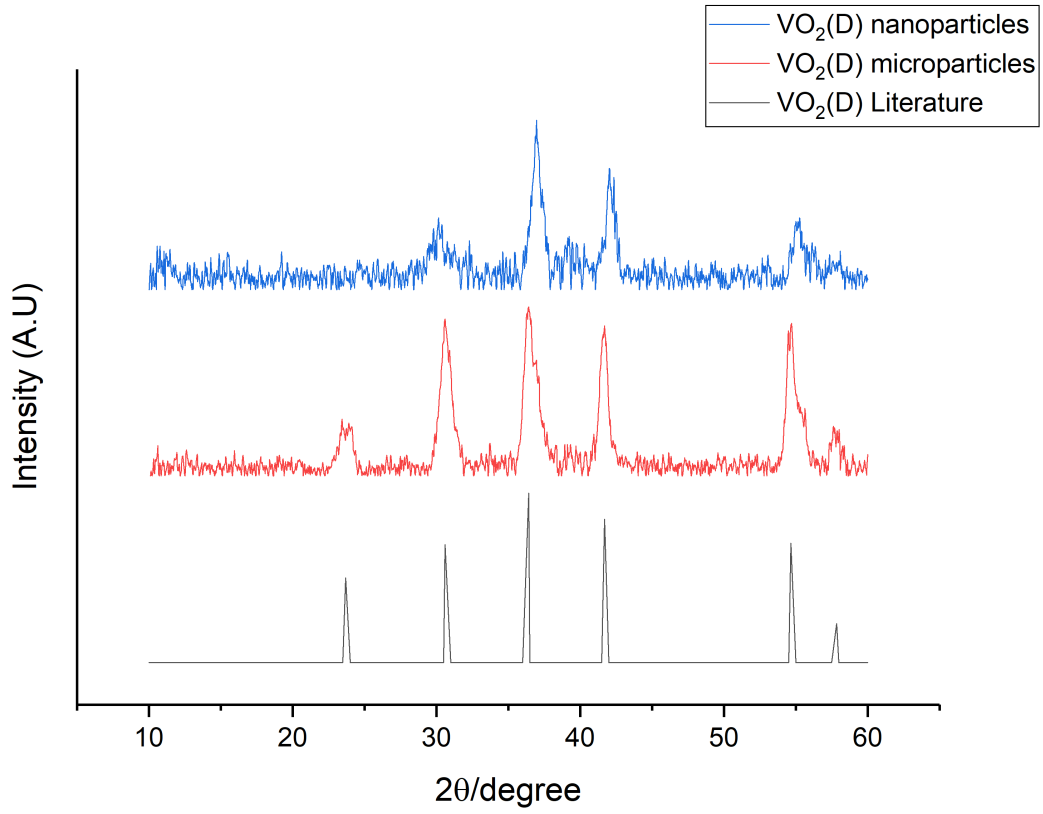

Figure 5.3: XRD pattern of VO_2(D) presented in the literature and VO_2(D) microparticles and nanoparticles prepared in this work

Figure 5.4 shows the XRD pattern of the as prepared VO_2(D) sample with 2wt% of $NiWO_4$ added as a seed. As can be seen in Figure 5.4, the crystallinity of the product has not improved, it means sharper peaks are not noticed and the obtained XRD pattern correspond to the VO_2(D) pattern reported in the literature [46]. No extra peaks that can be indexed to the nickel tungstate are shown. The presence of nickel tungstate in this reaction seems to not act as a template as no crystalline peaks that can be addressed to $NiWO_4$ are observed and moreover the obtained XRD pattern does not resemble to $NiWO_4$ XRD pattern, in our opinion. It can be possible that the broad peaks of VO_2(D) mask the nickel tungstate peaks. No conclusions can be drawn at this point about the new phase structure and its similarity to nickel tungstate.

As no conclusive results were obtained preparing VO_2(D) with $NiWO_4$ seed, VO_2(D) have been synthesized *via* hydrothermal syn-

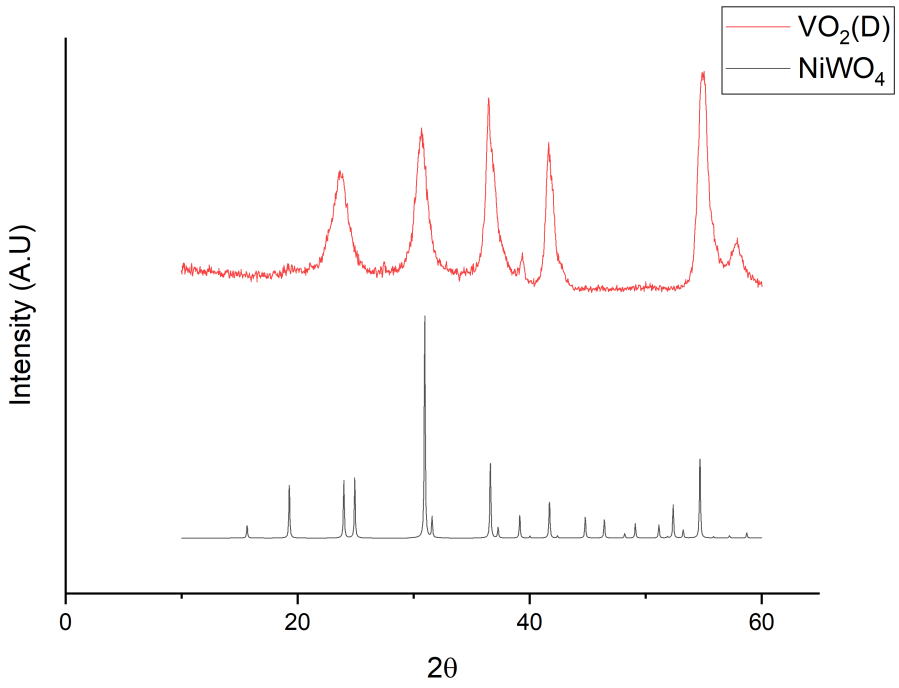

Figure 5.4: XRD pattern of the product obtained after synthesizing VO_2(D) with 2% of pure $NiWO_4$

thesis and studied in this work using different precursors and reaction times.

The X-Ray diffraction pattern of the obtained VO_2(D) sample was compared by a simple inspection of the peak position to all known vanadium Magneli phases and VO_2 polymorphs, and none of them, or a mixture of them, match the obtained pattern.

In Appendix B can be observed the obtained VO_2(D) XRD pattern of a sample prepared *via* hydrothermal synthesis in this work and the well known patterns of the vanadium Magneli phases and different polymorphs of VO_2. By inspection is impossible to fit all the obtained peaks to one or various vanadium phases, this suggests that the VO_2(D) phase is indeed a new phase.

Analysis such as Raman spectroscopy and X-Ray absorption near edge structure were performed to the samples to confirm that the obtained samples are indeed a new phase of vanadium(IV) oxide.

Raman spectroscopy is a near-surface analysis that studies the photon-phonon interactions [168], each compound have a defined spectrum as a fingerprint. Vanadium(IV) oxide is sensitive in the presence of air and oxidizes easily, hence it is very hard to obtain an actual pattern from VO_2 polymorph in powder form. Most of the VO_2 Raman analysis found in the literature are performed on films [169] [170], this is because films tends to oxidize slower than nanoparticles and microparticles due to its smaller surface area, therefore any surface analysis will be more accurate.

Raman spectroscopy was performed to the as prepared VO_2(D) powders. The obtained pattern is shown in Figure 5.5.

It is common for vanadium oxide analysis in powders to obtain V_2O_5 Raman spectrum, as result of the surface oxidation however, it worth mentioning that Raman spectrum of V_2O_5 and V_2O_3 are very similar, being actually very hard to distinguish between them if the data does not show well defined bands [171] [172].

The obtained Raman bands for the as prepared VO_2(D) powder show similarities to the V_2O_5 and V_2O_3 Raman spectra, as this is a surface analysis technique, the information does not provide any new evidence in the investigation of the new vanadium(IV) oxide phase.

Further analyses were performed to the sample to try to obtain a characteristic Raman spectrum for the newly reported VO_2(D) phase. The as prepared sample was placed in a glove box in nitrogen atmosphere, ground in a mortar and sealed into a 0.3 mm capillary.

Raman spectroscopy was performed on the samples inside the capillary, and no bands were observed, this is due to the difficulty to focus the laser in the sample through a curve surface (capillary). The sample was removed from the capillary and Raman analysis was performed immediately in order to avoid oxidation. The obtained Raman spectrum (Figure 5.6) shows three bands at 241 ± 1, 381 ± 1 and 713 ± 1 cm^{-1}. Those bands does not match to any Raman bands for vanadium reported

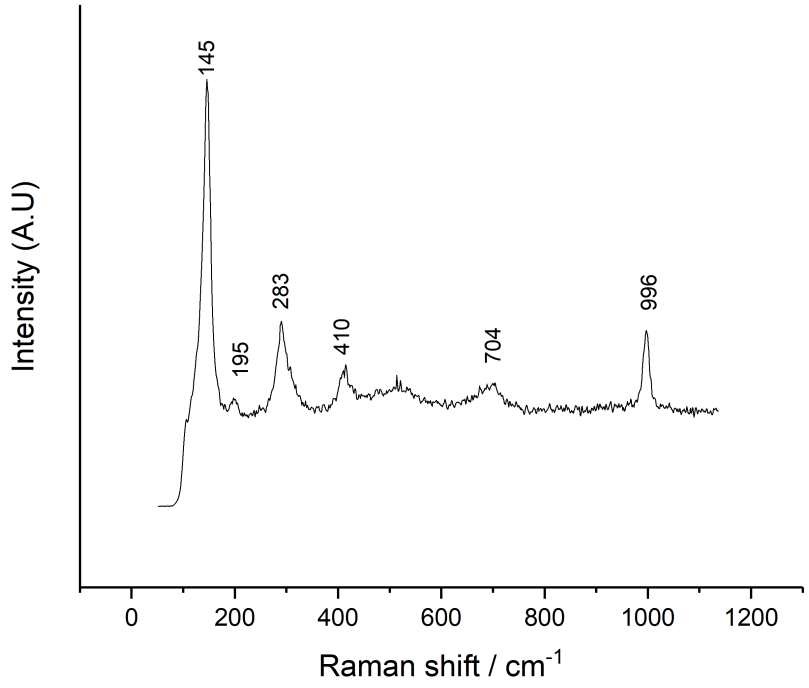

Figure 5.5: Raman spectroscopy of the as prepared VO_2(D) powder handled in air

in the literature to our knowledge.

This result suggests that this is the characteristic Raman spectrum for VO_2(D) phase and a demonstration that VO_2(D) phase is actually another vanadium oxide phase and not a mixture of phases, as this is not reported in the literature for any other vanadium polymorph or Magneli phase.

X-Ray absorption near edge structure (XANES) analysis give details on how X-Rays are absorbed by an atom [173] and in addition helps on the determination of the oxidation state of a compound [123]. As vanadium oxide have different phases and polymorphs, XANES was performed on the as prepared VO_2(D) samples in order to determine the oxidation state and compare the result with the existing XANES in the literature.

Figure 5.7 shows the XANES spectra of four VO_2(D) as prepared

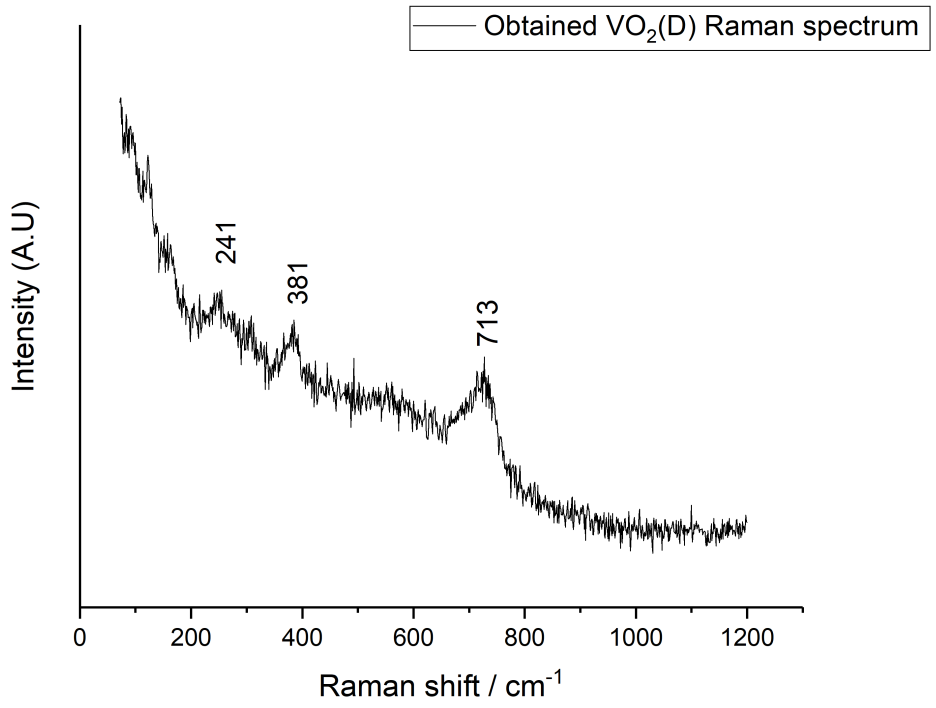

Figure 5.6: Raman spectroscopy of the as prepared VO_2(D) powder ground in nitrogen atmosphere and sealed into a 0.3 mm capillary

samples. Two of the samples, denoted as M1 and M3, represent VO_2(D) microparticles prepared using ammonium metavanadate as a precursor (experimental details in section 5.4). The other two samples, denoted as N1 and N2, represent VO_2(D) nanoparticles (experimental details in section 5.4), prepared using V_2O_5 as a precursor.

The pre-edge peak position is at $\approx$ 5465 eV and the intensity of the pre-edge compared to the edge provides information related to the oxidation state of the compounds [174]. In this case, the intensity of the pre-edge excludes the presence of V_2O_5, as the pre-edge of this one presents a pronounced peak, as can be see in Figure 5.8 where the XANES of V^0, V_2O_3, VO_2 and V_2O_5 are shown.

The pre-edge peak intensity of the as prepared samples also preclude the presence of pure vanadium metal. Analyzing the pre-edge peak intensity of the as-prepared VO_2(D) sample compared to the liter-

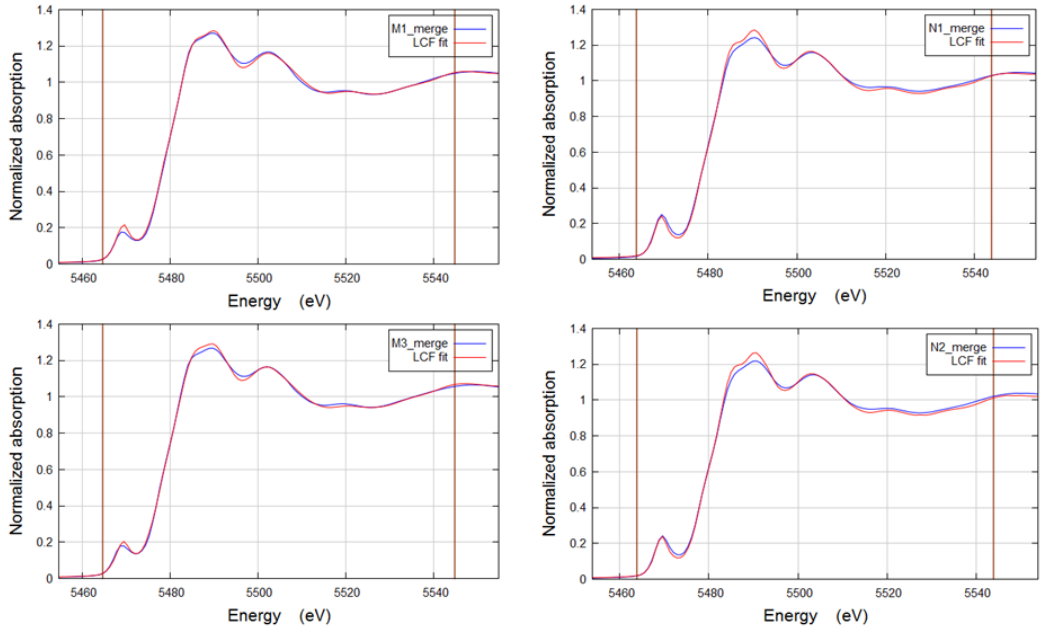

Figure 5.7: Normalized XANES spectra for the as prepared VO_2(D) microparticles M1 and M3 and VO_2(D) nanoparticles N1 and N2

ature 5.8, seems that the as-prepared VO_2(D) samples are mainly vanadium 4+, however, it is possible to also have vanadium 3+.

The relative calculated amounts (using Athena software) of vanadium 3+ and vanadium 4+ in the samples, after XANES spectra analysis are shown in table 5.3.

The results presented in table 5.3 suggests that for samples M1 and M3 (representing VO_2(D) microparticles) the bulk composition is mainly vanadium 4+ and the rest represents vanadium 3+. The vanadium 3+ is probably result of reduced vanadium 4+ during the hydrothermal synthesis reaction. On the other hand, the results presented in table 5.3 for samples N1 and N2 (representing VO_2(D) nanoparticles) suggests that almost 100 % of the sample is composed by vanadium 4+.

In table 5.3 can be observed a 10% difference in the vanadium 3+ and vanadium 4+ composition between samples M1 and M3, the difference is considerable and this can be due to several reasons. It is possible that during the hydrothermal synthesis the reduction of one of the samples occurs faster than the other, and this provokes the higher

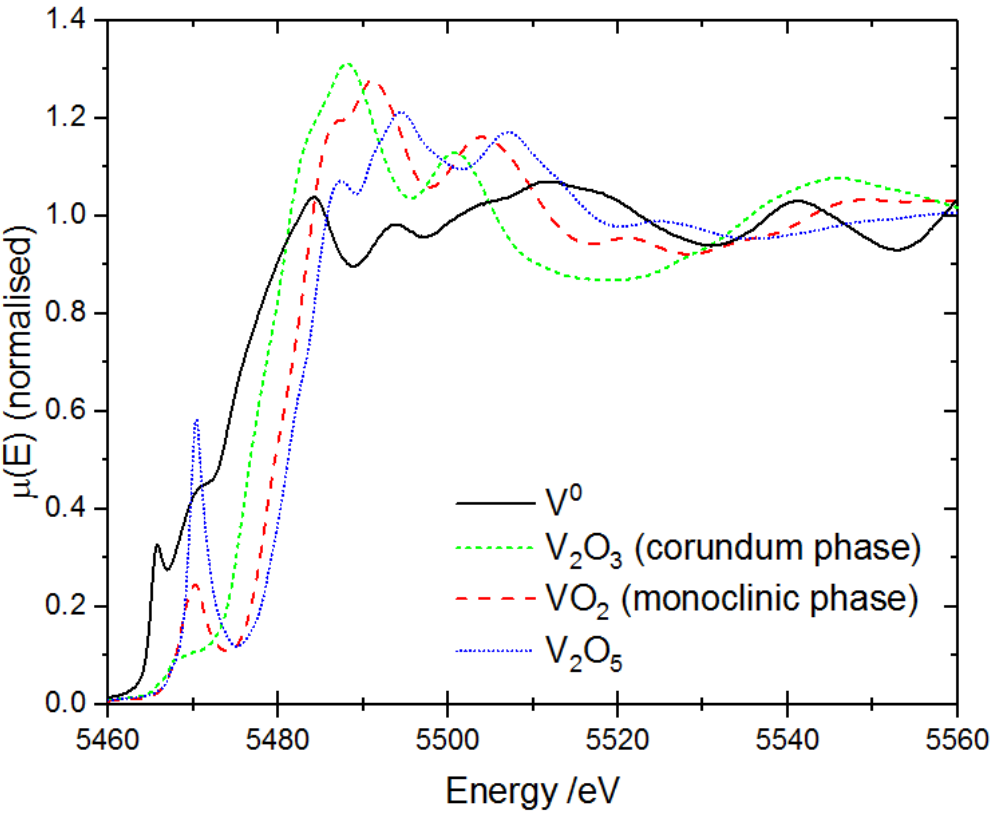

Figure 5.8: Normalized XANES spectra of V, V_2O_3, VO_2 and V_2O_5 reference samples in powder

Table 5.3: Oxidation state of VO_2(D) microparticles samples M1, M3 and VO_2(D) nanoparticles samples N1, N2 where: R is the residual factor: measure of the agreement between the model and the experimental results.

Sample	V3+ /at%	V4+ /at%	R factor
M1	25.9(8)	74.8(8)	0.0008192
M3	35.8(8)	65.7(8)	0.0009964
N1	7(1)	93(1)	0.0019344
N2	6(1)	92(1)	0.0021917

presence of vanadium 3+. Another possible reason for this difference in the vanadium 3+ content could be due to the pellet preparation. It must be remembered the vanadium phase diagram (chapter 2), where small changes in temperature or pressure leads to a different oxidation state or polymorph of vanadium. Small changes like the pressure inside the vessel due to bad sealing of the reactor, can lead into different products.

In the case of the nanoparticles samples, N1 and N2, the difference between them is not significant in terms of the vanadium 3+ and vanadium 4+ composition, actually, taking into account the uncertainty it can be said that there is no difference between N1 and N2 composition.

All the fittings were done using VO_2(M) as standard reference for vanadium 4+, however, as samples N1 and N2 (corresponding to VO_2(D) nanoparticles) have a very good fitting with the vanadium 4+ oxidation state (shown before in Figure 5.7), and there is no report in the literature for a VO_2(D) XANES spectrum (reported and suggested to be a newly VO_2 phase in the 4+ oxidation state [87] [44]), XANES spectrum from sample N1 was used as standard reference for VO_2(D) and samples M1 and M3 were fitted against this new reference. This was done in order to understand if VO_2(D) was indeed a new vanadium dioxide phase with a distinctive XANES spectrum.

In Figure 5.9A,B are shown the fittings of samples M1 and M3 respectively. The fitting is very good, but still there is an important part of the composition of samples M1 and M3 in the vanadium 3+ oxidation state as can be observed in Table 5.4.

Table 5.4: Oxidation state of VO_2(D) microcroparticles samples M1, M3 using as vanadium 4+ reference the as-prepared VO_2(D) nanoparticle sample N1. The R value represent the residual factor: measure of the agreement between the model (sample N1) and the experimental results.

Sample	N1/at%	V_2O_3/at%	R factor
M1	79(1)	22(1)	0.0017824
M3	69.9(9)	31.6(9)	0.0010698

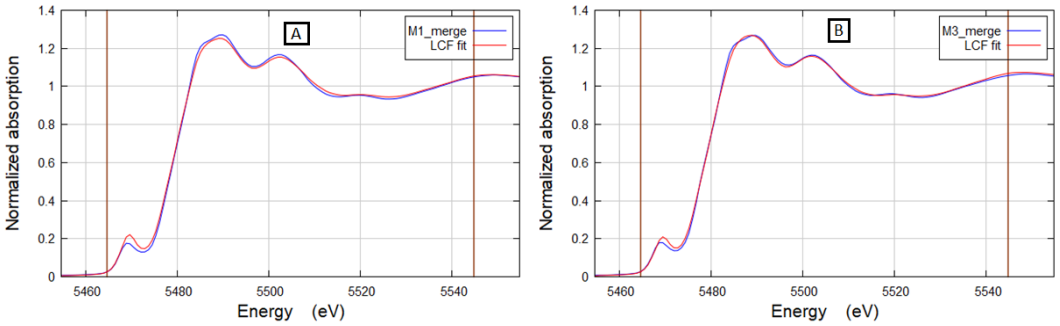

Figure 5.9: (A) Normalized XANES spectra against VO_2(D) standard (N1 sample) of samples M1 (B) Normalized XANES spectra against VO_2(D) standard (N1 sample) of samples M3

These good fittings against VO_2(D) nanoparticles and VO_2(D) microparticles confirm that, in fact, we can produce VO_2(D) nanoparticles and microparticles (with different morphologies), being these mainly vanadium 4+ and using different precursors.

On the other hand, these results presented here corroborate the ones obtained by XPS previously (chapters 3 and 4) where the as-prepared VO_2(D) microparticles and nanoparticles are composed not only by vanadium 4+ but also vanadium 3+.

The XANES results shows that VO_2(D) samples are mainly composed by vanadium 4+ with a component of vanadium 3+, besides that, XPS spectroscopy results also shows that VO_2(D) is a mixture of vanadium 3+ and vanadium 4+, while Raman spectroscopy and X-Ray diffraction results show a new Raman spectra and X-Ray pattern for the VO_2(D) microparticles and nanoparticles as-prepared samples. These results all together suggests that either VO_2(D) is indeed a new phase of vanadium(IV) oxide with over-reduced vanadium explaining the pres-

ence of vanadium 3+ on the samples, or it is new vanadium oxide but possibly a Magneli-like phase with vanadium 3+ present.

5.7.2 VO_2(D) structure elucidation and comparison with the literature

Liang Liu *et al.* suggests that the XRD pattern of the VO_2(D) resembles to the XRD pattern of nickel tungstate. Previously in Figure 5.2 was shown the VO_2(D) experimental pattern obtained by the authors compared to the nickel tungstate.

In order to compare the published results of VO_2(D) with the ones obtained in this work, Figure 5.10 shows the XRD pattern of the experimental VO_2(D) prepared in this work *via* hydrothermal synthesis compared to the nickel tungstate XRD pattern.

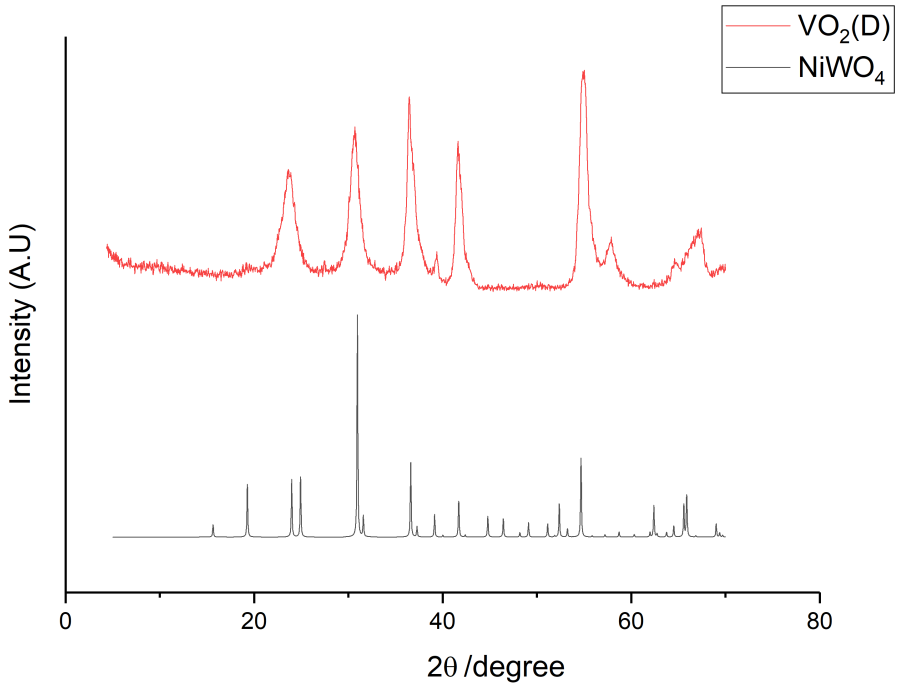

Figure 5.10: Simulated XRD pattern of nickel tungstate compared to the XRD pattern obtained from a prepared sample *via* hydrothermal synthesis

As can be observed in Figure 5.10 the VO_2(D) pattern and the nickel tungstate pattern have some similarities, however they are not identical.

The intensities are clearly not the same, nevertheless, the comparison is done between two completely different compounds even though the vanadium, nickel and tungsten have similar ionic radii, but completely different atomic number. According to our opinion it is not accurate to say that nickel tungstate and VO_2(D) XRD patterns resemble each other, in the present work.

Following with the published results in VO_2(D), as mentioned before, Liang Liu *et al.* shows a calculated VO_2(D) pattern replacing nickel (0.69 Å) and tungsten (0.74 Å) atoms of nickel tungstate by vanadium (0.72 Å) atoms [44] and the resultant calculated pattern and comparison with the experimental pattern is shown in Figure 5.2 [44].

In order to understand the results presented by the author and following the same analysis criteria used in the published work, different XRD patterns were simulated using nickel tungstate ($NiWO_4$) as referenced. It have to be remembered that each material has a different diffraction pattern, that is the reason why changing atoms in certain structure, the diffraction pattern changes. The simulated patterns were:

- A pattern replacing nickel atoms by vanadium atoms.
- A pattern replacing tungsten atoms by vanadium atoms.
- A pattern replacing nickel and tungsten atoms by vanadium atoms.

In Figure 5.11 are shown the resultant simulated patterns obtained.

As can be seen, and expected, all the obtained patterns are similar between them, except by the fact that the intensities of the peaks are different for each case. The only conclusion that can be drawn from this result is the fact that by replacing nickel and tungsten atoms by vanadium atoms in the nickel tungstate structure does not provide a XRD pattern that really fits the new VO_2(D) phase in our opinion.

In our opinion, the results shown by the authors regarding the VO_2(D) does not seem accurate, mainly because the XRD pattern of the experimental VO_2 does not resemble to nickel tungstate as VO_2(D)

XRD pattern shows 5 main peaks with strong intensity that can be recognized easily while nickel tungstate present only one peak with a strong intensity and several others with no strong intensities, that in our opinion do not match with the VO_2(D) XRD, therefore, the space group, crystal system and indexing of the synthesised VO_2 do not match the experimental results.

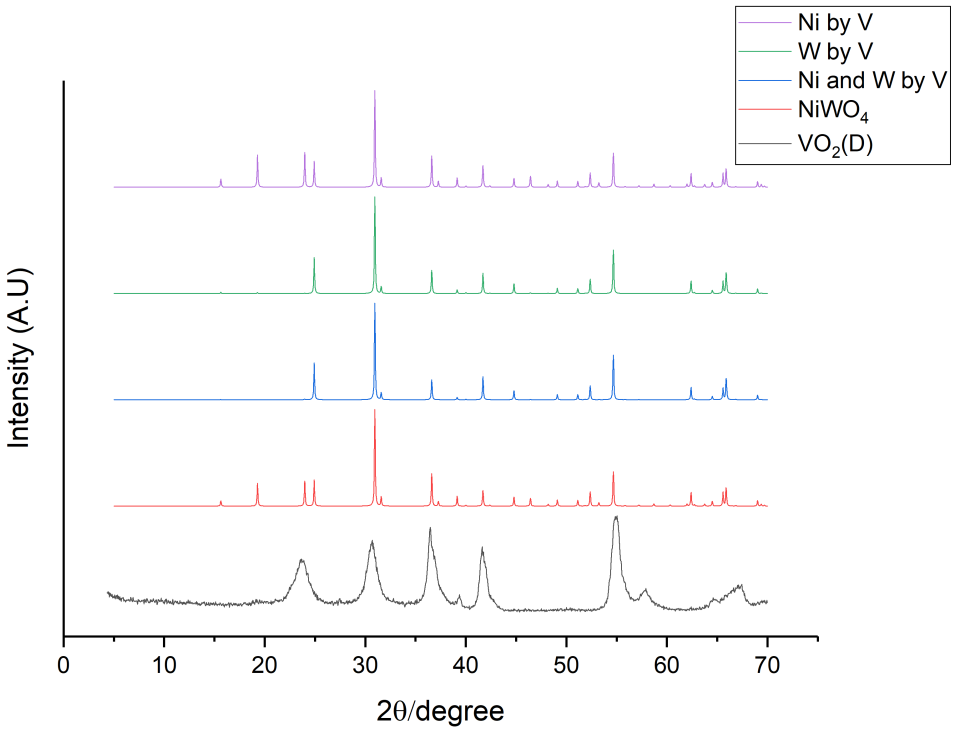

Figure 5.11: Nickel tungstate XRD pattern compared to other simulated patterns using as reference the $NiWO_4$: (A) a pattern replacing nickel atoms by vanadium atoms (B) a pattern replacing tungsten atoms by vanadium atoms (C) a pattern replacing nickel and tungsten atoms by vanadium atoms.

5.7.2.1 VO_2(D) proposal

To solve the structure of a new compound is not an easy task and even less when the experimental pattern to be solved does not have sharp peaks, as in the present case.

The easiest starting point to solve the structure of a new compound, as mentioned before, is using the pattern matching technique, adding the obtained pattern to a XRD database software and compare the ob-

tained pattern with the database. This technique was used in the present work using the software "Match!", and the most similar XRD pattern, according to the software, was nickel tungstate. It was shown previously that the nickel tungstate pattern does not fit to VO_2(D).

A manual pattern matching search was performed using the National Chemical Database Service database, where XRD patterns of binary and ternary oxides were searched in order to compare by simple eye inspection to the experimental VO_2(D) XRD pattern. The search was unsuccessful, as the XRD patterns found in the search were not similar to the experimental VO_2(D).

Manual pattern matching is often used as first step in the phase identification of new compounds, the process consist of searching (initially) for compounds that have the same molecular formula and compare the unknown compound XRD pattern with the database XRD patterns to check if there are coincidences, if no XRD pattern is similar, the search continues with compounds with a different formula (compared to the unknown compound) until a similar XRD pattern is found.

As mentioned before, the manual search of XRD patterns of binary and any other oxide (for example TiO_2, MnO_2, NbO_2 and so on following the formula XO_2 and then X_xO_x) was unsuccessful and lead to a the manual pattern matching using different formula than the unknown one.

Following these two unsuccessful searches, Dicvol program (mentioned before) was used to index the pattern. The information given to the program include the 2θ position of the six main peaks of the empirically obtained VO_2(D) XRD pattern and the wavelength used to collect the powder data.

The program output suggested 36 possible sets of lattice parameters that fit the input data. From the 36 solutions, 32 of them are monoclinic systems, 2 tetragonal systems and 2 orthorhombic system.

Using the suggested unit cell to each proposed system by the Dicvol program, and doing a manual search at the National Chemical Database

Service of the possible structures with a similar unit cell structure, it was possible to narrow the search to four compounds that present similar patterns to the VO_2(D). The four compounds are $CoCu_2O_3$, $LaNiO_2$, GaAs and FeB.

In Figure 5.12 can be seen the XRD pattern of the as prepared VO_2(D) sample, compared to the four compounds that according to our research, can possibly fit the XRD pattern of the VO_2(D).

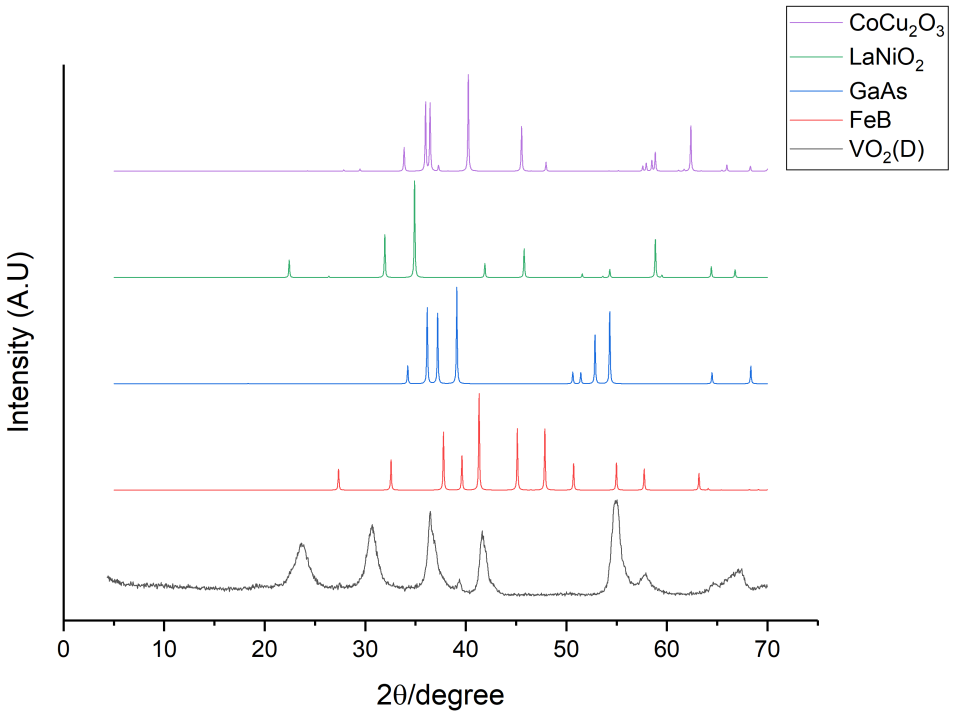

Figure 5.12: XRD patterns of $CoCu_2O_3$ (ICSD 33996), $LaNiO_2$ (ICSD 153058), GaAs (ICSD 43951) and FeB (ICSD 391329) compared to the XRD pattern of VO_2 selected to perform a refinement in order to propose a VO_2(D) structure

By simple inspection, seems that the compound $LaNiO_2$ is a good candidate to try a refinement and obtain a calculated XRD pattern to index the new D phase of vanadium(IV) oxide.

$LaNiO_2$ is a reduced form of $LaNiO_3$ perovskite [175] [176] with an orthorhombic crystal structure and was the closest match to VO_2(D) pattern obtained by us. XRD patterns were simulated by replacing La and Ni atoms by V atoms in the structure of $LaNiO_2$ as the first approach

done to the structure refinement (final refinement parameters are shown in appendix C).

Figure 5.13 A, B and C shows the structure and XRD pattern of $LaNiO_2$, $LaNiO_2$ with La and Ni atoms replaced by V atoms, and $LaNiO_2$ with La and Ni atoms replaced by V and with refined a, b and c parameters, respectively. It can be seen how the atomic structure change after the atoms replacement, as well as the intensities of the XRD patterns.

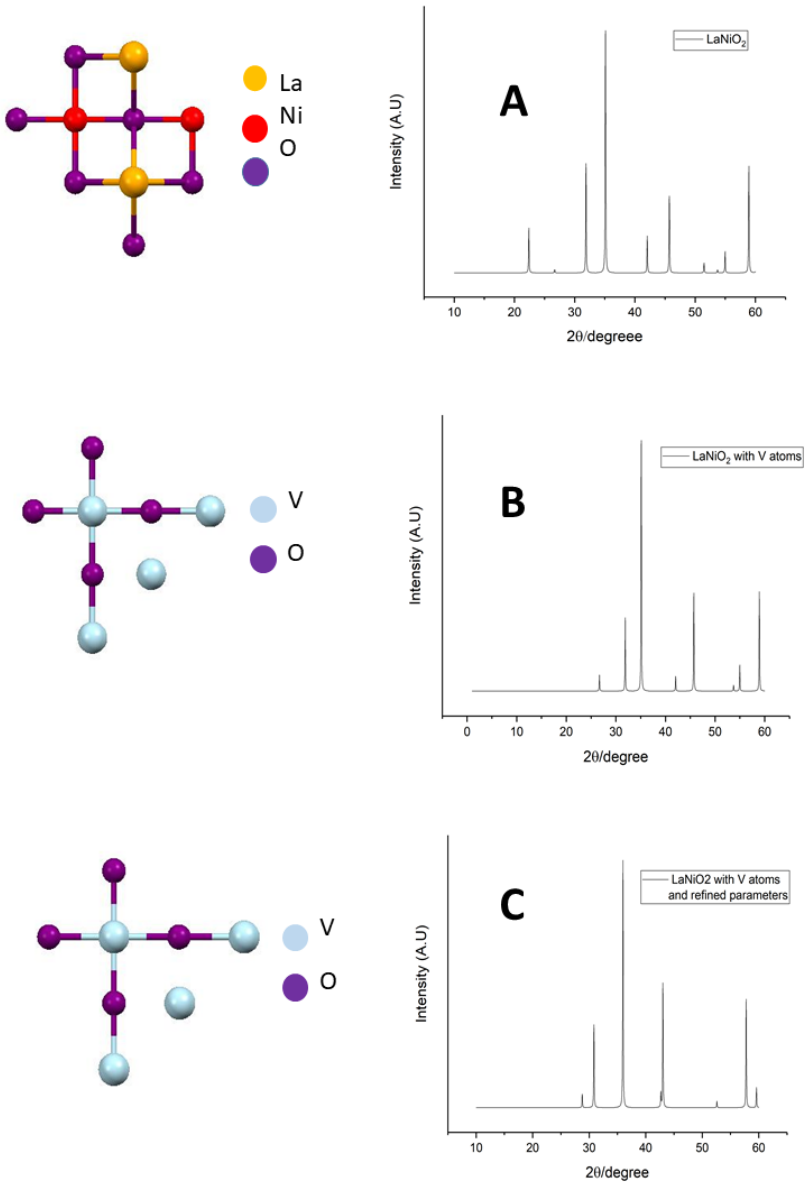

Figure 5.13: (A) $LaNiO_2$ crystal structure and XRD pattern (B) $LaNiO_2$ with replaced La and Ni by V vanadium atoms and XRD pattern (C) $LaNiO_2$ with replaced La and Ni by V vanadium atoms, modified a, b and c parameters and XRD pattern

Figure 5.14 shows the XRD pattern of the $LaNiO_2$ after the atoms replacement and changes in the lattice parameters of the $LaNiO_2$ structure compared with the VO_2(D) pattern.

The obtained pattern after refinement is still not identical to the VO_2(D) pattern, but seems to be a better fit than the nickel tungstate.

In appendix C are shown the parameters for the simulated XRD pattern after $LaNiO_2$ refinement.

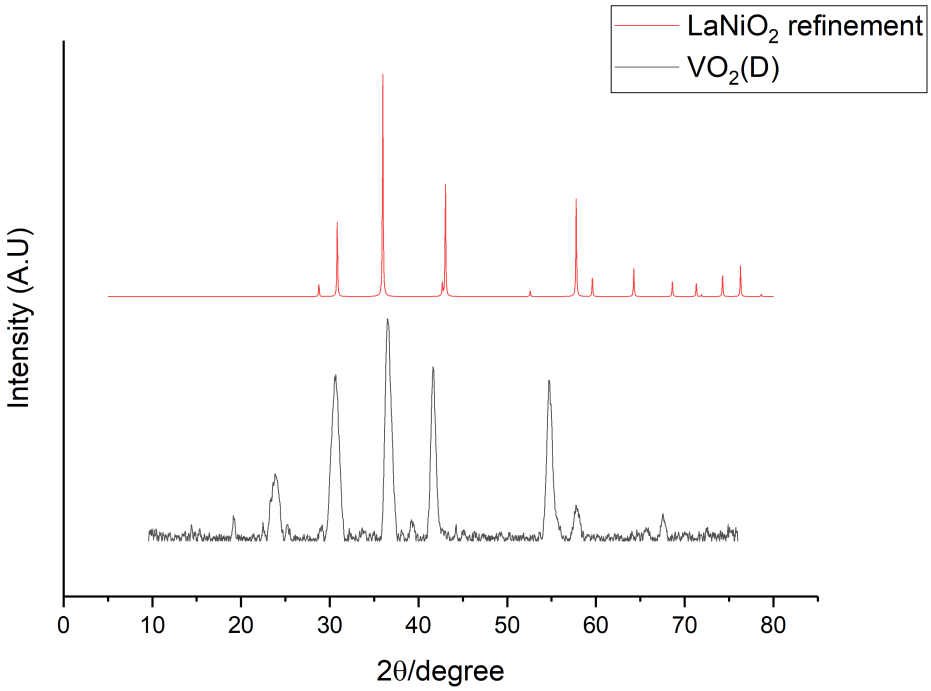

Figure 5.14: XRD pattern of the as prepared VO_2(D) sample compared to the $LaNiO_2$ XRD pattern after refinement

The obtained data was used to perform Rietveld refinement in order to properly solve the VO_2(D) structure new phase, unfortunately, the Rietveld refinement was unsuccessful and the proper phase identification of the VO_2(D) was not possible because the model is not close enough to correct the structure.

The proposed XRD pattern in Figure 5.14 may not represent the final structure of the VO_2(D) new phase, however, this proposal is, according to us, a closer guess to the real structure, compared to the nickel tungstate match proposed in the literature.

Despite the discrepancies between the published VO_2(D) structure and our views, the VO_2(D) pattern accepted in the literature will be the reference XRD pattern for all the presented experimental data results obtained in this work.

5.8 Conclusions

This chapter discusses the literature around the so called new phase of vanadium(IV) oxide, VO_2(D).

Experiments such as X-Ray diffraction, Raman spectroscopy and X-Ray absorption near edge structure makes us think that VO_2(D) is indeed a new polymorph of vanadium(IV) oxide.

In this work, a Raman spectrum is shown for the first time and is suggested to be the typical Raman spectrum for VO_2(D) with Raman shift bands at 241$\pm$1, 381$\pm$1 and 713$\pm$1 Raman shift / cm^{-1}.

XANES analysis provide evidence that the obtained powder (VO_2(D)) is mainly composed by vanadium 4+, this finding make more strong the thesis that VO_2(D) is a new phase of vanadium dioxide. XANES analysis were performed to VO_2(D) microparticles and nanoparticles samples prepared using different precursors (vanadium pentoxide and ammonium metavanadate).

Likewise, the inspection of the XRD pattern of the as prepared VO_2(D) compared to all known vanadium Magneli phases and vanadium(IV) oxide polymorphs XRD lead to the conclusion that the obtained VO_2 product is not a mixture of phases, and effectively is a new XRD pattern corresponding to VO_2(D).

Dicvol software was used in order to obtain a series of possible structures for the newly D phase, and from the obtained results, a structure is proposed. This suggested structure is a refinement of the $LaNiO_2$ however, the exact structure parameters could not be obtained after using Rietveld refinement.

5.9 Suggestions

Difficulties have been found in order to solve the structure of the new D phase of vanadium(IV) oxide. A crystalline XRD pattern of the VO_2(D) phase would be ideal in order to do a refinement.

Future work will focus on trying to grow a single crystal of VO_2(D).

A single crystal will provide an excellent XRD pattern for the refinement, this could be achieved performing the hydrothermal VO_2(D) reaction for long periods of time, or calcinating the VO_2(D) product at low temperatures and in different atmospheres (nitrogen, argon, air, vacuum) for long times.

Future works on the VO_2(D) phase identification will include powder X-Ray diffraction using synchrotron data. Synchrotron data will provide high quality in the XRD pattern, making easier the data refinement.

VO_2(D) has been synthesized only using ammonium metavanadate and vanadium pentoxide (used for the first time in this work to prepare VO_2(D)) as precursors, future work will include to trying different precursors and reactions times to obtain the same phase with improved crystallinity.

Chapter 6

Conclusions

6.1 Summary of results

This thesis has studied the synthesis of vanadium dioxide (VO_2) thin films and particles (nanoparticles and microparticles) aimed to be used for technological applications as smart windows. Sol-gel/spin coating technique and Aerosol-Assisted Chemical Vapour Deposition (AACVD) were the techniques used to synthesize vanadium dioxide thin films, while hydrothermal synthesis was the method used to prepare micro and nanoparticles of VO_2. Monoclinic VO_2 is a material with a metal to semiconductor transition phase at 68 °C (that can be reduced to room temperature by doping the material) that can be potentially used to coat windows in buildings to maintain a comfortable temperature inside without the excessive use of air conditioning and heating, hence reducing CO_2 emissions.

For the sol-gel/spin coating samples, vanadium(V) oxytriisopropoxide ($VO(OC_3H_7)_3$) was the precursor used. Thermochromic yellow transparent thin films of approximately 120 nm of thickness and a solar modulation response of $\approx$ 4-6 % were obtained after annealing them in a controlled atmosphere of nitrogen for 4 hours at 550 °C. On the other hand, monoclinic VO_2 dark and non uniform films were obtained *via* AACVD method using vanadyl acetylacetonate ($VO(acac)_2$) as a precursor, at temperatures between 540 to 560 °C, using nitrogen

as carrier gas.

Nanoparticles of a recently reported phase of vanadium dioxide (VO_2(D)) were prepared in this work using vanadium(V) oxide (V_2O_5) as a precursor *via* hydrothermal synthesis technique for the first time. pH of the initial solution needs to be fixed between 6.60 to 6.90 in order to obtain the desired phase. pH of the solution was altered using sodium hydroxide (NaOH).

The as-prepared nanoparticle morphology exhibit round/oval shapes with a diameter of 20-30 nanometers. The VO_2(D) nanoparticles do not have thermochromic properties between 0 to 300 °C, nevertheless, they do show an irreversible phase transition at $\approx$ 165 °C, from VO_2(D) to thermochromic VO_2(M). This is the lowest transition temperature reported to obtain monoclinic VO_2.

The nanoparticles of VO_2(M) obtained *via* VO_2(D) calcination at low temperature (180 °C for 2 hours) present thermochromic behavior with a switching temperature of 59 °C, lower than reported in the literature for bulk VO_2. Morphology of the nanoparticles after calcination is round/oval and the size is 20-30 nanometers.

Microparticles of the recently reported VO_2(D) phase with different morphologies were prepared in this work *via* hydrothermal synthesis using ammonium metavanadate (NH_4VO_3) as a precursor. VO_2(D) microparticles (1 to 5 μm) were obtained by changing the pH of the initial solution by adding NaOH. The obtained morphologies were: star/flower shape, circular fused plates shape, full spheres looking like a rubber ball shape, cross shaped and homogeneous round balls shape for pH 0.65, 0.98, 1.05, 1.52 and 3.51 respectively. Due to the different shape obtained with the same VO_2 phase, the particles could be used for different applications (to be investigated in the future).

Monoclinic VO_2 microparticles with different morphologies and sizes from 1 to 5 μm were obtained after calcination of VO_2(D) microparticles under a controlled nitrogen atmosphere for 2 hours at 350

°C with a switching temperature at 61 °C.

Microparticles and nanoparticles of the VO_2(D) phase were intended to be doped using tungsten (tungsten(IV) chloride and tungsten(VI) ethoxide), in order to reduce the transition temperature closer to room temperature, however, the obtained samples were not doped but tungsten-vanadium composite. It is possible to recognize by XRD the relevant peaks of tungsten oxide. Moreover, tungsten oxide tubes are observed by transmission electron microscopy imaging of the samples. The tungsten was not successfully incorporated into the lattice.

VO_2(M) thermochromic nanoparticles obtained *via* calcination of the the as prepared VO_2(D) nanoparticles were incorporated into a polymeric matrix of polyvinylpyrrolidone and spin coated into a glass substrate in order to obtain thermochromic thin films. The obtained film present a yellow/brown transparent colour with a solar modulation of 1.7-2.3 %.

The VO_2(D) phase was studied and a typical Raman spectrum for this phase was presented for the first time in this work showing Raman bands at 241$\pm$1, 381$\pm$1 and 713$\pm$1 cm^{-1}. Crystal structure of VO_2(D) suggested in the literature was questioned in this work, as the proposed pattern does not match the actual VO_2(D) pattern. An XRD pattern is proposed to be a more accurate pattern for the VO_2(D) phase. The proposed pattern is a manipulated and refined reduced form of $LaNiO_3$ perovskite with an orthorhombic crystal structure.

6.2 Future work

Taking into account the results obtained and presented in this work it is possible to list some considerations for future work:

- Prepare thin films *via* AACVD on different metal substrates like aluminium or silver, instead of glass. This could result in semiconductive films that can be used for other purposes apart from architectural applications, like semiconductors.

- Prepare nanoparticles and microparticles of the new phase, VO_2(D) using different precursors, and study if the transition temperature from VO_2(D) to VO_2(M) phase, particle size and reaction times varies considerably using different precursors.
- Dope the nanoparticles and microparticles of VO_2(D) using tungsten precursors in order to reduce the transition temperature from monoclinic to rutile phase, once the VO_2(D) was transformed into thermochormic VO_2.
- Dope the nano and microparticles of VO_2(D) using magnesium precursors in order to improve the light transmission in the visible range of the final thermochromic VO_2 particles.
- Grow a single crystal of VO_2(D) to facilitate the proper phase identification of the VO_2(D) phase.
- Improve the thermochromic behavior of the thin films prepared using VO_2(M) nanopaticles obtained *via* mild calcination of VO_2(D) nanoparticles.

Appendix A

List of samples prepared *via* spin coating and AACVD

Sample Number	Type	Method	Compound	Comments	Results
DP01	films	Spin coating	V-oxytripropoxide + Isopropyl alcohol	5 layers doped with W (5%)	These samples were done to understand the technique and the used compounds
DP02	films	Spin coating	V-oxytripropoxide + Isopropyl alcohol	5 layers doped with W (5%)	
DP03	films	Spin coating	V-oxytripropoxide + Isopropyl alcohol	10 layers doped with W (5%)	
DP04	films	Spin coating	V-oxytripropoxide + Isopropyl alcohol	5 layers doped with Sb (5%)	
DP05	films	Spin coating	V-oxytripropoxide + Isopropyl alcohol	10 layers doped with Sb (5%)	
DP06	films	Spin coating	V-oxytripropoxide + Isopropyl alcohol	2 layers doped with W (5%)	
DP07	films	Spin coating	V-oxytripropoxide + Isopropyl alcohol	2 layers doped with W (5%), sample heated during 40 min after deposition	
DP08	films	Spin coating	V-oxytripropoxide + Isopropyl alcohol	2 layers doped with W (5%), solution heated during 10 min	
DP09	films	Spin coating	V-oxytripropoxide + Isopropyl alcohol	2 layers doped with W (5%), solution heated during 10 min + sample heated after deposition	
DP11	films	Spin coating	V-oxytripropoxide + Isopropyl alcohol	W Bulk	
DP12	films	Spin coating	V-oxytripropoxide + Isopropyl alcohol	1 layer	

Figure A.1: List of samples prepared *via* spin coating

	films	Spin coating	V-oxytripropoxide + Isopropyl alcohol	Heated in air. Time: 10 hours. Temp: 500C. 1 layer	Amorphous/no film
DP13-1	films	Spin coating	V-oxytripropoxide + Isopropyl alcohol	Heated in air. Time: 10 hours. Temp: 500C. 2 layers	Amorphous/no film
DP14-1	films	Spin coating	V-oxytripropoxide + Isopropyl alcohol	Heated in air. Time: 10 hours. Temp: 500C. 3 layers	Amorphous/no film
DP15-1	films	Spin coating	V-oxytripropoxide + Isopropyl alcohol	Heated in air. Time: 10 hours. Temp: 500C. 4 layers	Amorphous/no film
DP16-1	films	Spin coating	V-oxytripropoxide + Isopropyl alcohol	Heated in air. Time: 10 hours. Temp: 500C. 5 layers	Amorphous/no film
DP17-1	films	Spin coating	V-oxytripropoxide + Isopropyl alcohol	Heated in NITROGEN. Time: 10 hours. Temp: 500C. 1 layer	Amorphous/no film
DP18-1	films	Spin coating	V-oxytripropoxide + Isopropyl alcohol	Heated in NITROGEN. Time: 10 hours. Temp: 500C. 2 layers	Amorphous/no film
DP19-1	films	Spin coating	V-oxytripropoxide + Isopropyl alcohol	Heated in NITROGEN. Time: 10 hours. Temp: 500C. 3 layers	Amorphous/no film
DP20-1	films	Spin coating	V-oxytripropoxide + Isopropyl alcohol	Heated in NITROGEN. Time: 10 hours. Temp: 500C. 4 layers	Amorphous/no film
DP21-1	films	Spin coating	V-oxytripropoxide + Isopropyl alcohol	Heated in NITROGEN. Time: 10 hours. Temp: 500C. 5 layers	Amorphous/no film
DP22	films	Spin coating	V-oxytripropoxide + Isopropyl alcohol	Unclean glass. 5 layers	Amorphous/no film
DP23	films	Spin coating	V-oxytripropoxide + Isopropyl alcohol	Unclean glass. 6 layers	Amorphous/no film
DP24	films	Spin coating	V-oxytripropoxide + Isopropyl alcohol	Unclean glass. 7 layers	Amorphous/no film
DP25	films	Spin coating	V-oxytripropoxide + Isopropyl alcohol	Clean glass. 5 layers. Annealed in N2: 15 hours at 500C	Amorphous/no film
DP26	films	Spin coating	V-oxytripropoxide + Isopropyl alcohol	Clean glass. 6 layers. Annealed in N2: 15 hours at 500C	Amorphous/no film
DP27	films	Spin coating	V-oxytripropoxide + Isopropyl alcohol	Clean glass. 7 layers. Annealed in N2: 15 hours at 500C	Amorphous/no film
DP28	films	Spin coating	V-oxytripropoxide + Isopropyl alcohol	Unclean glass. Doped with 5% W (0.09 gr) 10 min at 400 rpm. 5 layers	Amorphous/no film
DP29	films	Spin coating	V-oxytripropoxide + Isopropyl alcohol	Unclean glass. Doped with 5% W (0.09 gr) 10 min at 400 rpm. 6 layers	Amorphous/no film
DP30	films	Spin coating	V-oxytripropoxide + Isopropyl alcohol	Unclean glass. Doped with 5% W (0.09 gr) 10 min at 400 rpm. 7 layers	Amorphous/no film
DP31	films	Spin coating	V-oxytripropoxide + Isopropyl alcohol	Clen glass. Doped with 5% W (0.09 gr). 10 min at 400 rpm. 5 layers	Amorphous/no film
DP32	films	Spin coating	V-oxytripropoxide + Isopropyl alcohol	Clen glass. Doped with 5% W (0.09 gr). 10 min at 400 rpm. 6 layers	Amorphous/no film
DP33	films	Spin coating	V-oxytripropoxide + Isopropyl alcohol	Clen glass. Doped with 5% W (0.09 gr). 10 min at 400 rpm. 7 layers	Amorphous/no film

Figure A.2: List of samples prepared *via* spin coating

DP43	films	Spin coating	V-oxytripropoxide + Isopropyl alcohol	0.16 molar solution doped with 5% of W. 3 layers. Nitrogen atmosphere, 3 hours at 550C	V2O5
DP44	films	Spin coating	V-oxytripropoxide + Isopropyl alcohol	0.16 molar solution doped with 5% of W. aged 2 days. 3 layers. nitrogen atmosphere during 10 hours at 550 C.	tungsten
DP45	films	Spin coating	V-oxytripropoxide + Isopropyl alcohol	0.16 molar solution doped with 5% of W. aged 2 days. 4 layers. nitrogen atmosphere during 10 hours at 550 C.	tungsten
DP46	films	Spin coating	V-oxytripropoxide + Isopropyl alcohol	0.16 molar solution doped with 5% of W. aged 2 days. 5 layers. nitrogen atmosphere during 10 hours at 550 C.	tungsten
DP48	films	Spin coating	vanadyl acetylacetonate + Methanol + polyethylene glycol	aged 2 days. after 2nd layer, rinse with acetone and then deposit 3 more layers. 550 C,	Amorphous
DP49	films	Spin coating	vanadyl acetylacetonate + Methanol + polyethylene glycol	aged 2 days. 550 C, 3 hours in nitrogen	Amorphous
DP50	films	Spin coating	vanadyl acetylacetonate + Methanol + polyethylene glycol	aged 2 days. 550 C, 3 hours in nitrogen	Unknown
Dp51	films	Spin coating	vanadyl acetylacetonate + Methanol + polyethylene glycol	aged 6 days. 550 C, 10 hours nitrogen	Amorphous
Dp52	films	Spin coating	vanadyl acetylacetonate + Methanol + polyethylene glycol	aged 6 days. 550 C, 10 hours nitrogen	Amorphous
DP53	films	Spin coating	V-oxytripropoxide + Isopropyl alcohol	0.12 molar solution. 25 layers. Put in plate 250 C during 3 min, then in the furnace air atmosphere, does not arrive in temp, finally in	Unknown
DP54	films	Spin coating	V-oxytripropoxide + Isopropyl alcohol	0.12 molar solution. 20 layers. 10 hours at 550 C in nitrogen. The nitrogen was empty when I arrive, So	Unknown
DP55	films	Spin coating	V-oxytripropoxide + Isopropyl alcohol	0.12 molar solution. 20 layers. 10 hours at 550 C in nitrogen. The nitrogen was empty when I arrive, So	VO2(m)
DP56	films	Spin coating	V-oxytripropoxide + Isopropyl alcohol	0.12 molar solution. 20 layers. 10 hours at 550C in nitrogen atmosphere	mixed phases
DP57	films	Spin coating	V-oxytripropoxide + Isopropyl alcohol	0.12 molar solution. 15 layers. 10 hours at 550C in nitrogen atmosphere	VO2(m)
DP58	films	Spin coating	vanadyl acetylacetonate, Methanol, polyethylene glycol	10 layers. 10 hours at 550C in nitrogen atmosphere	VO2(m)
DP59	films	Spin coating	V-oxytripropoxide + Isopropyl alcohol	0.12 molar solution, deposited on a glass with a layer of titanium oxide. Layer around 600-900 nm. 10 layers. 10 hours at 550C in nitrogen atmosphere	mixed phases

Figure A.3: List of samples prepared *via* spin coating

DP81	films	AACVD	vanadyl acetilacetonate + Ethanol	Temp 560C on copper	Inconclusive results
DP82	films	AACVD	vanadyl acetilacetonate + Ethanol	Temp 560C on glass	Unknown
DP83	films	AACVD	vanadyl acetilacetonate + Ethanol	Temp 560C on iron	Inconclusive results
DP84	films	AACVD	vanadyl acetilacetonate + Ethanol	Temp 560C on copper	Inconclusive results
DP85	films	AACVD	vanadyl acetilacetonate + Ethanol	Close to the. aacvd. Temp 545C on glass	mixed phases
DP86	films	AACVD	vanadyl acetilacetonate + Ethanol	With titania film Temp 545C on glass	VO2(b)
DP87	films	AACVD	vanadyl acetilacetonate + Ethanol	Far from the reactor. Temp 545C on glass	VO2(b)
DP88	films	Spin coating	V-oxytripropoxide + acetic acid (2x) +isopropyl	annealing 10 hours 550C. 10 layers	Amorphous
DP89	films	Spin coating	V-oxytripropoxide + acetic acid (2x) +isopropyl	annealing 10 hours 550C. 10 layers	Amorphous
DP90	films	Spin coating	V-oxytripropoxide + acetic acid (4x) +isopropyl	annealing 10 hours 550C. 10 layers	Amorphous
DP91	films	Spin coating	V-oxytripropoxide + acetic acid (4x) +isopropyl	annealing 10 hours 550C. 5 layers	Unknown
DP92	films	AACVD	vanadyl acetilacetonate + Ethanol	Temp 550 on glass	Amorphous
DP93	films	Spin coating	V-oxytripropoxide + Citric Acid acid+isopropyl	5 layers on glass	unknown
DP94	films	Spin coating	V-oxytripropoxide + Citric Acid acid+isopropyl	5 layers on glass	unknown
DP95	films	Spin coating	V-oxytripropoxide + Citric Acid acid+isopropyl	10 layers on glass	unknown
DP96	films	Spin coating	V-oxytripropoxide + Citric Acid acid+isopropyl	10 layers on glass	unknown
DP97-ht	Powders	Hydrothermal Synthesis	V2O5 + oxalic acid	280 c during 5 hours.	VO2(m)
DP98	films	Spin coating	V-oxytripropoxide + Acetic	5 layers	VO2(m)
DP99	films	Spin coating	V-oxytripropoxide + Acetic Acid+isopropyl	5 layers	Amorphous
DP100	films	Spin coating	V-oxytripropoxide + Acetic Acid+isopropyl	5 layers y secado 1 min a 70C	Amorphous
DP101	films	Spin coating	V-oxytripropoxide + Citric Acid acid+isopropyl	5 layers	VO2(m)
DP102	films	Spin coating	V-oxytripropoxide + Citric Acid acid+isopropyl	5 layers	VO2(m)
DP103	films	Spin coating	V-oxytripropoxide + Citric Acid acid+isopropyl	5 layers dried during 1 min at 70C	VO2(m)
DP104	films	AACVD	Ethanol + vanadyl acetilacetonate	555 C on glass	mixed phases
DP105	films	Spin coating	V-oxytripropoxide + Acetic Acid+isopropyl	5 layers.aged 4 days	Amorphous
DP106	films	Spin coating	V-oxytripropoxide + Acetic Acid+isopropyl	5 layers.aged 4 days	Unknown
DP107	films	Spin coating	V-oxytripropoxide + Citric Acid acid+isopropyl	5 layers.aged 4 days	Unknown
DP108	films	Spin coating	V-oxytripropoxide + Citric Acid acid+isopropyl	5 layers.aged 4 days	Unknown
DP109	Powder	Hydrothermal Synthesis	DI Water + oxalic acid + V2O5		VO2(b)
DP110	films	Spin coating	V-oxytripropoxide + Acetic Acid+isopropyl	5 layers	Unknown
DP111	films	Spin coating	V-oxytripropoxide + Acetic Acid+isopropyl	5 layers	Unknown

Figure A.4: List of samples prepared *via* spin coating and AACVD

DP112	films	Spin coating	V-oxytripropoxide + Acetic	5 layers. Aged 4 days (en	Unknown
DP116	films	Spin coating	V-oxytripropoxide + Acetic		Tungsten oxide
DP117	films	Spin coating + hydrothermal synthesis	V2O5 + oxalic acid. Enjuagado con DI Water y propanol		Mixed phases
DP118	films	Spin coating + hydrothermal synthesis	V2O5 + oxalic acid. Enjuagado con DI Water y propanol		Mixed phases
DP119	films	Spin coating + hydrothermal synthesis	V2O5 + oxalic acid. Enjuagado con ethyl acetate		Amorphous
DP121	films	Spin coating	V-oxytripropoxide + Acetic Acid+isopropyl	10 layers	Unknown
DP122	films	Spin coating	V-oxytripropoxide + Acetic Acid+isopropyl + 0.10 gr WCl6	5 layers	Tungsten oxide
DP123	Powder	Hydrothermal Synthesis	V2O5 + oxalic acid + 0.4637 gr de WCl		VO2(b)
DP124	films	Spin coating	V-oxytripropoxide + acetic acid	15 layers	Unknown
DP125	films	Spin coating	V-oxytripropoxide + Acetic Acid+isopropyl + polymer solutin	5 layers	Unknown
DP126	films	Spin coating	Hydrothermal Synthesis yellow liquid + polymer solution	5 layers	PDMS
DP127	films	Spin coating	yellow Hydrothermal Synthesis liquid	2 layers	PDMS
DP128	films	Spin coating	Powder (DP123) + polymer solution	5 layers	VO2(b)
DP129	films	Spin coating	Ethanol + vanadyl acetilacetonate	Flow 1. temp550 C	unknown
DP130	films	Spin coating	V-oxytripropoxide + Acetic	550	Amorphous
DP131	films	Spin coating	V-oxytripropoxide + Acetic Acid+isopropyl + silane	550	Amorphous
DP132	films	Spin coating	V-oxytripropoxide + Acetic Acid+isopropyl + WCl	550	Tungsten
DP133	films	Spin coating	V-oxytripropoxide + Acetic Acid+isopropyl + WCl + silane	550	Amorphous
DP134	films	Spin coating	polystyrene + tolueno + DI Water +	4 layers	Polymer
DP135	films	Dip coating	polystyrene + tolueno + DI Water + Powder + silane	dipped	polymer
DP136	films	Spin coating	V-oxytripropoxide + Acetic Acid+isopropyl	20 layers	VO2(m)
DP137	films	Spin coating	V-oxytripropoxide + Acetic Acid+isopropyl	20 layers	VO2(m)
DP138	aacvd	Spin coating	Ethanol + vanadyl acetilacetonate	flow=1.5 550C	VO2(m)
DP139	films	Spin coating	V-oxytripropoxide + Acetic	20 layers. Spin 20 seg	
DP141	films	Spin coating	V-oxytripropoxide + Citric Acid+isopropyl	20 layers. Spin 20 seg	Unknown
DP145	films	Spin coating	V-oxytripropoxide + Acetic Acid+isopropyl	15 layers. N2 during 10 hours at 580C. Aged 5 days	
DP146	films	Spin coating	V-oxytripropoxide + Acetic Acid+isopropyl	15 layers. Aged 5 days. N2 during 10 hours at 580C	VO2(m)
DP149	films	Spin coating	V-oxytripropoxide + Acetic Acid+isopropyl+WCl	15 layers	Tungsten
DP150	films	Spin coating	V-oxytripropoxide + Acetic Acid+isopropyl+WCl	15 layers	Tungsten
DP156	block		Block of VO2 Powder + PDMS	fayza	PDMS
DP157	films	Reflux+Spin coating	green solution by reflux.	5 layers. 330C. 3 hours. 5	

Figure A.5: List of samples prepared *via* spin coating and dip coating

Appendix B

Simulated XRD pattern of all vanadium Magneli phases and polymorphs

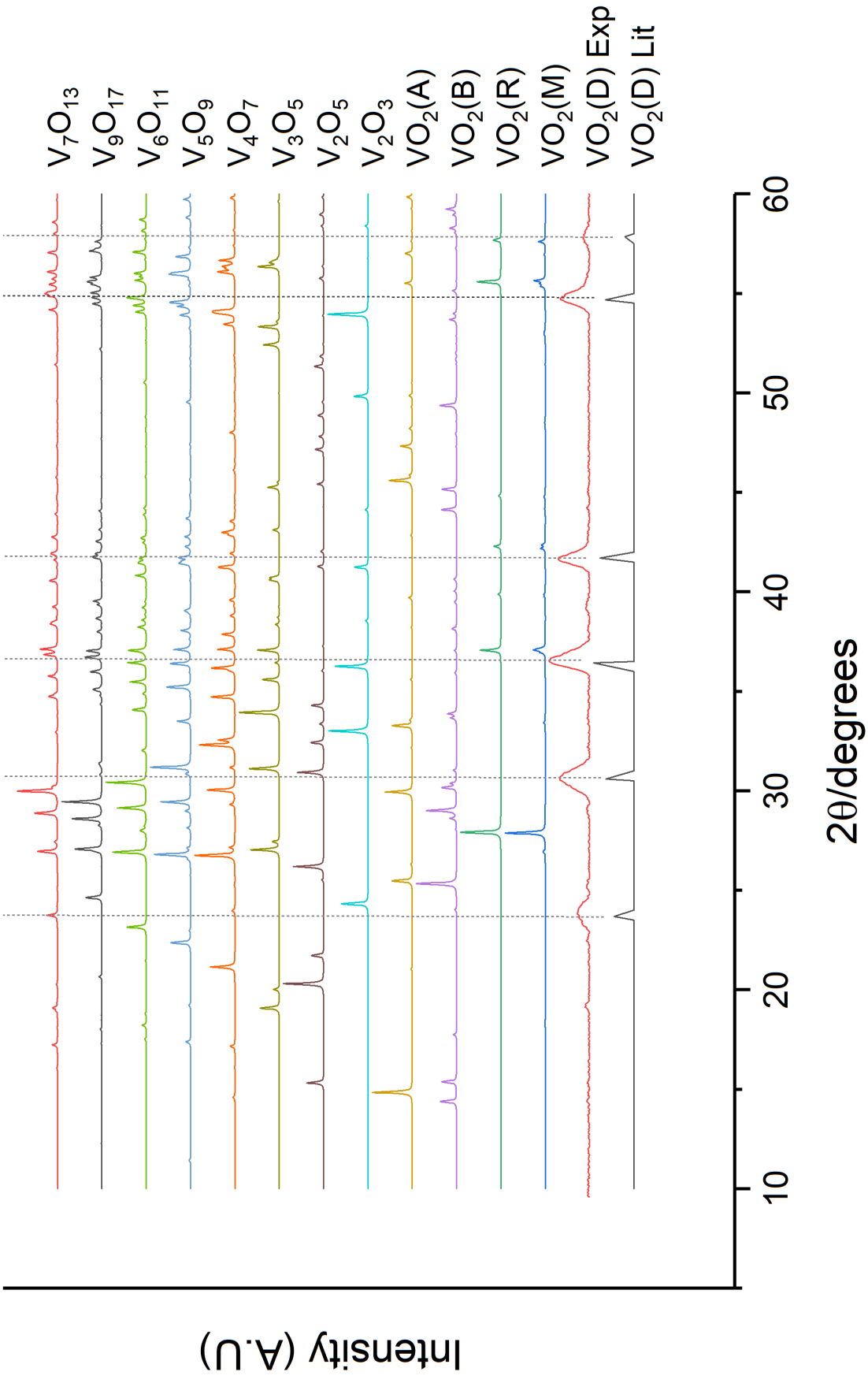

Figure B.1: Simulated XRD pattern of: VO_2(M), VO_2(R) and XRD pattern of the as-prepared VO_2(D) *via* hydrothermal synthesis in this work

Appendix C

$LaNiO_2$ refinement parameters using vanadium ions

```
_cell_length_a 4.200(1)
_cell_length_b 4.000(1)
_cell_length_c 3.100(1)
_cell_angle_alpha 90.
_cell_angle_beta 90.
_cell_angle_gamma 90.
_cell_volume 52.5
_cell_formula_units_Z 1
_symmetry_space_group_name_H-M 'P 4/m m m'
_symmetry_Int_Tables_number 123
_refine_ls_R_factor_all 0.07
loop_
_symmetry_equiv_pos_site_id
_symmetry_equiv_pos_as_xyz
1 'y, x, -z'
2 '-y, -x, -z'
3 '-y, x, -z'
4 'y, -x, -z'
5 '-x, y, -z'
6 'x, -y, -z'
7 'x, y, -z'
8 '-x, -y, -z'
9 '-y, -x, z'
10 'y, x, z'
11 'y, -x, z'
12 '-y, x, z'
13 'x, -y, z'
14 '-x, y, z'
15 '-x, -y, z'
16 'x, y, z'
loop_
_atom_type_symbol
_atom_type_oxidation_number
V3+ 3
V1+ 1
O2- -2
loop_
_atom_site_label
_atom_site_type_symbol
_atom_site_symmetry_multiplicity
_atom_site_Wyckoff_symbol
_atom_site_fract_x
_atom_site_fract_y
_atom_site_fract_z
_atom_site_B_iso_or_equiv
_atom_site_occupancy
_atom_site_attached_hydrogens
V1 V3+ 1 d 0.5 0.5 0.5 . 1. 0
V1 V1+ 1 a 0 0 0 . 1. 0
O1 O2- 2 f 0.5 0 0 . 1. 0
```

Figure C.1: $LaNiO_2$ refinement parameters using vanadium ions

Appendix D

VO_2(D) structural and crystallographic parameters suggested by Liang Liu *et al.* [44]

compound name	vanadium dioxide (VO_2)			
space group	P2/C (No. 13)			
Z	2			
crystal system	monoclinic			
lattice parameters	a = 4.5968 Å, b=5.6844 Å, c=4.9133 Å, β=89.39°			
cell volume	128.4 Å^3			
label	site	x	y	z
O(1)	4g	0.22	0.11	0.96
O(2)	4g	0.26	0.38	0.39
V(1)	2f	0.50	0.653	0.25
V(2)	2e	0.00	0.180	0.25

Figure D.1: VO_2(D) structural and crystallographic parameters suggested by Liang Liu et al. [44]

Bibliography

[1] Lingxiao Li, Bucheng Li, Jie Dong, and Junping Zhang. Roles of silanes and silicones in forming superhydrophobic and superoleophobic materials. *Journal of Materials Chemistry A*, 4:13677–13725, 2016.

[2] Y. Gao, C. Cao, L. Dai, H. Luo, M. Kanehira, Y. Ding, and Z. L. Wang. Phase and shape controlled VO_2 nanostructure by antimony doping. *Energy and Environmental Science*, pages 8708–8715, 2012.

[3] S. Ji, F. Zhang, and P. Jin. Preparation of high performance pure single phase VO_2 nanopowder by hydrothermally reducing the V_2O_5 gel. *Solar Energy Materials and Solar Cells*, 95(12):3520–3526, 2011.

[4] R. Li, S. Ji, Y. Li, Y. Gao, H. Luo, and P. Jin. Synthesis and characterization of plate-like VO_2(M)@SiO_2 nanoparticles and their application to smart window. *Materials Letters*, 110:241–244, 2013.

[5] L. Mai, Q. Wei, Q. An, X. Tian, Y. Zhao, X. Xu, L. Xu, L. Chang, and Q. Zhang. Nanoscroll Buffered Hybrid Nanostructural VO_2 (B) Cathodes for High-Rate and Long-Life Lithium Storage. *Advance Materials*, 2:2969–2973, 2013.

[6] C. Nethravathi, C. R. Rajamathi, M. Rajamathi, U. K. Gautam, X. Wang, D. Golberg, and Y. Bando. N Doped Graphene VO_2 (B) Nanosheet-Built 3D Flower Hybrid for Lithium Ion Battery. *Applied Materials and Interface*, 2, 2013.

[7] C. Hu, H. Xu, X. Liu, F. Zou, L. Qie, Y. Huang, and X. Hu. VO_2/TiO_2 Nanosponges as Binder-Free Electrodes for High- Performance Supercapacitors. *Scientific Reports*, pages 1–8, 2015.

[8] X. Xiao, S. Li, H. Wei, D. Sun, Y. Wu, G. Jin, F. Wang, and Y. Zou. Synthesis and characterization of VO_2(B)/graphene nanocomposite for supercapacitors. *Journal of Materials Science: Materials in Electronics*, 2:4226–4233, 2015.

[9] X. Pan, Y. Zhao, G. Ren, and Z. Fan. Highly conductive VO_2 treated with hydrogen for supercapacitors . *ChemComm*, pages 3943–3945, 2013.

[10] H. T. Kim, B. G. Chae, D. H. Youn, S. L. Maeng, G. Kim, K. Y. Kang, and Y. S. Lim. Mechanism and observation of Mott transition in VO_2 -based two- and three-terminal devices. *New Journal of Physics*, 6, 2004.

[11] M. Soltani, M. Chaker, E. Haddad, and R. Kruzelesky. 1 x 2 optical switch devices based on semiconductor-to-metallic phase transition characteristics of VO_2 smart coatings. *Measurement Science and Technology*, (1), 2006.

[12] International Energy Agency. Transition to Sustainable Buildings. Technical report, 2013.

[13] Buildings. https://ec.europa.eu/energy/en/topics/energy-efficiency/buildings. Technical report.

[14] T. D. Manning. *Atmospheric pressure chemical vapour deposition*. PhD thesis, University College London, 2004.

[15] C. Liu, N. Wang, and Y. Long. Multifunctional overcoats on vanadium dioxide thermochromic thin films with enhanced luminous transmission and solar modulation , hydrophobicity and anti-oxidation. *Applied Surface Science*, 283:222–226, 2013.

[16] L. Zhao, L. Miao, C. Liu, C. Li, T. Asaka, Y. Kang, Y. Iwamoto, S. Tanemura, H. Gu, and Huirong Su. Solution-Processed VO_2-SiO_2 Composite Films with Simultaneously Enhanced Luminous Transmittance, Solar Modulation Ability and Anti-Oxidation property. *Scientific Reports*, pages 1–11, 2014.

[17] A. Taylor, I. P. Parkin, N. Noor, M. S. Brown, and I. Papakonstantinou. A bioinspired solution for spectrally selective thermochromic VO_2 coated intelligent glazing. *Optics Express*, 21(May):3914–3918, 2013.

[18] Z. P. Wu, A. Miyashita, S. Yamamoto, H. Abe, I. Nashiyama, K. Narumi, and H. Naramoto. Molybdenum substitutional doping and its effects on phase transition properties in single crystalline vanadium dioxide thin film. *Journal of Applied Physics*, 86(1999), 2010.

[19] N. R. Mlyuka, G. a. Niklasson, and C. G. Granqvist. Mg doping of thermochromic VO_2 films enhances the optical transmittance and decreases the metal-insulator transition temperature. *Applied Physics Letters*, 95(17):2–4, 2009.

[20] L. Dai, S. Chen, J. Liu, Y. Gao, J. Zhou, Z. Chen, C. Cao, H. Luo, and M. Kanehira. F-doped VO_2 nanoparticles for thermochromic energy-saving foils with modified color and enhanced solar-heat shielding ability. *Physical Chemistry Chemical Physics*, pages 11723–11729, 2013.

[21] P. Jin, S. Nakao, and S. Tanemura. Tungsten doping into vanadium dioxide thermochromic films by high-energy ion implantation and thermal annealing. *Thin Solid Films*, pages 151–158, 1998.

[22] J. C. Lee, G. V. Jorgenson, and R. J. Lin. Thermochromic Materials Research for Optical Switching. In *Proceeding SPIE 0692*, 1986.

[23] J A Mejia, R Rodriguez, and A Armienta. Aquifer Vulnerability Zoning, an Indicator of Atmospheric Pollutants Input? Vanadium in the Salamanca Aquifer, Mexico. *Water Air Soil Pollut*, pages 95–100, 2007.

[24] F. Pintchovski, W. S. Glaunsinger, and A. Navrotsky. Experimental study of the electronic and lattice contributions to the VO_2 transition. *Journal of Physics and Chemistry of Solids*, 39, 1978.

[25] C. H. Griffiths and H. K. Eastwood. Influence of stoichiometry on the metal-semiconductor transition in vanadium dioxide. *Journal of Applied Physics*, 2201(1974), 2012.

[26] A. S. Barker, H. W. Verleur, and H. J. Guggenheim. Infrared Optical Properties of Vanadium Dioxide Above and Below the Transition Temperature. *Physical Review Letters*, 17(26):1286–1289, 1966.

[27] J. B. Goodenough. The Two Components of the Crystallographic Transition in VO_2*. *Journal of Solid State Chemistry*, pages 490–500, 1971.

[28] R. Molaei, R. Bayati, S. Nori, D. Kumar, J. T. Prater, and J. Narayan. Diamagnetic to ferromagnetic switching in VO_2 epitaxial thin films by nanosecond excimer laser treatment. *Applied Physics Letters*, 103(25):2–6, 2013.

[29] F. Guinneton, L. Sauques, J. C. Valmalette, F. Cros, and J. R. Gavarri. Optimized infrared switching properties in thermochromic vanadium dioxide thin films: role of deposition process and microstructure. *Thin Solid Films*, 446:287–295, 2004.

[30] F. Guinneton, L. Sauques, J. C. Valmalette, F. Cros, and J. R. Gavarri. Comparative study between nanocrystalline powder and thin film of vanadium dioxide VO_2: electrical and infrared properties. *Journal of Physics and Chemistry of Solids*, 62:1229–1238, 2001.

[31] C. Moffatt and A. Wigstein. Sol-gel synthesis of VO_2 thin films and the effects of W and Re doping. Technical Report June, 2005.

[32] H. Jerominek, F. Picard, N. R. Swart, M. Renaud, M. Lévesque, M. Lehoux, S. Castonguay, M. Pelletier, G. Bilodeau, D. Audet, T. D. Pope, and P. Lambert. Micromachined, uncooled, VO_2-based, IR bolometer arrays. Technical Report 60, 1996.

[33] K. N. Wood, R. O. Hayre, and S. Pylypenko. Recent progress on nitrogen/carbon structures designed for use in energy and sustainability applications. *Energy and Enviromental Science*, pages 1212–1249, 2014.

[34] Z. Chen, Y. Gao, L. Kang, C. Cao, S. Chen, and H. Luo. Fine crystalline VO_2 nanoparticles: synthesis, abnormal phase transition temperatures and excellent optical properties of a derived VO_2 nanocomposite foil. *Journal of Materials Chemistry A*, 2(8):2718, 2014.

[35] X. Tan, T. Yao, R. Long, Z. Sun, Y. Feng, H. Cheng, X. Yuan, W. Zhang, Q. Liu, C. Wu, Y. Xie, and S. Wei. Unraveling Metal-insulator Transition Mechanism of VO_2 Triggered by Tungsten Doping. *Scientific Reports*, pages 1–6, 2012.

[36] L. Perez-Lombard, J. Ortiz, and C. Pout. A review on buildings energy consumption information. *Energy and Buildings*, 40:394–398, 2008.

[37] M. A. Brown and F. Southworth. Mitigating climate change through green buildings and smart growth. *Environment and Planning A*, 40:653–676, 2008.

[38] V. V. Maslyuk, A. Bagrets, V. Meded, A. Arnold, F. Evers, M. Brandbyge, T. Bredow, and I. Mertig. Organometallic Benzene-Vanadium Wire: A One-Dimensional Half-Metallic Ferromagnet. *Physical Review Letters*, 97, 2006.

[39] G. Silversmit, D. Depla, H. Poelman, G. B. Marin, and R. De Gryse. Determination of the V2p XPS binding energies for different vanadium oxidation states (V5+ to V0+). *Journal of Electron Spectroscopy and Related Phenomena*, 135(2-3):167–175, 2004.

[40] H. Katzke, P. Toledano, and W Depmeier. Theory of morphotropic transformations in vanadium oxides. *Physical Review B*, pages 1–7, 2003.

[41] U. Schwingenschl and V. Eyert. The vanadium Magneli phases V_nO_{2n1}. *Annalen der Physik*, 510(9):475–510, 2004.

[42] Y. Li, S. Ji, Y. Gao, H. Luo, and M. Kanehira. Core-shell VO_2@TiO2 nanorods that combine thermochromic and photocatalytic properties for application as energy-saving smart coatings. *Scientific Reports*, 3:1370, 2013.

[43] J. Nag and R. F. Haglund Jr. Synthesis of vanadium dioxide thin films and nanoparticles. *Journal of Physics: Condensed Matter*, 20(26):264016, 2008.

[44] L. Liu, F. Cao, T. Yao, Y. Xu, M. Zhou, B. Qu, B. Pan, C. Wu, S. Wei, and Yi Xie. New-phase VO_2 micro/nanostructures: investigation of phase transformation and magnetic property. *New Journal of Chemistry*, 36(3):619, 2012.

[45] Z. Song, L. Zhang, F. Xia, N. A. S. Webster, J. Song, B. Liu, H. Luo, Y. Gao, and G. Yanfeng. Controllable synthesis of VO_2(D) and their conversion to VO_2(M) nanostructures with thermochromic phase transition properties. *Inorganic Chemistry*, 3(8):1035–1042, 2016.

[46] L. Zhong, M. Li, H. Wang, Y. Luo, J. Pan, and G. Li. Star-shaped VO_2(M) nanoparticle films with high thermochromic performance. *CrystEngComm*, 17(30):5614–5619, 2015.

[47] Y. Oka, S. Sato, T. Yao, and N. Yamamoto. Crystal Structures and Transition Mechanism of VO_2(A). *Journal of Solid State Chemistry*, 598(141):594–598, 1998.

[48] Y. Oka, T. Yao, and N. Yamamoto. Powder Crystal Structure of VO_2(A). *Journal of Solid State Chemistry*, 1990.

[49] Y. Oka, T. Yao, and N. Yamamoto. Phase transition and V4+-V4+ pairing in VO_2(B). *Journal of Solid State Chemistry*, 105, 1993.

[50] D. Hagrman, J. Zubieta, C. J. Warren, L. M. Meyer, M. M. .J. Treacy, and R. C. Haushalter. A New Polymorph of VO_2 Prepared by Soft Chemical Methods. *Journal of Solid State Chemistry*, 182(138):178–182, 1998.

[51] L. Whittaker, C. Jaye, Z. Fu, D. A. Fischer, and S. Banerjee. Depressed Phase Transition in Solution-Grown VO_2 Nanostructures. *Journal of the American Chemical Society*, (18):8884–8894, 2009.

[52] T. Yao, X. Zhang, Z. Sun, S. Liu, Y. Huang, Y. Xie, C. Wu, X. Yuan, W. Zhang, Z. Wu, G. Pan, F. Hu, L. Wu, Q. Liu, and S. Wei. Understanding the Nature of the Kinetic Process in a VO_2 Metal-Insulator Transition. *Physical review letters*, pages 2–5, 2010.

[53] J. H. Park, J. M. Coy, T. S. Kasirga, C. Huang, Z. Fei, S. Hunter, and D. H. Cobden. Measurement of a solid-state triple point at the metalinsulator transition in VO_2. *Nature*, 500(7463):431–434, 2013.

[54] W. Zhang, L. Shi, K. Tang, and Y. Yu. A facile fabriaction of VO_2(A) micro-nanostructures with controlled shape and its electrochemical behavior in lithium ion batteries. *Chemistry Letters*, 41:104–106, 2012.

[55] Y. Zhang, X. Tan, C. Huang, C. Meng, Y. Zhang, X. Tan, C. Huang, and C. Meng. Hydrothermal treatment with VO_2(B) nanobelts for synthesis of VO_2(A) and W doped VO_2(M) nanobelts. *Materials Research Innovations*, 10:295–302, 2016.

[56] N. Ganganagappa and A. Siddaramanna. One step synthesis of monoclinic VO_2(B) bundles of nanorods: Cathode for Li ion battery. *Materials Characterization*, 68:58–62, 2012.

[57] Shuyi Li. *VO_2-based Thermochromic and Nanothermochromic Materials for Energy-Efficient Windows : Computational and Experimental Studies*. PhD thesis, Uppsala University, 2013.

[58] I. P. Parkin and T. D. Manning. Intelligent Thermochromic Windows. *Chemistry for Everyone*, 83(3):393–400, 2006.

[59] H. Futaki and M. Aoki. Effects of Various Doping Elements on the Transition Temperature of Vanadium Oxide Semiconductors. *Japanese Journal of Applied Physics*, 8(8), 1969.

[60] W. Burkhardt, T. Christmann, B. K. Meyer, W. Niessner, D. Schalch, and A. Scharmann. W- and F-doped VO_2 films studied by photoelectron spectrometry. *Thin Solid Films*, 345:229–235, 1999.

[61] J. Livage and M. Curie. Optical and electrical properties of vanadium oxides synthesized from alkoxides. *Coordination Chemistry Reviews*, 192:391–403, 1999.

[62] P. Kiri, M. E. A. Warwick, I. Ridley, and R. Binions. Fluorine doped vanadium dioxide thin films for smart windows. *Thin Solid Films*, 520:1363–1366, 2011.

[63] J. Zhou, Y. Gao, X. Liu, Z. Chen, L. Dai, C. Cao, H. Luo, M. Kanahira, C. Sun, and L. Yan. Mg-doped VO_2 nanoparticles: hydrothermal synthesis, enhanced visible transmittance and decreased metal-insulator transition temperature. *Physical Chemistry Chemical Physics*, 15(20):7505–11, 2013.

[64] M. J. Powell. *VO_2 Thin Films and Nanoparticles, from Chemical Vapour Deposition and Hydrothermal Synthesis, for Energy Efficient Applications*. PhD thesis, University College London, 2015.

[65] E. U. Donev. *Metal-semiconductor transitions in nanoscale vanadium dioxide-thin films, subwavelenght holes, and nanoparticles*. PhD thesis, Vanderbilt University, 2008.

[66] R. Lopez, T. E. Haynes, and L. A. Boatner. Size effects in the structural phase transition of VO_2 nanoparticles. *Physical Review B*, 65:1–5, 2002.

[67] S. Y. Li, G. a. Niklasson, and C. G. Granqvist. Nanothermochromics: Calculations for VO_2 nanoparticles in dielectric hosts show much improved luminous transmittance and solar energy transmittance modulation. *Journal of Applied Physics*, 108(6):1–8, 2010.

[68] L. Kang, Y. Gao, H. Luo, Z. Chen, J. Du, and Z. Zhang. Nanoporous Thermochromic VO_2 Films with Low Optical Constants, Enhanced Luminous Transmittance and Thermochromic Properties. *Applied and Materials Interfaces*, 3:135–138, 2011.

[69] G. Guzman, R. Morineau, and J. Livage. Synthesis of vanadium dioxide thin films from vanadium alkoxides. *Materials Research Bulletin*, 29(5):509–515, 1994.

[70] Y. Takahashi and M. Kanamori. Preparation of VO_2 films by organometallic chemical vapour deposition and dip-coating. *Journal of Materials Science*, 24:192–198, 1989.

[71] S. Lu, L. Hou, and F. Gun. Structure and optical property changes of sol-gel derived VO_2 thin films. *Advanced Materials*, 9(3):244–246, 1997.

[72] H. Wang, X. Yi, S. Chen, S. He, and X. Fu. Reactive Ion Beams Sputtering of Vanadium Oxides Films for Uncooled Microbolometer. *International Journal of Infrared and Millimeter Waves*, 26(3):421–431, 2005.

[73] X. J. Wang, H. D. Li, Y. J. Fei, X. Wang, Y. Y. Xiong, Y. X. Nie, and K. A. Feng. XRD and Raman study of vanadium oxide thin films deposited on fused silica substrates by RF magnetron sputtering. *Applied Surface Science*, 177:8–14, 2001.

[74] T. D. Manning, I. P. Parkin, C. Blackman, and U. Qureshi. APCVD of thermochromic vanadium dioxide thin films solid solutions V_{2-x} M_xO_2 (M=Mo , Nb) or composites VO_2 : SnO_2. *Journal of Materials Chemistry*, 15:4560–4566, 2005.

[75] T. D. Manning, I. P. Parkin, M. E. Pemble, and D. Sheel. Intelligent Window Coatings : Atmospheric Pressure Chemical Vapor Deposition of Tungsten-Doped Vanadium Dioxide. *Chemistry of Materials*, 16(13):744–749, 2004.

[76] T. Maruyama and Y. Ikuta. Vanadium dioxide thin films prepared by chemical vapour deposition from vanadium(III) acetylacetonate. *Journal of Materials Science*, 28:5073–5078, 1993.

[77] G. T. Chandrappa, N. Steunou, S. Cassaignon, C. Bauvais, and J. Livage. Hydrothermal synthesis of vanadium oxide nanotubes from V_2O_5 gels. *Catalysis Today*, 78(1-4 SPEC.):85–89, 2003.

[78] A. Sahin. *Hydrothermal Synthesis and Characterization of Transition Metal Oxides*. PhD thesis, 2004.

[79] M. Shandilya, R. Rai, and J. Singh. Review: hydrothermal technology for smart materials. *Advances in Applied Ceramics*, 2016.

[80] T. Chirayil, P. Y. Zavalij, and M. S. Whittingham. Hydrothermal Synthesis of Vanadium Oxides. *Chemistry of Materials*, 10:2629–2640, 1998.

[81] B. Liu and H. C. Zeng. Hydrothermal Synthesis of ZnO Nanorods in the Diameter Regime of 50 nm. *Journal of The American Chemical Society*, pages 4430–4431, 2003.

[82] V. Subramanian, H. Zhu, R. Vajtai, P. M. Ajayan, and B. Wei. Hydrothermal Synthesis and Pseudocapacitance Properties of MnO_2 Nanostructures. *Journal of Physical Chemistry B*, pages 20207–20214, 2005.

[83] S. Yang, P. Y. Zavalij, and M. S. Whittingham. Hydrothermal synthesis of lithium iron phosphate cathodes. *Electrochemistry Communications*, 3(May):505–508, 2001.

[84] H. Zhang, L. Wang, H. Xiong, L. Hu, B. Yang, and W. Li. Hydrothermal Synthesis for High-Quality CdTe nanocrystals. *Advanced Materials*, (20):1712–1715, 2003.

[85] H. Yin, Y. Wada, T. Kitamura, S. Kambe, and S. Murasawa. Hydrothermal synthesis of nanosized anatase and rutile TiO_2 using amorphous phase TiO_2. *Journal of Materials Chemistry*, 2001.

[86] J. H. Son, J. Wei, D. Cobden, G. Cao, and Y. Xia. Hydrothermal synthesis of monoclinic VO_2 micro- and nanocrystals in one step and their use in fabricating inverse opals. *Chemistry of Materials*, 22(10):3043–3050, 2010.

[87] D. Teixeira, R. Quesada-Cabrera, M. J. Powell, G. K. L. Goh, G Sankar, I P Parkin, and R G Palgrave. Particle size, morphology and phase transitions in hydrothermally produced VO_2(D). *New Journal of Chemistry*, 41:9216–9222, 2017.

[88] J. Y. Suh, R. Lopez, L. C. Feldman, and R. F. Haglund. Semiconductor to metal phase transition in the nucleation and growth of VO_2 nanoparticles and thin films. *Journal of Applied Physics*, 1209(2004):1–6, 2012.

[89] P. W. Voorhees. The Theory of Ostwald Ripening. *Journal of Statistical Physics*, 38:231–252, 1985.

[90] X. M. Lin, C. M. Sorensen, and K. J. Klabunde. Digestive ripening, nanophase segregation and superlattice formation in gold nanocrystal colloids. *Journal of Nanoparticle Research*, pages 157–164, 2000.

[91] M. A. Watzky and R. G. Finke. Transition Metal Nanocluster Formation Kinetic and Mechanistic Studies. A New Mechanism When Hydrogen Is the Reductant: Slow, Continuous Nucleation and Fast Autocatalytic Surface Growth. *Journal of the American Chemical Society*, pages 10382–10400, 1997.

[92] E. J. H. Lee, C. Ribeiro, E. Longo, and E. R. Leite. Oriented Attachment: An Effective Mechanism in the Formation of Anisotropic Nanocrystals. *The Journal of Physical Chemistry B*, pages 20842–20846, 2005.

[93] N. T. K. Thanh, N. Maclean, and S. Mahiddine. Mechanisms of Nucleation and Growth of Nanoparticles in Solution. *Chemical Reviews*, 3(1), 2014.

[94] V. K. La Mer. Nucleation in Phase Transitions. *Industrial and Engineering Chemistry*, 44(6), 1952.

[95] K. L. Choy. Special Issue on Aerosol-Assisted Chemical Vapor Deposition. *Chemical Vapor Deposition*, pages 581–582, 2006.

[96] X. Hou and K. L. Choy. Processing and Applications of Aerosol-Assisted Chemical Vapor Deposition. *Chemical Vapor Deposition*, pages 583–596, 2006.

[97] C. E. Morosanu. *Thin films by chemical vapour deposition*. Elsevier, 1990.

[98] R. G. Palgrave and I. P. Parkin. Aerosol Assisted Chemical Vapor Deposition Using Nanoparticle Precursors A Route to Nanocomposite Thin Films. *Journal of the American Chemical Society*, (17):1587–1597, 2006.

[99] P. Marchand, I. A. Hassan, I. P. Parkin, and C. J. Carmalt. Aerosol-assisted delivery of precursors for chemical vapour deposition: expanding the scope of CVD for materials fabrication. *Dalton Transactions*, 42(26):9406–22, 2013.

[100] L. L. Hench and J. K. West. The Sol-Gel Process. *Chemical Reviews*, 90:33–72, 1990.

[101] J. Livage, M. Henry, and C. Sanchez. Sol-Gel chemistry of transition metal oxides. *Progress in Solid State Chemistry*, 1989.

[102] D. P. Partlow, S. R. Gurkovich, K. C. Radford, and L. J. Denes. Switchable vanadium oxide films by a sol-gel process. *Journal of Applied Physics*, 443(1991), 2004.

[103] A. E. Gash, T. M. Tillotson, J. H. Satcher, L. W. Hrubesh, and R.L. Simpson. New sol-gel synthetic route to transition and main-group metal oxide aerogels using inorganic salt precursors. *Journal of Non-Crystalline Solids*, 285:22–28, 2001.

[104] C. J. Brinker, A. J. Hurd, P. R. Schunk, G. C. Frye, and C. S. Ashley. Review of sol-gel thin film formation. *Journal of Non-Crystalline Solids*, 148:424–436, 1992.

[105] D. B. Hall, P. Underhill, and J. M. Torkelson. Spin coating of thin and ultrathin polymer films. *Polymer Engineering and Science*, 38(12):2039–2045, 1998.

[106] I. E. Wachs. Catalysis science of supported vanadium oxide catalysts. *The Royal Society of Chemistry*, 42:11762–11769, 2013.

[107] K. Kosuge. The phase diagram and phase transition of the V2O3-V2O5 system. *Journal of Physics and Chemistry of Solids*, 28:1613–1621, 1967.

[108] Y. Shtmizu, K. Nagase, N. Miura, and N. Yamazoe. Electrochromic properties of spin-coated V_2O_5 thin films Youichi. *Solid State Ionics*, 56:490–495, 1992.

[109] Y. Dachuan, X. Niankan, Z. Jingyu, and Z. Xiulin. High quaility vanadium dioxide films prepared by an inorganic sol-gel method. *Materials Research Bulletin*, 31(3):335–340, 1996.

[110] F. Beteille and J. Livage. Optical Switching in VO_2 Thin Films. *Journal of Sol-Gel Science and Technology*, 13:915–921, 1998.

[111] L. Kang, Y. Gao, and H. Luo. A Novel Solution Process for the Synthesis of VO_2 Thin Films with Excellent Thermochromic Properties. *Applied Materials and Interfaces*, 1(10):2211–2218, 2009.

[112] I. P. Parkin, R. Binions, C. Piccirillo, C. Blackman, and T. D. Manning. Thermochromic Coatings for Intelligent Architectural Glazing. *Journal of Nano Research*, 2:1–20, 2008.

[113] Cl. Piccirillo, R. Binions, and I. P. Parkin. Synthesis and characterisation of W-doped VO_2 by Aerosol Assisted Chemical Vapour Deposition. *Thin Solid Films*, 516(8):1992–1997, 2008.

[114] Y. Wang and C. Chen. Facile Growth of Thermochromic VO_2 Nanostructures with Greatly Varied Phases and Morphologies. *Inorganic Chemistry*, 52, 2013.

[115] Z. Zhang, Y. Gao, Z. Chen, J. Du, C. Cao, L. Kang, and H. Luo. Thermochromic VO_2 Thin Films: Solution-Based Processing, Improved Optical Properties, and Lowered Phase Transformation Temperature. *Langmuir*, 26(8):10738–10744, 2010.

[116] G. Guzman, F. Beteille, R. Morineau, and J. Livage. Electrical switching in VO_2 sol-gel films. *Journal of Materials Chemistry*, 6:505–506, 1996.

[117] B. Chae, H. Kim, S. Yun, B. Kim, Y. Lee, D. Youn, and K. Kang. Highly Oriented VO_2 Thin Films Prepared by Sol-Gel Deposition. *Electrochemical and Solid-State Letters*, 9:2005–2007, 2006.

[118] A. Bahadori-jahromi, A. Rotimi, A. Mylona, P. Godfrey, and D. Cook. Impact of Window Films on the Overall Energy Consumption of Existing UK Hotel Buildings. *Sustainability*, pages 1–23, 2017.

[119] S. Li, G. A. Niklasson, and C. G. Granqvist. Thermochromic fenestration with VO_2-based materials: Three challenges and how they can be met. *Thin Solid Films*, pages 3823–3828, 2012.

[120] H. Y. Xu, Y. H. Huang, S. Liu, K. W. Xu, F. Ma, and P. K. Chu. Effects of annealing ambient on oxygen vacancies and phase transition temperature of VO_2 thin films. *RSC Advances*, pages 79383–79388, 2016.

[121] X. Liu, R. Ji, and Y. Zhang. Annealing process and mechanism of glass based VO_2 film from V oxidation in pure oxygen atmosphere. *Optical and Quantum Electronics*, 48(10):1–10, 2016.

[122] A. J. T. Naik, C. Bowman, N. Panjwani, M. E. A. Warwick, and R. Binions. Electric field assisted aerosol assisted chemical vapour deposition of nanostructured metal oxide thin films. *Thin Solid Films*, 544:452–456, 2013.

[123] M. J. Powell, I. Godfrey, R. Quesada-cabrera, D. Malarde, D. Teixeira, H. Emerich, R. G. Palgrave, C. J. Carmalt, I. P. Parkin, and G. Sankar. Qualitative XANES and XPS Analysis of Substrate Effects in VO_2 Thin Films: A Route to Improving Chemical Vapor Deposition Synthetic Methods ? *The Journal of Physical Chemistry C*, 2017.

[124] C. Piccirillo, R. Binions, and I. P. Parkin. Synthesis and functional properties of vanadium oxides: V_2O_3, VO_2, and V_2O_5 deposited on glass by aerosol-assisted CVD. *Chemical Vapor Deposition*, 13(APRIL):145–151, 2007.

[125] C. Piccirillo, R. Binions, and I. P. Parkin. Nb-doped VO_2 thin films prepared by aerosol-assisted chemical vapour deposition. *European Journal of Inorganic Chemistry*, (25):4050–4055, 2007.

[126] M. E. A. Warwick and R. Binions. Electric field assisted aerosol assisted chemical vapor deposition of nanostructured metal oxide thin films. *Surface & Coatings Technology*, 230:28–32, 2013.

[127] C. B. Greenberg. Undoped and doped VO_2 films grown from $VO(OC_3H_7)_3$. *Thin Solid Films*, 110:73–82, 1983.

[128] M. A. Sobhan, R. T. Kivaisi, B. Stjerna, and C. G. Granqvist. Thermochromism of sputter deposited $W_xV_{1-x}O_2$ films. *Solar Energy Materials and Solar Cells*, 44:451–455, 1996.

[129] Andriy Romanyuk Ã, Roland Steiner, Laurent Marot, and Peter Oelhafen. Temperature-induced metal semiconductor transition in W-doped VO_2 films studied by photoelectron spectroscopy. *Solar Energy Materials and Solar Cells*, 91:1831–1835, 2007.

[130] S. Y. Li, G. A. Niklasson, and C. G. Granqvist. Thermochromic undoped and Mg-doped VO_2 thin films and nanoparticles: Optical properties and performance limits for energy efficient windows. *Journal of Applied Physics*, (2014), 2015.

[131] Y. Gao, S. Wang, H. Luo, C. Cao, Y. Liu, Z. Chen, and M. Kanehira. Enhanced chemical stability of VO_2 nanoparticles by the formation of SiO_2/VO_2 core shell structures and the application to transparent and flexible VO_2-based composite foils with excellent thermochromic properties for solar heat control. *Energy and Environmental Science*, 5:6104–6110, 2012.

[132] S. Wang, M. Liu, L. Kong, Y. Long, X. Jiang, and A. Yu. Recent progress in VO_2 smart coatings: Strategies to improve the thermochromic properties. *Progress in Materials Science*, 81:1–54, 2016.

[133] M. Moein and R. Binions. Sol-gel approaches to thermochromic vanadium dioxide coating for smart glazing application. *Solar Energy Materials and Solar Cells*, 159:52–65, 2017.

[134] S. Y. Li, G. a. Niklasson, and C. G. Granqvist. Nanothermochromics with VO_2-based core-shell structures: Calculated luminous and solar optical properties. *Journal of Applied Physics*, 109(11):1–5, 2011.

[135] N. R. Mlyuka, G. a. Niklasson, and C.G. Granqvist. Thermochromic VO_2-based multilayer films with enhanced luminous transmittance and solar modulation. *Physica Status Solidi (A)*, 206(9):2155–2160, 2009.

[136] J. Shi, S. Zhou, B. You, and L. Wu. Preparation and thermochromic property of tungsten-doped vanadium dioxide particles. *Solar Energy Materials and Solar Cells*, 91:1856–1862, 2007.

[137] X. B. Chen, J. H. Shin, H. T. Kim, and Y. S. Lim. Raman analyses of co-phasing and hysteresis behaviors in V_2O_3 thin film. *Journal of Raman Spectroscopy*, (April):2025–2028, 2012.

[138] J. F. Watts and J. Wolstenholme. Electron Spectroscopy: some basic concepts. In *An Introduction to Surface Analysis by XPS and AES*, volume 3. 2003.

[139] M. Demeter, M. Neumann, and W. Reichelt. Mixed-valence vanadium oxides studied by XPS. *Surface Science*, 456:41–44, 2000.

[140] G. A. Sawatzky and D. Post. X-ray photoelectron and Auger spectroscopy study of some vanadium oxides. *Physical Review B*, 20(4), 1979.

[141] B. Horvath, J. Strutz, and E. G. Horvath. Preparation, Properties, and ESCA Characterization of Vanadium Surface Compounds on Silicagel. I. *Zeitschrift für anorganische und allgemeine Chemie*, 192:181–192, 1981.

[142] Y. Zhou, Y. Cai, X. Hu, and Y. Long. Temperature-responsive hydrogel with ultra-large solar modulation and high luminous transmission for smart window applications. *Journal of Materials Chemistry A: Materials for Energy and Sustainability*, 2:13550–13555, 2014.

[143] Ch. V. Subba, E. H. Walker, S. A. Wicker, Q. Williams, and R. Kalluru. Synthesis of VO_2(B) nanorods for Li battery application. *Current Applied Physics*, 9(6):1195–1198, 2009.

[144] Y. Zhang and Y. Huang. A facile hydrothermal synthesis of tungsten doped monoclinic vanadium dioxide with B phase for supercapacitor electrode with pseudocapacitance. *Materials Letters*, 182:285–288, 2016.

[145] K. Zhao, L. Teng, Y. Tang, and X. Chen. Branched titanium oxide / vanadium oxide composite nano fi bers formed by electrospinning and dipping in vanadium sol. *Ceramics International*, 40:15335–15340, 2014.

[146] P. Phoempoon and L. Sikong. Phase Transformation of VO_2 Nanoparticles Assisted by Microwave Heating. *The Scientific World Journal*, 2014.

[147] B. Lei, W. Qin, G. Kang, C. Peng, and J. Wu. Desert Rose-Shaped Zircon Synthesized by Low-Temperature Hydrothermolysis. *Journal of the American Ceramic Society*, 1633:1626–1633, 2015.

[148] R. Lopez, L. A. Boatner, T. E. Haynes, L. C. Feldman, and R. F. Haglund. Synthesis and characterization of size-controlled vanadium dioxide nanocrystals in a fused silica matrix. *Journal of Applied Physics*, 4031(2002):1–7, 2010.

[149] L. Kang, Y. Gao, Z. Zhang, J. Du, C. Cao, Z. Chen, and H. Luo. Effects of Annealing Parameters on Optical Properties of Thermochromic VO_2 Films Prepared in Aqueous Solution. *Journal of Physical Chemistry C*, pages 1901–1911, 2010.

[150] S. R. Popuri, M. Miclau, A. Artemenko, C. Labrugere, A. Villesuzanne, and M. Pollet. Rapid Hydrothermal Synthesis of VO_2 (B) and Its Conversion to. *Inorganic Chemistry*, 2, 2013.

[151] M. B. Sahana, G. N. Subbanna, and S. A. Shivashankar. Phase transformation and semiconductor-metal transition in thin films of deposited by low-pressure metalorganic chemical vapor deposition. *Journal of Applied Physics*, 6495(2002), 2010.

[152] F. Gracia, F. Yubero, J. P. Espinos, and A. R. Gonzalez-Elipe. First nucleation steps of vanadium oxide thin films studied by XPS inelastic peak shape analysis. *Applied Surface Science*, 252:189–195, 2005.

[153] J. Mendialdua, R. Casanova, and Y. Barbaux. XPS studies of V_2O_5, V_6O_{13}, VO_2 and V_2O_3. *Journal of Electron Spectroscopy and Related Phenomena*, 71:249–261, 1995.

[154] R. J. Colton, A. M. Guzman, and J. W. Rabalais. Electrochromism in some thin-film transition-metal oxides characterized by x-ray electron spectroscopy. *Journal of Applied Physics*, 49(409), 2008.

[155] C. Sanchez, J. Livage, and G. Lucazeau. Infrared and Raman Study of Amorphous V_2O_5. *Journal of Raman Spectroscopy*, 12(1):3–7, 1982.

[156] Crystal Structures. https://web.iit.edu/sites/web/files/departments/academic-affairs/academic-resource-center/pdfs/Crystal_Structures.pdf. Technical report, Illinois institute of technology.

[157] A. Boultif and D. Lou. Indexing of Powder Diffraction Patterns for Low-Symmetry Lattices by the Successive Dichotomy Method. *Journal of Applied Crystallography*, pages 987–993, 1991.

[158] M. Sakata and Cooper M. J. An Analysis of the Rietveld Profile Refinement Method. *Journal of Applied Crystallography*, pages 554–563, 1979.

[159] R. A. Young, P. E. Mackie, and R. B. Von Dreele. Application of the Pattern-Fitting Structure-Refinement Method to X-ray Powder Diffractometer Patterns. *Journal of Applied Crystallography*, pages 262–269, 1977.

[160] Y. Du, Y. Zhu, S. Xi, P. Yang, H. O. Moser, M. B. H. Breese, and A. Borgna. XAFCA: a new XAFS beamline for catalysis research. *Journal of Synchrotron Radiation*, pages 839–843, 2015.

[161] B. Y. Qu, L. Liu, Y. Xie, and B. C. Pan. Theoretical study of the new compound VO_2(D). *Physics Letters A*, 375:3474–3477, 2011.

[162] M. Li, X. Wu, L. Li, Y. Wang, D. Li, J. Pan, S. Li, L. Sun, and G. Li. Defect-mediated phase transition temperature of VO_2 (M) nanoparticles with excellent thermochromic performance and low threshold voltage. *Journal of Materials Chemistry A*, pages 4520–4523, 2014.

[163] R. Prendergast. *Structure determination of small and large molecules using single crystal X-ray crystallography*. PhD thesis, University of Manchester, 2010.

[164] Dept. of Chemistry & Biochemistry. Steps in Structure Determination. http://xrayweb.chem.ou.edu/notes/steps.html. Technical report.

[165] J. Cockcroft. *Advanced Certificate in Powder Diffraction on the Web. Course Material Master Index*. 2007.

[166] Xiangying Chen, Xiong Wang, Zhenghua Wang, Junxi Wan, Jianwei Liu, and Yitai Qian. An ethylene glycol reduction approach to metastable VO_2 nanowire arrays. *Nanotechnology*, 15, 2004.

[167] Michael H Huang, Amer Choudrey, and Peidong Yang. Ag nanowire formation within mesoporous silica. *ChemComm*, (March):1063–1064, 2000.

[168] Y. Hong-Tao, F. Ke-Cheng, W. Xue-JIn, L. Chao, H. Chen-JUan, and N. Yu-Xin. Effect of nonstoichiometry on Raman scattering of VO_2 films. *Chinese Physics*, 13(1):82–84, 2004.

[169] C. M. Foster, R.P. Chiarello, H. L. M. Chang, H. You, T. J. Zhang, and H. Frase. Raman scattering and x-ray diffractometry studies of epitaxial TiO_2 and VO_2 thin films and multilayers on alpha-Al_2O_3. *Journal of Applied Physics*, 3(1993), 2014.

[170] K. Shibuya, J. Tsutsumi, and A. Sawa. Fabrication and Raman scattering study of epitaxial VO_2 films on MgF_2 (001) substrates. *Applied Physics Letters*, 2013.

[171] C. Julien, G. A. Nazri, and O. Bergstrom. Raman Scattering Studies of Microcrystalline V6O13. *Physica Status Solidi (b)*.

[172] Y. Hu, Z. Li, Z. Zhang, and D. Meng. Effect of magnetic field on the visible light emission of V_2O_5 nanorods. *Applied Physics Letters*, (2009):1–4, 2017.

[173] Matthew Newville. Fundamentals of XAFS. Technical report, University of Chicago, 2004.

[174] J. E. Penner-Hahn. X-ray Absorption Spectroscopy. In *Comprehensive Coordination Chemistry II*, pages 159–186. 2005.

[175] B. Y. M. Crespin, P. Levitz, and L. Gatineau. Reduced Forms of $LaNiO_3$ Perovskite. *Journal of the Chemical Society*, pages 1181–1194, 1983.

[176] M. Crespin, O. Isnard, F. Dubois, J. Choisnet, and P. Odier. $LaNiO_2$: Synthesis and structural characterization. *Journal of Solid State Chemistry*, 178:1326–1334, 2005.